The Seasonal Cycle of CO_2 fluxes in the Southern Ocean: a model spatial scale sensitivity analysis

Ndunisani Precious Mongwe

Taught Masters

Thesis presented for the Degree of

Master of Science

Department of Oceanography

University of Cape Town

April 2014

UNIVERSITY OF CAPE TOWN

IYUNIVESITHI YASEKAPA • UNIVERSITEIT VAN KAAPSTAD

Abstract

A recent study by Lenton et al., 2013, compared the mean seasonal cycle of air-sea CO_2 flux in the Southern Ocean(SO) over 1990 – 2009 period using five ocean biogeochemical models(BGMs) and atmospheric and ocean inversion models with monthly mean observations for the year 2000. This was done using a set of geographic boundaries to defined sub-domains of the SO consistent with the Regional Carbon Cycle and Assessment and Processes (RECCAP) protocol. Lenton et al., 2013 found that the seasonal cycle anomaly of the five BGMs better resolved observations of the air-sea CO_2 flux seasonal cycle in the SAZ, but was generally out phase with observations in the polar zone. In this study two setups of the ocean biogeochemical model NEMO PISCES was used to investigate the characteristics of the air-sea CO_2 flux seasonal cycle in the Southern Ocean in the period 1993- 2006. The study focused on two aspects i.e. (i) the sensitivity of air-sea CO_2 flux seasonal cycle to model resolution: comparing the ORCA2-LIM-PISCES (2^o x 2^o cos Ø) and PERIANT05 (NEMO-PISCES) (0.5^o x 0.5^o cos Ø) model configurations relative to climatological mean observations for the year 2000 (Takahashi et al., 2009) , and (ii) the sensitivity of air-sea CO_2 flux seasonal cycle to zonal boundary definition: comparing the air-sea CO_2 flux seasonal cycle and annual fluxes for three different boundaries i.e. Lenton 2013 RECCAP boundaries (44^oS – 58^oS and south of 58^oS), geographic boundaries (40^oS -50^oS and south of 50^oS) and dynamic boundaries (Sub-Antarctic Zone and Antarctic Zone, defined using climatological frontal positions). The seasonal cycle of the air-sea CO_2 flux in ORCA2 was found to be out of phase and overestimated the CO_2 flux compared to observations in almost all the sub-regions considered. The use of dynamic boundaries was found not to improve resolving observations seasonal cycle of air-sea CO_2 flux in both ORCA2 and PERIANT05. Boundary definition was found to affect the magnitude of ORCA2 annual air-sea CO_2 fluxes surface area based, where sub-regions of larger surface area gave larger annual CO_2 uptake and vice versa. This was mainly because ORCA2 air-sea CO_2 fluxes were found to show a general CO_2 in-gassing bias and spatially uniform in most parts of the SO and hence integration over a larger surface area gave larger annual fluxes. On the contrary PERIANT05 air-sea CO_2 fluxes spatial variability was not uniform in most parts of the SO however influenced by regional processes and hence annual fluxes were found not surface area based. The poor spatial representation and seasonal cycle sensitivity of ORCA2 air-sea CO_2 fluxes was found to be primarily due to lack or weak winter CO_2 entrainment and biological CO_2 draw down during the summer season. PERIANT05 on the contrary showed the effect of winter CO_2 entrainment, however maintains lack of or weak biological CO_2 draw down in the seasonal cycle. PERIANT05 was also found to show major weakness in the spatial representation of air-sea CO_2 fluxes north of the polar front with relative to T09 observations.

Supervisors

CSIR: Dr Pedro .M.S Monteiro

Ocean Systems and Climate, Natural Resource & Environment (NRE),

Council for Scientific and Industrial Research (CSIR), South Africa

UCT: Dr Howard Waldron

Department of Oceanography

University of Cape Town, South Africa

Acknowledgements

I would like to acknowledge my supervisor Dr Pedro Monteiro for his support and patience in guiding me to develop an understanding and articulation of my findings in this project. I would also like to acknowledge Dr Howard Waldron for his assistance in articulating this work in writing. Thanks to Dr Nicolette Chang who ran the NEMO PISCES model used in this project and her assistance in processing the model output. Thanks to Dr Alessandro Tagliabue for assistance with setting up the model and the Centre for High Performance Computing (CHPC) for providing the resources and computing time to run this experiment. I would also like to thank Dr Julie Deshayes, Dr Issufo Halo, Dr Bjorn Backeberg for their assistance in Matlab data processing.

Table of contents

1. Introduction

The exchange of CO_2 between the ocean and atmosphere forms an important part of the global carbon cycle and a key determinant in the future of earth systems (Gruber et al., 2009; Fung et al., 2005). The Southern Ocean (SO) plays a key role in ocean – atmosphere exchange of CO_2 and the global carbon budget (Lovenduski et al., 2007; Takahashi et al., 2012). The SO only covers about 20% of the global ocean, however takes up about a third of the total oceanic annual CO_2 uptake (Mikaloff Fletcher et al., 2006; Gruber et al., 2009, Sabine et al., 2004), slowing down the accumulation of CO_2 in the atmosphere and thus the rate of climate change (Lenton et al 2013). Consequently the SO is a critical sink and provides long term storage of anthropogenic CO_2 (Takahashi et al 2012). The importance of the SO in the global CO_2 budget is a result of *inter alia* its unique connection of the interior and surface ocean, allowing a significant air-sea ventilation of CO_2 (Lenton et al., 2013; Gonzalez et al., 2011). One of the critical features of the SO contribution to this unique CO_2 ventilation is the impact of westerly winds in surface waters in high latitudes. Westerly winds deflect surface waters of the Antarctic Circumpolar Current (ACC), resulting in the northern movement of surface water driven by Ekman transport. This deflected surface water is replenished by deep ocean CO_2 saturated water, causing a strong change in the air-sea gradient leading to a CO_2 outgassing in high latitudes. The interaction of these deep ocean waters with surface and sub-surface waters dominates the air-sea CO_2 flux dynamics of the SO (Anderson et al., 2009; Gonzalez et al., 2011; Lenton et a., 2013; NcNeil et al., 2007). This characteristic of the SO makes it a key component of the global climate system and carbon budget (Le Quèrè et al., 2007, 2009). It has been described as the single most important CO_2 sink in the world oceans (Gruber et al., 2009).

At the current rate of climate change, processes regulating the sea-air CO_2 gas exchange are expected to change, leading to positive and negative feedbacks (Sarmiento et al., 1998; Gruber et al., 2004; Fung et al., 2005). Several studies in the past have suggested that the SO CO_2 sink has weakened over time in response to climate change and is projected to continue weakening in the future, (e.g. Le Quèrè et al., 2007; Lovenduski et al., 2007, Takahashi et al., 2012). However some studies propose a strengthening of the CO_2 sink, thus the predicted evolution of the CO_2 sink in the SO is still under debate (Zickfeld et al., 2008; Sarmiento et al., 1998; Sarmiento et al., 1995; Sabine et al 1999; Le Quèrè et al., 2007, 2010). A recent review by Thompson et al., 2011, proposes that the observed reduction of stratospheric ozone has an ability to weaken the long term CO_2 uptake of the SO. The reduction of stratospheric ozone is known to cause an intensification of the circulation vortex which enhances westerly winds in high latitudes, characterized as the positive phase of the Southern Annual Mode (SAM), (Solomon and Thomson, 2002; Son et al., 2011). This intensification

of the westerlies strengthens the CO_2 outgassing by accelerating the rate of surface water deflection in high latitudes (Ekman transport) and hence increasing the exposure of deep ocean CO_2 saturated waters. Thompson et al., 2011 propose that in recent years, the SAM index has become more positive as result of climate change and the evolution of this process in the future is likely to weaken the long term CO_2 uptake of the SO.

Although the SO plays a critical role in the storage and circulation of anthropogenic CO_2 in the world ocean, it still remains one of the poorly sampled regions with respect to carbon (Monteiro et al., 2010). Most of the available observations south of 20^{o}S only regularly cover a 3 month period, (Takahashi et al., 2009). The partial availability of observations introduces a critical gap in the quantitative understanding of air-sea CO_2 interaction in the SO. Most ocean models still struggle to reproduce the observed air-sea CO_2 fluxes in these sub-regions, especially south of 58^{o}S (e.g. Lenton et al., 2013). To this extent, previous studies applied different approaches to estimate air-sea CO_2 fluxes of the SO, including biogeochemistry models, Ocean inversion models, atmospheric inversion models and empirical gas exchange parameterization (e.g. Roy et al., 2003, 2011, Sarmiento et al., 1998, Matzl et al., 2006, 2009, Takahashi et al., 1998, 2002, 2009). Different modelling approaches gave different magnitudes of CO_2 annual fluxes (e.g. Gruber et al., 1996, 1998; Poisson and Chen 1991; Duffy and Caldeira., 1997; Mikaloff Fletcher et al., 2007; Gruber et al 1996; Roy et al., 2003). However a recent inter-model comparison study of air-sea CO_2 annual fluxes has shown a convergence of model results in annual air-sea CO_2 fluxes (Gruber et al., 2009). These findings are encouraging, however agreement on annual fluxes alone does not hold the key in assessing the ability of ocean models to resolve observations air-sea CO_2 fluxes. It is essential to take into account seasonal cycle sensitivity, (Lenton et al., 2013).

In response to such concerns, a recent paper published by Lenton et al., 2013 under the global carbon project assessed the air-sea CO_2 fluxes seasonal cycle in the SO over 1990 -2009. In this study Lenton et al., 2013 used five ocean biogeochemical models, ocean inversion models, atmospheric models and observations from Takahashi et al., 2009. Lenton et al., 2013 found that though the five ocean biogeochemical models agreed on CO_2 fluxes at the annual scale, none of the models could reproduce both the phase and magnitude of the observations of the air-sea CO_2 fluxes intra-annually, especially south of 58^{o}S. Furthermore Lenton et al., 2013 found that of the five ocean biogeochemical models, two (NEMO-Plankton 5 and NEMO-PISCES (2^o x 2^o cos Ø)) overestimates the annual CO_2 fluxes compared the other three (CCSM_BEC, CCSM_ETH and CSIRO). Given that the seasonal cycle is the dominant mode of variability in the SO (Thomalla et al., 2011), the inability of these ocean models to reproduce the seasonal cycle is concerning (Lenton et al., 2013). These

findings bring into question current understanding of the air-sea CO_2 fluxes of the SO in ocean models. Furthermore, the different air-sea CO_2 flux seasonal variability in these ocean biogeochemical models question whether long term CO_2 projections made from these models are based on true ocean –atmosphere CO_2 interaction processes.

Though simulation of biogeochemical parameters has improved overtime in Earth Systems Models (EMS), most of the current state of the art biogeochemical ocean models from the latest Coupled Model Intercomparison Project Phase 5 (CMIP5; Anav et al., 2013) have a spatial resolution of 1^o to 2^o. This resolution still does not resolve some of the fine scale feature important in processes driving air-sea CO_2 fluxes i.e. mesoscale and sub-mesoscale eddies, surface waves and etc. However though the use of high-resolution biogeochemical models has an advantage of resolving fine scale features, the level of complexity involved in their parameterization also create a challenges in representation of surface ocean biogeochemical dynamics (e.g. Treguier et al 2014). In this study the impact of resolution in the seasonal cycle of air-sea CO_2 flux is investigated by comparing the model output of the PERIANT05 (0.5^o x 0.5^o) and ORCA2 (2^o x 2^o) configurations of the NEMO PICECES biogeochemical model. Note that besides resolution, ORCA2 and PERIANT05 simulations has other differences including spin periods, atmospheric pCO_2 forcing and etc. which may also be the source of difference their outputs (see Appendix B).

In the Lenton et al., 2013 study, sub-domains of the SO were divided geographically as accordance to the Regional Carbon Cycle Assessment and Processes project (RECCAP; Canadell et al., 2011) protocol. The use of geographically defined boundaries in assessing the air-sea CO_2 fluxes has however been questioned by some of the recent studies because of their inability to depict distinct regions of the air-sea CO_2 fluxes, (e.g. Sèfèrian et al., 2012). In Lenton et al., 2013 for example the use of geographic boundaries was also found to be problematic, defining the SO as south of 44^oS excluded some parts of the Sub-Antarctic Zone which is an important CO_2 sink. When the northern boundary was extended to 40^oS, annual CO_2 fluxes almost doubled (Lenton et al., 2013). Concerns of boundary definition is a well-known phenomenon in ocean modelling however their quantitative effects on the seasonal cycle of air-sea CO_2 flux and CO_2 annual fluxes have not been previously investigated. Thus in addition to the assessment of the impact of resolution on air-sea flux, this project also seeks to investigate the quantitative effect of zonal boundary definition in the estimation of air-sea CO_2 flux at the seasonal and annual scale in the SO.

2. Literature review

This chapter gives an overview background of the carbon dioxide (CO_2) literature and description of fundamental processes governing the atmosphere-ocean CO_2 interaction. This chapter is organized into four sections *viz*;

I. Section 2.1 gives a brief overview background of CO_2 and its significance as an earth system study.
II. Section 2.2 describes some of the main processes regulating the air-sea CO_2 interaction i.e. ocean CO_2 chemistry, biological processes and air-sea gas exchange
III. Section 2.3 focuses on the Southern Ocean (SO) as an important CO_2 sink, describing features responsible for the SO significance as a component of the global carbon cycle and goes on to describe the specific focus and aim of this study.

2.1 Carbon dioxide

Carbon dioxide (CO_2) is one of the most important life sustaining substances in the biosphere, typically because it acts as a source of carbon which is a principal element of all live beings (Revelle 1985). Carbon is found in all living substances and many inorganic materials, it accounts for about half of the earth's planet dry mass (Sulzman, 2000). CO_2 has three major reservoirs i.e. land, ocean and atmosphere and its circulation between these reservoirs is referred to as the Carbon cycle. In the three reservoirs, the atmosphere is the smallest reservoir (storing about 750 Gt), most of the carbon in the atmosphere occurs as CO_2 with a small fraction of methane (CH_4), carbon monoxide (CO) and Chlorofluorocarbon (CFC). The terrestrial biosphere (land, including plants and animals) is the second largest reservoir, storing about 2200Gt. And the ocean is the largest reservoir by far, storing about 39 000Gt of carbon. The balance of carbon among these three reservoirs is referred to as the carbon budget (Sulzman, 2000).

Since the beginning of the industrial revolution in the 1750s, CO_2 gas has being increasing in the atmosphere as a result of burning of fossil fuel for energy, cement production and land use change (Le Quèrè et al., 2009). Early studies in the 1900s found that the increase of CO_2 in the atmosphere has an ability to alter long term climate through a process currently known as the greenhouse effect (e.g. Arrhenius 1896). CO_2 is one among several atmospheric gases known as greenhouse gases. These gases have the ability to absorb terrestrial radiation through the infrared wavelength and re-emit the energy to earth (Sarmiento and Gruber, 2006). The concept of the greenhouse effect is as follows. Earth receives radiation from the sun through short wavelengths and radiates it back to

space in long wavelengths, greenhouse gases in the atmosphere absorb this radiation and re-emit the energy to earth, warming the planet to present day ambient temperatures and making it habitable. In the absence of these atmospheric gases, radiation would only warm up the earth until it reaches an equilibrium temperature of -18^{o}C, which is not favorable for habitability, (Lammer et al., 2009). Given that CO_2 is one of main greenhouse gasses, elevated concentrations of CO_2 in the atmosphere can alter the re-emission of energy resulting in an increase of average temperatures, (Sorenson, 2011).

The concept of the alteration of long term climate, commonly referred to as climate change, was first documented by Svante Arrhenius in 1896. In this study, Arrhenius, 1896 proposed that variations in the atmospheric CO_2 concentration contributed to the long-term climate change. Although this phenomenon was known since the 1990s, only in 1957 were actual measurements of atmospheric CO_2 commenced by Charles Keeling and Roger Revelle, attempting to get a clearer understanding of the global carbon cycle. Revelle and Keeling monitored two atmospheric CO_2 remote stations, one at the South Pole and one in Hawaii. These two stations have continued almost un-interrupted since, and are still providing useful CO_2 data to date (Keeling 1958, Bopp and Le Quèrè, 2010). In the past few decades, quantification of the land and oceanic CO_2 sink has drawn much interest since they give a first-order evaluation of atmospheric CO_2, (Bopp and Le Quèrè, 2010). One of the main reasons for these studies was because a long-term change in climate systems has implications for environmental change, including *inter alia* sea-level rise and alterations of terrestrial-marine ecosystems, which in turn could affect the socio-economic stability of human society (ICCCEA 2003; HLPE report 3).

The atmospheric CO_2 concentration increases at half the rate of the human-induced CO_2 emissions because the ocean acts as a large sink of CO_2 (among others), absorbing about half of the emitted CO_2 annually (Prentice et al., 2001; Le Quèrè et al., 2007). The Southern Ocean absorbs about half of the annual oceanic CO_2 uptake alone, slowing down the rapid accumulation of CO_2 in the atmosphere (Takahashi et al., 2012). Several studies have reported that processes regulating oceanic and atmospheric CO_2 are likely to change due to global warming, leading to negative and positive feedbacks in the global climate system (e.g. Sarmiento et al., 1998; Joos et al 1999; Le Quèrè et al., 2007; Fung et al., 2005).

Thus the study of interannual variability of processes regulating atmosphere-ocean CO_2 interaction over the last few decades may help determine the future evolution of CO_2 concentrations in the atmosphere (Lovenduski et al., 2007). The next section explores the atmospheric and oceanic CO_2 circulation, but mainly focuses on oceanic CO_2 processes and circulation mechanisms.

2.2 Atmosphere – ocean CO_2 interaction and circulation

This section describes oceanic CO_2 processes (oceanic CO_2 chemistry) and goes on to investigate biological process and air-sea gas exchange impact *viz.* atmospheric – oceanic CO_2 interaction.

2.2.1 Ocean CO_2 chemistry

When CO_2 dissolves in seawater, it first forms carbonic acid (H_2CO_3), which is very unstable and dissociates immediately to form a bicarbonate ion (HCO_3^-), which further dissociates to form a carbonate ion (CO_3^{2-}), equation 2.1 - 2.3. These reactions are fast enough that thermodynamic equilibrium can be assumed (Sarmiento and Gruber, 2006).

$$CO_{2(g)} + H_2O \leftrightarrow H_2CO_3 \qquad K_0 = \frac{[H_2CO_3]}{pCO_2} \tag{2.1}$$

$$H_2CO_3 \leftrightarrow H^+ + HCO_3^- \qquad K_1 = \frac{[H^+][HCO_3^-]}{[H_2CO_3]} \tag{2.2}$$

$$HCO_3^- \leftrightarrow H^+ + CO_3^{2-} \qquad K_2 = \frac{[H^+][CO_3^{2-}]}{[HCO_3^-]} \tag{2.3}$$

Summation of equation 2.1 – 2.3 give the primary buffering of CO_2 in seawater, equation 2.4 (Bopp and Le Quèrè, 2010).

$$CO_{2(aq)} + H_2O + CO_3^{2-} \leftrightarrow 2HCO_3^- \tag{2.4}$$

Where K_0 is the solubility coefficient of CO_2 in seawater, given in mol kg^{-1} atm^{-1}, CO_2 solubility reflects the efficiency at which moles of carbon pass in and out of the air-sea interface, and is predominantly driven by temperature and salinity. K_1 and K_2 are the dissociation constants of H_2CO_3 and HCO_3^- respectively. There are different magnitudes of these constants from previous studies (e.g. Mehrbach et al., 1973; Dickson and Millero., 1987; Millero et al., 1993, 2006; Lueker, 1998).

The speciation of CO_2 (aq), CO_3^{2-} and HCO_3^- in seawater are 0.5%, 89% and 10.5 % respectively. The summation of CO_2 (aq), CO_3^{2-} and HCO_3^- gives the total Dissolved Inorganic Carbon (DIC), i.e. total concentration of inorganic oceanic carbon. DIC is a very useful measure in the oceanic CO_2 circulation as will be evident later in the text. The proportions of CO_2 (aq), CO_3^{2-} and HCO_3^- in sea water are highly dependent on pH, where high pH results in more CO_2 and low pH results in more

CO_3^{2-}, see figure 2.1. The current ocean pH is about 8.2, shown by the dotted line in figure 2.1 as are the current oceanic proportions of CO_2, CO_3^{2-} and HCO_3^-.

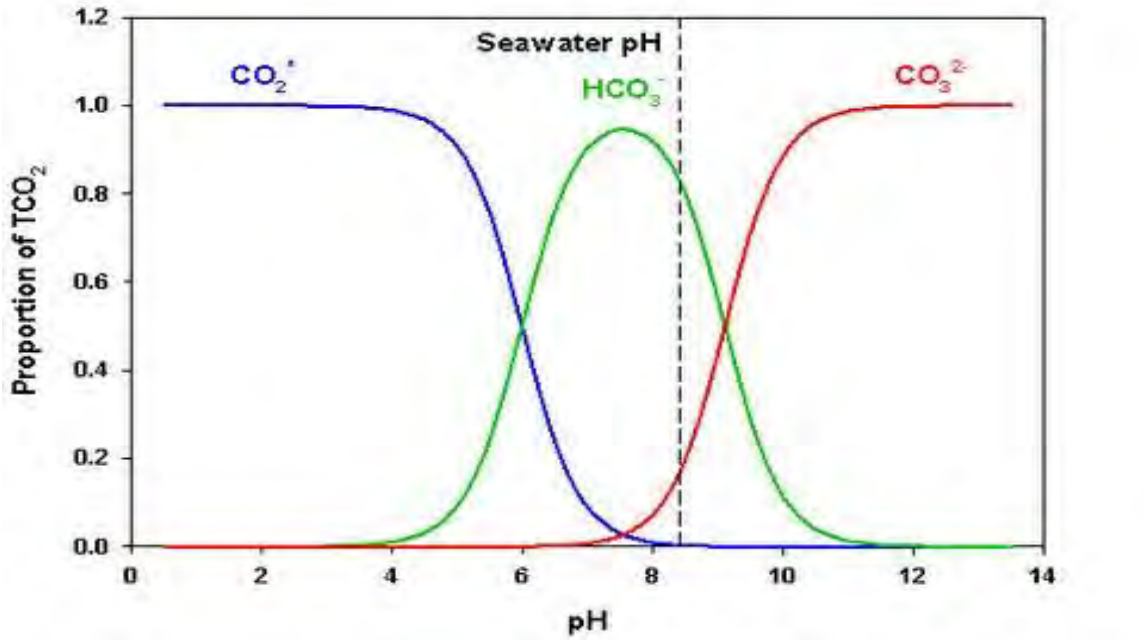

Figure 2.1 Speciation diagram for CO_2 in sea water showing the relative proportion of each species, the dotted line shows the current seawater pH (taken from http://www.advancedaquarist.com/2008/12/chemistry)

The air-sea CO_2 equilibrium in the ocean takes longer relative to other gases e.g. oxygen (Sarmiento and Gruder, 2006). For a mixed layer of 40m, the air-sea CO_2 equilibrium has a timescale of 6 months. This longer timescale of equilibrium is mainly because only about 5% of the CO_2 molecules dissolving in the air-sea interface contribute to the change of CO_2 concentration in the ocean, the other 95% react with carbonate ions already present in the mixed layer to form two carbonate ions, equation 2.5. Thus the efficiency of dissolving CO_2 in seawater is dependent on the availability of carbonate ions. This is one of the key reasons why the ocean has a large storage capacity for CO_2 (Bopp and Le Quèrè, 2010).

$$H_2CO_2 + CO_3^{2-} \leftrightarrow 2HCO_3^- \qquad (2.5)$$

Another useful quantity in the carbon cycle and descriptor of the carbonate system (CO_2, HCO_3^-,CO_3^{2-}, H^+, OH) is total alkalinity (TAlk), (Wolf- Gladrow et al.,2007). Total alkalinity is defined as the excess of proton acceptors over donors with respect to the chosen zero level of the protons (Dickson, 1981; Wolf- Gladrow et al., 2007).

$$TAlk = [HCO_3^-] + 2[CO_3^{2-}] + [B(OH)_4^-] + [OH^-] - [H^+]$$ + Minor anions of weak acids. (2.6)

DIC and TAlk are conservative with respect to mixing and temperature changes in the ocean and hence are used as state variables in ocean carbon models (Wolf-Gladrow et al., 2007; Sarmiento and Gruber 2006).

The partial pressure of the CO_2 gradient (ΔpCO_2) between the atmosphere and ocean gives the thermodynamic forcing for the oceanic anthropogenic CO_2 uptake (Takahashi et al., 2009; Wanninkhof et al., 2009). Thus surface pCO_2 variability plays a key role in controlling the influx of CO_2 into the ocean. Consequently surface pCO_2 distributions play a central role in controlling the oceanic annual CO_2 uptake. To study the pCO_2 surface variability one has to investigate the variability of the components of DIC (CO_2 (aq), CO_3^{2-} and HCO_3^-) and the processes controlling them. To illustrate this relationship, below equations 2.1 – 2.3 are further simplified and solved for pCO_2 to give equation 2.7. Equation 2.6 can also be further simplified using the definition of Alk (2.5) and DIC, to also give equation 2.8; (Sarmiento and Gruber, 2006).

$$pCO_2 = \frac{K_2}{K_0 K_1} \frac{[HCO_3^-]}{[CO_3^{2-}]} \qquad (2.7)$$

$$pCO_2 \approx \frac{K_2}{K_0 K_1} \frac{(2.DIC - Alk)^2}{Alk - DIC} \qquad (2.8)$$

From equation 2.8, surface pCO_2 distributions can be assessed by a knowledge of the dissociation constants (K_0, K_1 & K_2), DIC and Alk. The relationship of temperature with the carbonate system is shown in figure 2.2. Solubility of CO_2 (K_0) shows a strong inverse relation with temperature, on the other hand K_1 and K_2 have a direct proportional relation with temperature, see figure 2.2. From this figure one can infer that surface pCO_2 will be low in the tropics and high in higher latitudes on the premise of latitudinal temperature gradient. However this presumption is not entirely true since other factors including biological activity, ocean transport and mixing play a role in the CO_2 uptake as will be illustrated later in the text (Sarmiento and Gruber, 2006).

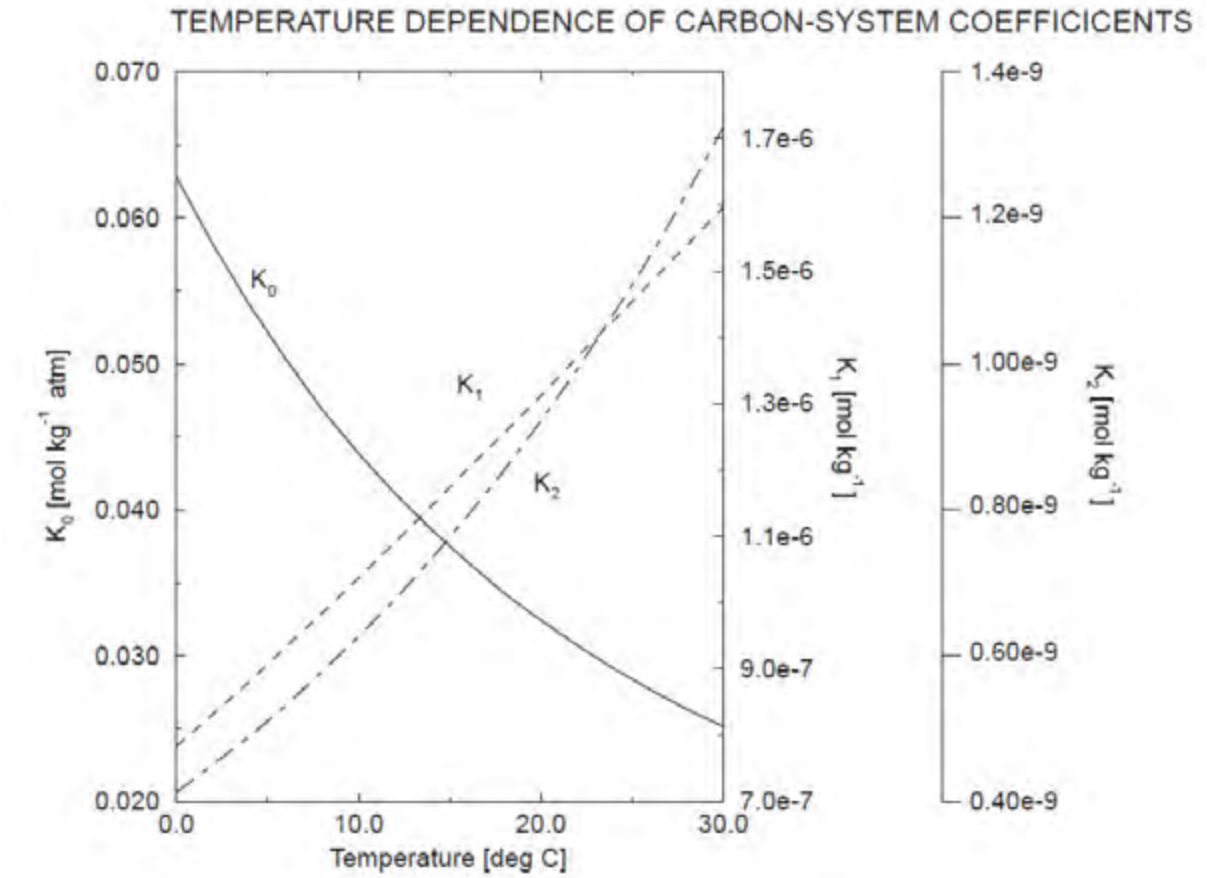

Figure 2.2 CO_2 solubility plot (K_o) and the first (K_1) and second dissociation constants (K_2) of carbonic acid plotted against temperature (Sarmiento and Gruber 2006)

Sensitivity experiments on the influence of temperature and salinity on CO_2 solubility designed by Sarmiento and Gruber (2006), showed that temperature is more of a dominant regulator of CO_2 solubility than salinity. From this experiment it was found that at a given set of standard conditions, a rise of 1^{o}C results in a 13 µatm increase of pCO_2 and only 9µatm in salinity. Also, given that salinity only varies slightly in absolute terms compared to temperature in the world oceans, temperature variability is a more important factor in the variability of surface pCO_2 (Sarmiento and Gruber, 2006). High latitude waters have high CO_2 solubility due to lower Sea Surface Temperatures (SST) and high densities in these waters drive them to the deep ocean via subduction. Because of this mechanism, deep ocean waters hold more CO_2 saturated waters relative to surface seawaters owing to the conditions under which they were formed. In contrast to high latitudes, in the tropics, CO_2 solubility is reduced by high SSTs and CO_2 saturated waters are upwelled by ambient ocean circulation. The overall interaction of these processes is termed the solubility pump, (Bopp and Le Quèrè, 2010).

In addition to the solubility pump, biological activity and mixed layer dynamics play a key role in the air-sea CO_2 fluxes (Williams and Follows, 2011). The next section explores the influence of biological activity in oceanic CO_2 uptake.

2.2.2 Biological process

Biological processes play a major role in the distribution of chemical species in the ocean. If it was not for of the influence of biological activity, most chemicals in the ocean would be distributed uniformly in a manner similar to salinity (Sarmiento and Gruber, 2006). The influence of biological activity in air-sea CO_2 interaction is by means of two major processes i.e. (i) photosynthetic CO_2 uptake and the reverse process of respiration and remineralisation, (ii) formation of $CaCO_3$ shells by ocean organisms through a process called calcification (Bopp and Le Quèrè, 2010). Photosynthesis takes place in the upper surface ocean at the sub-region commonly referred to as the euphotic zone. During photosynthesis CO_2 is reduced by marine organisms (phytoplankton) to form organic matter in the presence of sunlight and nutrients, the chemical reaction is given as follows.

$$106CO_2 + 16NO_2^- + HPO_4^{2-} + 68H_2O \leftrightarrow C_{106}H_{175}O_{42}N_{16}P + 150O_2 \qquad (2.9)$$

The overall productivity in the euphotic zone is generally limited by the availability of sunlight, nutrients (nitrate, phosphate, silicate and micronutrients including iron) and stratification in some parts of the ocean (Gruber and Sarmiento, 2006; Thomalla et al., 2011). About half of the fixed carbon in the euphotic zone is converted back to CO_2 through respiration by both auto- and heterotrophs (reverse of photosynthesis). The remaining fixed carbon constitutes the Net Primary Production (NPP) of the ocean, (Bopp and Le Quèrè, 2010). The estimation of this from global remote sensing observations and models gives a figure between 35 and 70 $PgCyr^{-1}$ (Carr et al., 2006). A fraction of the NPP is exported to the deeper layers of the ocean in the form of Particulate Organic Carbon (POC), which includes dead and living organisms. The downward flux of POC is referred to as the export material and it accounts for about 11 $PgCyr^{-1}$ at 100m depth (Schitzer et al., 2002). Dissolved Organic Carbon (DOC) is also produced during photosynthesis and transported to the deep ocean by physical processes. A portion of the downwelling DOC is remineralised to DIC by bacterial respiration and then transported back to the mixed layer via physical processes (Bopp and Le Quèrè., 2010). This entire mechanism is referred to as the soft-tissue pump, also known as the Biological pump (Volk and Hoffert., 1985).

The formation and dissolution of calcite or aragonite is the second major biological process in the ocean as stated above, where marine organisms (Coccolithophorids, pteporods and foraminifers) form $CaCO_3$ shells. The chemical reaction of process is as follows;

$$Ca_2^{+} + CO_3^{2-} \leftrightarrow CaCO_3 \qquad (2.10)$$

The formation and dissolution of a single molecule of calcium carbonate ($CaCO_3$) changes the ratio of TAlk twice as much as DIC. This is because one mole of CO_3^{2-} contributes two moles to the formation of a single mole in the Alk equation (2.6), but one mole to DIC formation. Thus formation and dissolution of calcium carbonate shells have a direct implication for surface CO_2 concentrations. When marine organisms produce calcite shells (which die in the surface ocean), their shells sink to the deep ocean, drawing down CO_3^{2-} from the mixed layer. More than half this carbonate production is dissolved in the water column. This process is referred to as the carbonate pump (Bopp and Le Quèrè, 2010). In situ measurements give an estimation of about 0.6 $PgCyr^{-1}$ at 100m depth for the carbonate pump (Milliman, 1993).

The combined effect of biological activity, CO_2 solubility and mixed layer dynamics in the surface ocean is reflected in the overall air-sea CO_2 gas exchange. The next section describes basic principles of air-sea gas change.

2.2.3 Air-sea gas exchange

The flux (F) of a nonreactive soluble gas across the air-sea interface can be defined as a result of the gas transfer velocity coefficient (*k*) (which provides the kinetic forcing) and the concentration gradient (thermodynamic forcing) between the upper layer (atmosphere) and the boundary layer (ocean), (Wanninkhof et al., 2009) . For CO_2, the gas exchange between the air-sea interface is given by equation 2.11.

$$F = k \times K_0 \times (pCO_{2w} - pCO_{2a}) = k \times K_0 \times \Delta pCO_2 \qquad (2.11)$$

Where K_0 is the CO_2 solubility, pCO_{2w} is the CO_2 partial pressure of seawater and pCO_{2a} is the atmospheric CO_2 partial pressure. The net flux into the ocean is expressed as a negative value by convention (Wanninkhof et al., 2013). The gas transfer velocity coefficient (*k*) is defined by equation 2.10. where $<U^2>$ denotes the second moment of the mean wind speed at 10m above sea surface and Sc is the Schmidt number Sc [kinetic viscosity of water/diffusion of coefficient of CO_2 in sea water], (Wanninkhof et al., 2013)

$$k = 0.0251 \times (Sc/660)^{-0.5} < U^2 > \quad (2.13)$$

$$Sc = 2073.1 - 125.62 \times SST + 3.6276 \times SST^2 - 0.04319 \times SST^3 \quad (2.14)$$

There are several parameterizations of the gas transfer velocity from previous studies. Some studies suggested higher order polynomials and various forcing functions (e.g. McNeil et al., 2009; Jackson et al., 2012; Nightingale et al., 2000). For this study the quadratic equation has been chosen in accordance with Wanninkhof et al 2009, where it was established to be optimum for global-scale analysis.

Other factors influencing the gas transfer velocity include surface films, bubble entrainment, and boundary layer stabilities (Broecker et al., 1978, Few et al., 1990, Wallance and Wirick ., 1992, McNeil and d'Asaro., 2007, Ho et al., 1997, Takagaki and Komori., 2007, Erickson et al., 1993). Figure 2.3 summarizes factors influencing the air-sea CO_2 flux and variables relating to this process. The thermodynamic forcing is mainly driven by SST, ocean transport and biological processes in the surface ocean, see figure 2.2. The kinetic forcing, on the other hand, is mainly influenced by wind stress, slope and boundary layer dynamics, (Wanninkhof et al., 2009).

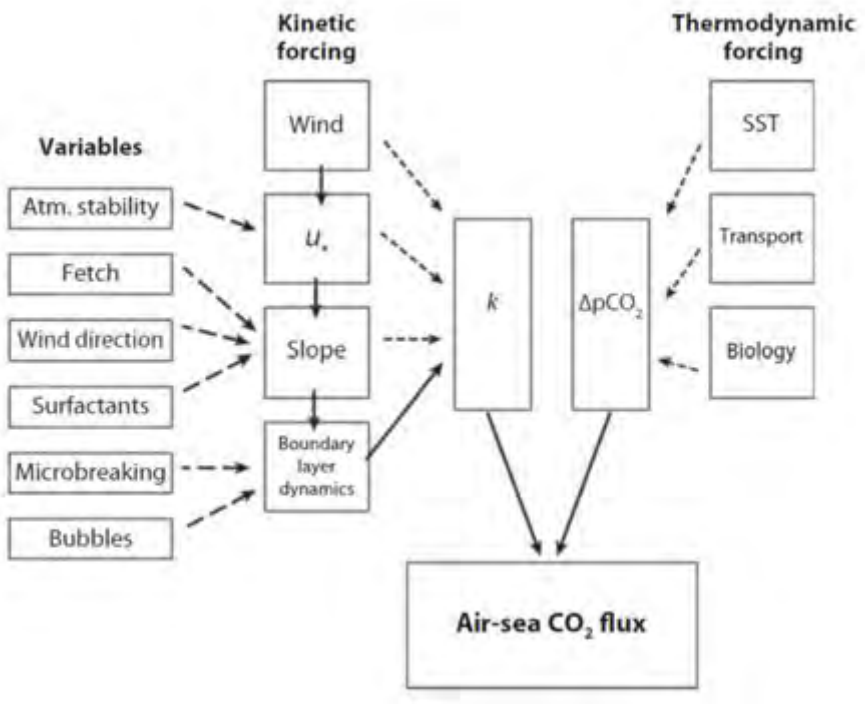

Figure 2.3 Simplified schematic of factors influencing the air-sea CO_2 fluxes, kinetic forcing factors given on the left and the thermodynamic forcing factors on the right (taken from Wanninkhof et al., 2009)

The global ocean air-sea CO_2 fluxes computed from a compilation of about 3 million in situ surface CO_2 measurements collected since 1970, and referenced to the year 2000 by Takahashi et al., 2009 shows that air-sea CO_2 fluxes are not uniform over most of the ocean, see figure 2.4. Figure 2.4 shows some regions of the ocean to be major CO_2 sink zones (North Atlantic, North Pacific and south part Southern Ocean) and other regions to be CO_2 outgassing zones (equatorial regions and south of the Polar front in the Southern Ocean). The spatial and temporal variability of the air-sea CO_2 fluxes is mainly controlled by the processes described above.

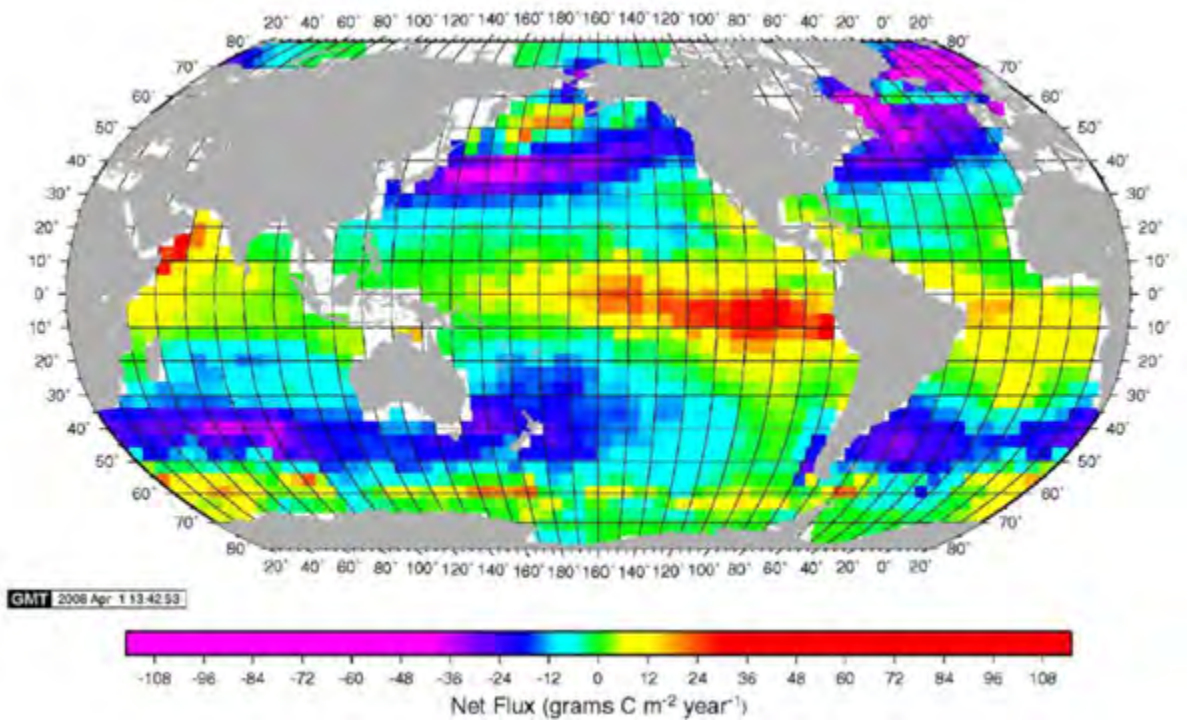

Figure 2.4 Climatological mean annual air-sea CO_2 fluxes in $gCm^{-2}yr^{-1}$ for the reference year 2000. This figure is based on 3.0 million surface water pCO_2 measurements obtained since 1970 (taken Takahashi et al., 2009).

From figure 2.4, note that the Southern Ocean is one of the major CO_2 sink regions in the global ocean, mainly at the Sub-Antarctic Zone (between 40^oS – 60^oS). Sabine et al., 2004, proposed that about 60% of the CO_2 in the global ocean is stored in the Southern hemisphere and more than 40% of it is found between 14^oS – 50^oS, in the SAZ. The next section further explores the Southern Ocean as a major CO_2 sink and reasons why this is the case.

2.3 Southern Ocean

2.3.1 Circulation, transport and mixing of SO water masses

The SO forms a major part of the global ocean circulation (Pardo et al., 2012), see figure 2.5. Rintoul et al., 2001 describes the SO as a cross road of the global ocean circulation. Water masses of the SO are divided by several frontal positions, separating different water masses in accordance with their origin, chemical and physical properties (Orsi et al., 1995). Moving from the south, the SO fronts are as follows; southern ACC boundary front, Polar Front (PF), Sub-Antarctic Front (SAF) and the Subtropical Front (STF), (Graham, 2013). The Antarctic Circumpolar Current (ACC) forms a major feature of the SO, flowing eastwards around the SO and driven by the westerly winds (shown by the hatched area in figure 2.5. The ACC is the largest current of the world oceans and it dominates the dynamics of the SO. It connects the Pacific, Atlantic and Indian Ocean basins of the SO as shown in figure 2.5, Rintoul et al., 2012.

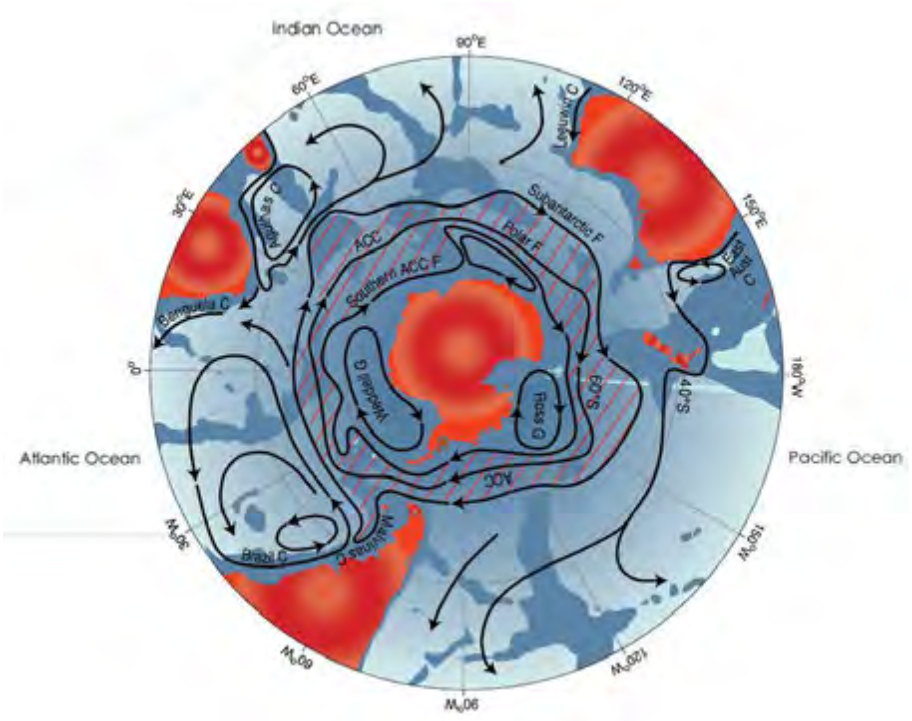

Figure 2.5 The Southern Ocean, the hatched area showing the ACC body flow, black lines show the varies currents and frontal positions of the Southern Ocean. (taken from http://takvera.blogspot.com/2011/12/ocean-acidification-warning-to-climate.html)

Westerly winds play a key role in the air-sea CO_2 flux of the SO. They cause a deflection of surface waters (Ekman transport) just south of the PF and exposing subsurface water, leading to a wind driven upwelling (Gruber and Sarmiento, 2006). This wind driven upwelling brings deep ocean CO_2 saturated waters to the surface, known as Circumpolar Deep Water (CDW), see figure 2.6. Because this newly upwelled water is rich in CO_2 and nutrients, it shifts the air-sea pCO_2 gradient to the atmosphere resulting in CO_2 outgassing, see figure 2.6. Some portion of the newly upwelled CDW is immediately subducted into the deep ocean south of the PF, forming Antarctic Bottom Water (AABW). The other portion moves northwards in the sub-surface Ekman layer and eventually forms two water masses i.e. the Antarctic Intermediate and Water (AAIW) and the Sub-Antarctic Mode Water (SAMW), (Marinow et al 2006).

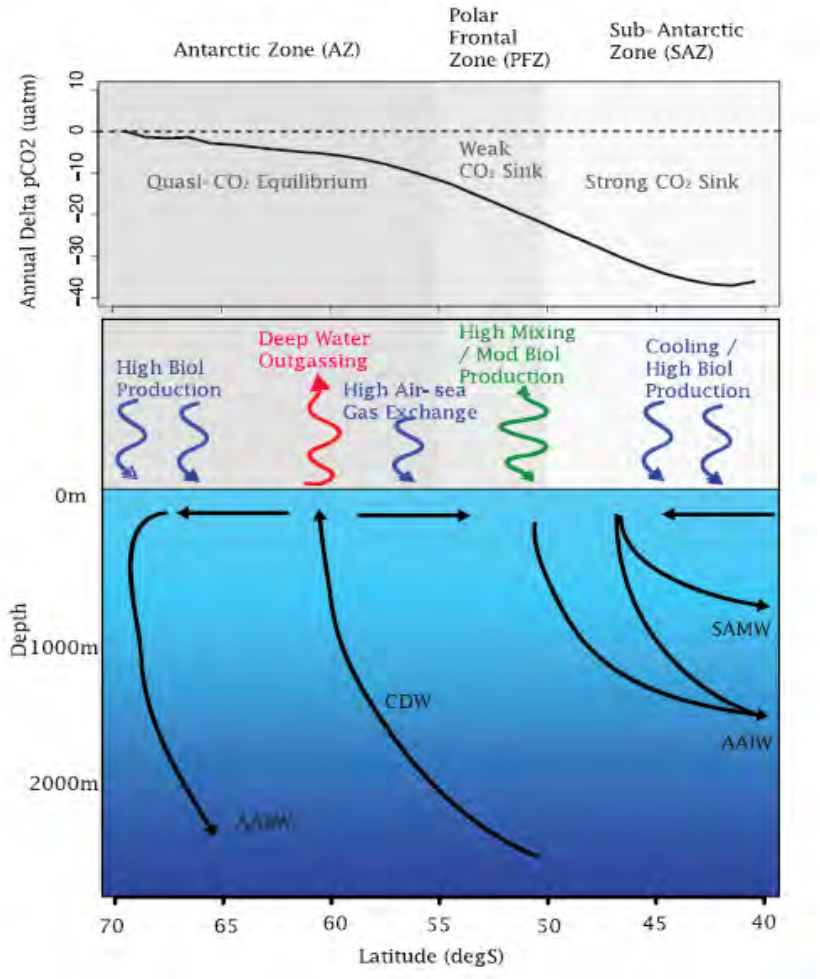

Figure 2.6 Southern Ocean water masses circulation and the corresponding air-sea CO_2 flux in response to deep ocean circulation.

The SAMW has a non-varying temperature and salinity and as result it typically has a deep mixed layer depth (MLD). This characteristic allows SAMW to play a central role in ventilating the SO (Speer et a., 1995, McCartney 1982). SAMW is therefore the main conduit of nutrients from the SO to the

upwelling regions of the equatorial Pacific. SAMW also plays a key role in the primary production occurring around 40°S, where the AAIW meets with subtropical waters, (Sallèè et al., 2006). The distribution and composition of these water masses are affected by the seasonal cycle. For example some large expanses of surface waters south of the ACC fall in to the AAIW in summer and become part of the CDW in winter (ludicone et al., 2008). The SAMW forms in winter, when vertical mixing is enhanced (Sokolov et al., 2008). The connection of deep waters with surface waters in the SO plays an central role in modulating global climate systems by transporting and storing heat, fresh water, nutrients and anthropogenic CO_2 (Lovenduski and Gruber, 2005)

MLD seasonal variability is crucial in the SO water masses formation and distribution. During winter, when surface waters are cooler and the buoyancy flux is weak, MLD deepens, strengthening vertical mixing and the entrainment of deep waters, (Dong et al., 2008). The MLD retreats towards summer, when surface waters become warmer. Thereafter the presence of nutrients, sunlight and stratification promotes primary production, taking up CO_2, (Solokov et al., 2008; Thomalla et al., 2011). Winter deepening of the MLD is not uniform in the SO. In some zones, e.g. south of Australia, the MLD is 600-700m in winter while only 100m in some other sub-regions such as the central Atlantic Ocean, (Dong et al., 2008). In summer however the MLD shallows throughout the SO as SST increases, reaching a maximum depth of only about 60m (Rintoul and England, 2002).

Globally, the SO provides the single most important region for CO_2 uptake (Gruber et al., 2009). One of the other key features of the SO, separating its dynamics from other parts of the ocean, is the superimposition of natural and anthropogenic fluxes. The SO is a strong source of natural CO_2 and an anthropogenic CO_2 sink at the same time (Gruber et al., 2009). The natural CO_2 source has existed since pre-industrial times and anthropogenic uptake has increased since the industrial revolution. Evolution of the SO as a major sink for CO_2 is a matter of some debate. Some studies propose a decreasing sink and others an increasing CO_2 sink (e.g. Le Quere et al., 2007, 2009; Zickfeld et al., 2008; Lovenduski et al 2007; Fung et al., 2005; Sarmiento et al., 1998; Gruber et al 2009).

The seasonal cycle is the dominant mode of variability in the SO (Thomalla et al., 2011), thus air-sea CO_2 flux variability is inevitably affected by seasonal variability in the SO. The next section describes the air-sea CO_2 flux seasonal cycle and puts it into perspective as the focus of this study.

2.3.2 Air-sea CO_2 flux seasonal cycle

The study of air-sea gas exchange has been of intensive scientific interest for more than half a century typically because of its significance in the biogeochemical cycling of climate and health related gases, (Wanninkhof et al., 2009). Of particular importance are changes in the oceanic

absorption of CO_2, which contribute to the mitigation of the greenhouse effect, (Le Quèrè et al., 2009; IPCC 2007; Takahashi et al., 2012). Variables driving the air-sea gas exchange have been studied over time and are well understood, (e.g. Weiss, 1974; Ho et al., 1997, 2004, 2006; Wanninkhof et al., 1992, 2009,2013; Nightingale et al., 2000). However the intra –annual interplay of these variables driving the seasonal cycle of air-sea CO_2 flux has only received attention in recent studies (e.g. Metzl et al., 2006, 2009; Rodgers et al., 2008; Lenton et al., 2012; 2013). One of the limitations on the study of air-sea CO_2 fluxes has been the lack of in situ data in most parts of the ocean with respect to CO_2, more especially in the Southern Ocean (Monteiro et al., 2010). Given the importance of the Southern Ocean (SO) as a key component of the climate system and the global carbon cycle, (Le Quèrè et al., 2007, 2010; Lovenduski et al., 2008; Takahashi et al., 2012), understanding of the seasonal cycle of air-sea CO_2 flux is significance, particularly for the quantification of long term evolution of CO_2 concentrations in the atmosphere.

The importance of the seasonal cycle in understanding long term oceanic CO_2 storage was well articulated by Rodgers et al 2008 in the North Atlantic. In this study they established that understanding long term CO_2 storage rests on resolving the air-sea CO_2 flux seasonal cycle because of its ability to provide knowledge of the annual timescale of oceanic CO_2 uptake. Thus, evolution of the magnitudes and drivers of the CO_2 sink, as result of climate change, can be tracked by studying the evolution of the air-sea CO_2 flux seasonal cycle. To this extent several studies have recently researched the air-sea CO_2 flux seasonal cycle in the SO (e.g. Metzl et al., 2009; Takahashi et al., 2009; Lenton et a., 2013, Anav et al., 2013).

In previous studies of air-sea CO_2 flux in the SO it was established that the major part of the Permanent Open Ocean Zone (POOZ) acts as a CO_2 source in winter influenced by vertical mixing, whereby the entrained CO_2 drive the air-sea pCO_2 gradient to the atmosphere as mentioned above (e.g. Metzl et al., 2006, 2009; McNeil et al., 2007; Takahashi et al., 2009). In summer this region is dominated by CO_2 in-gassing driven by biological activity, given favorable conditions as stated above, (Metzl et al., 2006; Rysgaard et al., 2011). The seasonal cycle of air-sea CO_2 flux in the Seasonal Ice Zone (SIZ; south of 58^{o}S) was found to be mainly influenced by the seasonal formation and depletion of sea ice (Cox and Weeks., 1983). In autumn, as SST begins decreasing, sea ice forms a porous crystal matrix filled with brine which is high in DIC, CO_2 and other gases from the rejected dissolved salts (Guild et al., 2002). The super-saturation of CO_2 in the brine solution causes a strong air-sea pCO_2 gradient leading to a CO_2 outgassing through the ice pores (Nomura et al., 2006). Some portion of the brine solution is sub-ducted to the deep ocean due to its high density (Shcherbine et al., 2003; Rusgaard et al., 2011). With the onset of winter, ice pores close due to contraction, capping the air-

sea CO_2 flux completely for about a month and half (Rysgaard et al., 2007). The air-sea CO_2 flux resumes again during spring-summer, as the permeability of the ice become restored (Cox and Weeks., 1983). As summer progresses, sea ice melting accelerates dilution of the brine solution, weakening the air-sea pCO_2 gradient and primary production is activated, causing an air-sea CO_2 flux into the ocean. Primary production in the SIZ continues until the end of summer in February (Rysgaard et al., 1999, 2011). A conceptual model of this process is shown in figure 2.7.

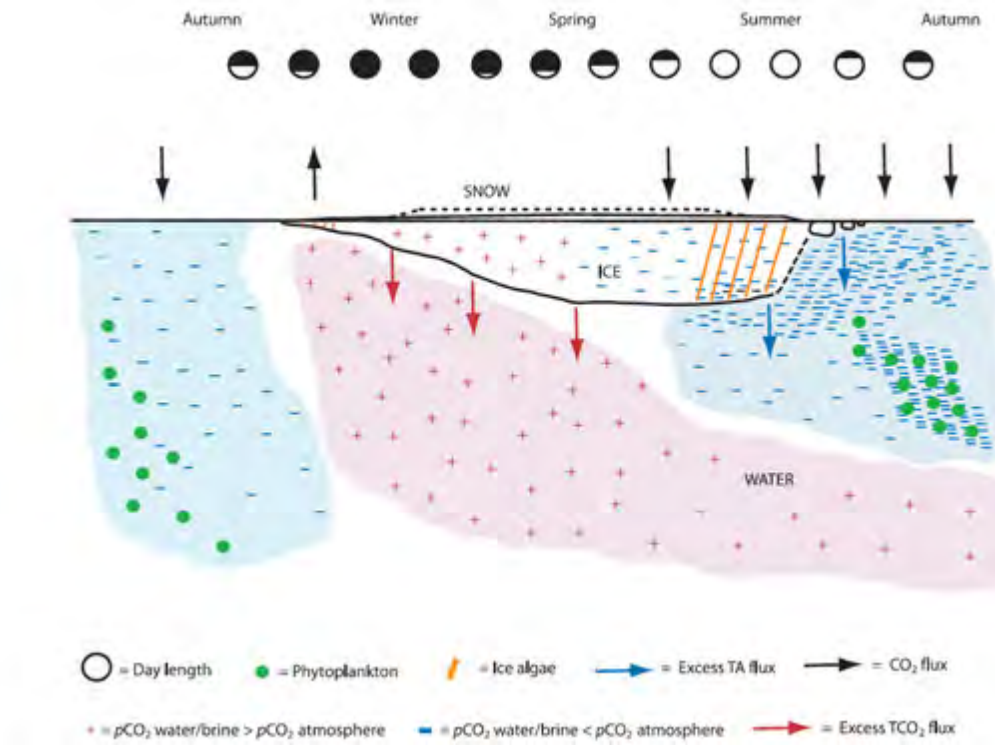

Figure 2.7 The conceptual model of the seasonal cycle of air-sea CO_2 flux at the SIZ, covering the upper 100m. TCO_2 stands for DIC according to terminology of the text (taken from Rysgaard et al., 2011)

In the past, several studies have applied different methods to estimate the air-sea CO_2 fluxes in the SO, including surface ocean partial pressure of CO_2 (pCO_2) from observations with empirical gas exchange parameterization, prognostic ocean biogeochemical models, atmospheric inversion models and ocean inversion models (e.g. Gruber et al., 2009; Mikaloff Fletcher et al., 2007; Metzl et al., 2006, 2009; Takahashi et al., 1993, 2002, 2009, 2012; Lenton et al., 2006, 2013). These studies have shown that the air-sea CO_2 flux is not uniform in the SO, reporting high spatial and temporal variability. However given the limited number of CO_2 observations in the SO with respect to carbon (Monteiro et al., 2010), the full characterization of the SO air-sea CO_2 flux seasonal cycle still remains a challenge, especially south of the polar front. Most of the ocean models still struggle to resolve the observed seasonal cycle of air-sea CO_2 flux and CO_2 annual fluxes south of the polar front. Some models are notable for their ability to resolve the seasonal signal at most sub-regions of the SO, (e.g

Lenton et al., 2013). The spatial and temporal paucity of observations in the SO presents a challenge because processes occurring in one season can be compensated for in another season (Lenton et al., 2012). The recent instigation of winter sampling capabilities in the SO i.e. ice breaker vessels, ocean wave gliders and sea gliders, is anticipated to increase the SO measurements data coverage which will ultimately help improve understanding of the air-sea CO_2 flux dynamics in these sub-regions.

Some studies previously investigated the air-sea CO_2 seasonal cycle on a regional scale in the SO (e.g. Metzl et al., 2006, 2009), however given the strong spatial and temporal variability of the air-sea CO_2 flux, findings from these studies cannot be extrapolated to the whole SO (Metzl et al., 2006; Lenton et al., 2012). Furthermore, previous studies have proposed that basins' contribution to the zonal mean annual air-sea CO_2 fluxes may not be uniform (e.g. Lenton et al., 2012). Most previous studies investigating the air-sea CO_2 flux seasonal cycle at the SO have used geographically defined boundaries to divide sub-domains of the SO. A recent study by Sèfèrian et al., 2012 has however shown that the use of geographic boundaries may be problematic given their inability to depict distinct regions of the air-sea CO_2 fluxes. The use of geographical boundaries have a potential to mix CO_2 outgassing and in-gassing zones which might inhibit the elucidation of regional variability of air-sea CO_2 fluxes and could result in a distorted seasonal cycle.

One of the most recent works on air-sea CO_2 flux characterization of the SO was published by Lenton et al., 2013, done as part of the global carbon project under the Region Carbon Cycle Assessment and Processes project (RECCAP; Canadell et al., 2011). Lenton et al., 2013 used five biogeochemical models (CCSM_BEC, CCSM_ETH, CSIRO, NEMO-Plankton 5 and NEMO-PISCES (2^o x 2^o cos Ø)), atmospheric inversion models, ocean inversion models, and observations from Takahashi et al., 2009, see figure 2.8. In this study, Lenton et al., 2013 used the Atmospheric Tracer Transport Model Inter-comparison Project (TRANSCOM) boundaries to define sub-domains of the SO which are specifically set to geographically defined boundaries consistent with the RECCAP protocol. The use of geographic boundaries was found to be problematic in Lenton et al., 2013. For example defining the SO as south of 44^oS excluded a major part of the SAZ (major CO_2 sink zone) and when the boundary was changed to 40^oS, the annual CO_2 flux almost doubled.

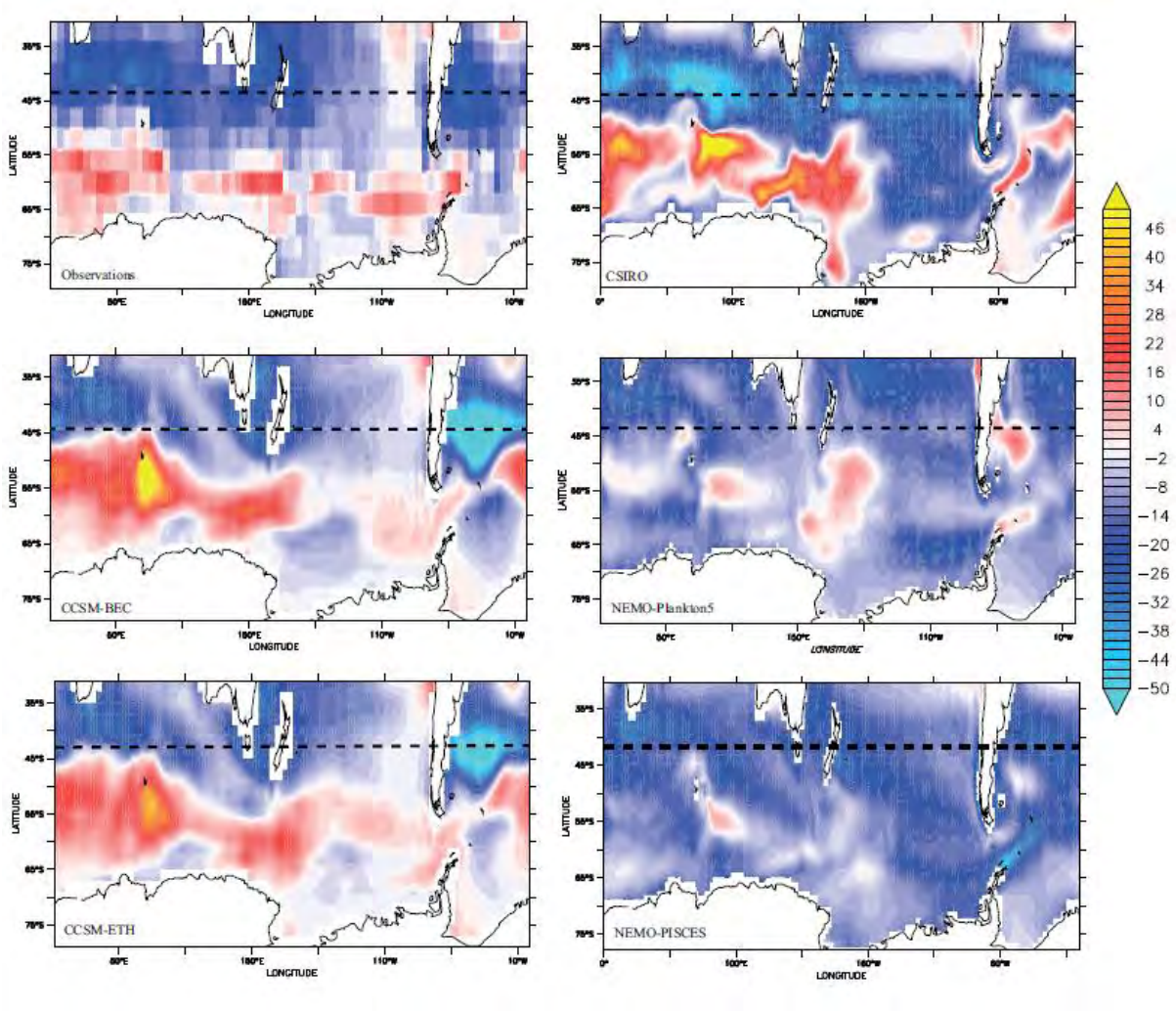

Figure 2.8 Spatial maps of the annual mean air-sea CO_2 flux of the five ocean biogeochemical models applied in Lenton et al., 2013 and the T09 observations (top left figure) in $gCm^{-2}yr^{-1}$. The dotted line marks RECCAP boundary 44°S. Negative reflect fluxes into the ocean

The findings of Lenton et al., 2013 showed that some biogeochemical models better simulated the air-sea CO_2 flux seasonal cycle in the Sub-Antarctic zone (44°S – 58°S) with respect to the Takahashi et al., 2009(T09) observations, but none was able to reproduce the air-sea CO_2 flux seasonal cycle south of 58°S. The biogeochemistry models, NEMO-Plankton 5 and NEMO-PIESES, were found to overestimate annual fluxes relative to the observations and the other three models, showing a general CO_2 in-gassing bias, see figure 2.8. Interestingly, Lenton et al., 2013 found that though ocean biogeochemical models agree on the annual air-sea CO_2 fluxes, none of the models could reproduce both the phase and amplitudes of the T09 observations air-sea CO_2 flux seasonal cycle in the selected sub-regions. Given that the seasonal cycle is the dominant mode of variability in the SO (Thomalla et al., 2011), poor simulation of air-sea CO_2 flux seasonal cycle is concerning, particularly when making future projections, (Lenton et al., 2013).

This study is an extension of the work of Lenton et al., 2013 using the NEMO PISCES biogeochemical model at two different spatial resolutions, investigating *inter alia;*

a) Whether the air-sea CO_2 fluxes temporal variability of the seasonal cycle can be improved by using a higher resolution. This is investigated by comparing the ORCA2-LIM-PISCES (2^o x 2^o cos Ø) and PERIANT05 (NEMO-PISCES) (0.5^o x 0.5^o cos Ø) model configurations relative to decadal mean observations for the year 2000 (Takahashi et al., 2009).
b) The sensitivity of the air-sea CO_2 flux seasonal cycle to zonal boundary definition. This is investigated by comparing the seasonal cycle of air-sea CO_2 flux and annual fluxes using the Lenton 2013 RECCAP boundaries (44^oS – 58^oS and south of 58^oS) , a different set of geographic boundaries closer to the STZ and PF boundaries (40^oS – 50^oS and south of 50^oS) and dynamic boundaries (Sub-Antarctic zone (SAZ) and Antarctic zone (AZ) defined using mean frontal positions)
c) The contribution made by SO basins (Pacific, Atlantic and Indian Ocean) to the zonal mean air-sea flux CO_2 seasonal cycle and CO_2 annual fluxes.

3. Methods

3.1 Datasets

The datasets used for this study include observations from:

- Takahashi et al., 2009, surface CO_2 observations (http://www.ldeo.columbia.edu/res/pi/CO2/carbondioxide/pages/air_sea_flux_2000.html),
- Mixed layer Depth (MLD) data from the Ifremer institute website (http://www.ifremer.fr/cerweb/deboyer/mld/home.php)
- Model output from the Nucleus for European Modelling of the Ocean (NEMO) and the Pelagic Interaction Scheme for Carbon and Ecosystem studies (PISCES) biogeochemistry model, (Aumont and Bopp, 2006).

3.1.1 Observations

The Takahashi et al., 2009 (T09) observations dataset is comprised of a compilation of about 3 million surface measurements of oceanic partial pressure of CO_2 (pCO_2) globally, obtained from 1970 – 2007. The T09 climatological mean distribution of surface pCO_2 observations has a spatial resolution of 4^o (latitude) x 5^o (longitude). The data was corrected for reference year 2000, with the mean –rate of CO_2 for the different years calculated from the time-trend analysis. This was done by using the deseasonalized surface water CO_2 data in portions of the North Atlantic, North Pacific, south Pacific and the Southern Ocean (Bates, 2001). The net air-sea CO_2 flux (F_{CO_2}) in T09 observations were estimated using the equation 3.1, where U_{10} is the wind speed 10m above sea surface, taken from the 1975- 2005 NCEP-DOE AMIP-II Reanalysis (R-2) wind speed data.

$$F_{CO_2} = 0.251 \times (U_{10})^2 \times (Sc/660)^{-0.5} \times K_0 \times (pCO_{2W} - pCO_{2a}) = k \times K_0 \times \Delta pCO_2 \quad (3.1)$$

$$InK_0 = -60.24 + 93.45\left(\frac{100}{T}\right) + 23.36In\left(\frac{T}{100}\right) + S\left(0.026 - 0.024\left(\frac{T}{100}\right) + 0.0047\left(\frac{T}{100}\right)^2\right) \quad (3.2)$$

$$Sc = 2073.1 - 125.62 \times SST + 3.6276 \times SST^2 - 0.043219 \times SST^3 \quad (3.3)$$

$$k = 0.251 \times (Sc/660) < U_{10}^2 > \quad (3.4)$$

Where k is the CO_2 gas transfer velocity coefficient, which is a function of wind speed (U_{10}) and the Schmidt number [kinematic viscosity of water) / diffusion coefficient of CO_2 in sea water], (Sc/660),

K_0, is the CO_2 solubility coefficient and is a function of temperature and salinity (Weiss, 1974), and ΔpCO_2 is the air-sea CO_2 partial pressure gradient. The air-sea pCO_2 gradient provides the thermodynamic driving potential of the CO_2 flux and k, the kinetic forcing as a function of CO_2 solubility in sea water. The net air-sea CO_2 flux into the ocean is expressed as a negative value by convention (Wanninkhof et al., 2013). The quadratic parameterization of the transfer velocity (*k;* equation 3.4) and coefficient of 0.251 was chosen in accordance with Wanninkhof et al., 2009, where it was established to be optimum for global scale analysis.

The T09 observations composed of a total of 1759 $4^{o}x5^{o}$ grid boxes globally, 30% of the boxes have measurements spanning 6 or more months and 50% have 3 or less months. Most boxes in the northern hemisphere have 6 or more months of observations, while south of $20^{o}S$ most boxes have only 3 or less measurements, most of which are in summer (Takahashi et al., 2009). This is partly due to the historical lack of capabilities for winter sampling in the Southern Ocean (SO) as result of the presence of ice in the Seasonal Ice Zone (Metzl et al., 2006), for example some regions of the eastern Pacific Ocean are yet to be sampled (Lenton et al., 2013). The lack of surface pCO_2 observations in the SO is well known, (Monteiro et al., 2010). The lack of observations in the SO introduces a limitation in the analysis of the air-sea CO_2 fluxes in some of its regions, more especially because the SO has high spatial and temporal air-sea CO_2 fluxes variability (Metzl et al., 2006). To account for the paucity of surface measurements, the T09 data were corrected for the reference year 2000 as indicated above.

For the observations MLD data, the 2008 updated version of the climatological de Boyer Montégut et al., 2004 MLD dataset was used. The data was extracted in the form of a 2^{o} x 2^{o} climatological mean over 1941 – 2008 and the methodology used to construct the dataset is presented in de Boyer Montègut et al., 2004. In the following analysis, the influence of the ΔpCO_2, CO_2 solubility coefficient (K_0), SST, MLD and transfer velocity coefficient (*k*) in driving air-sea CO_2 flux seasonal cycle is investigated in the T09 observations and therefore compared with NEMO PISCES model output.

3.1.2 NEMO PISCES

The ocean biogeochemistry model NEMO PISCES (Aumont and Bopp, 2006) was run on two configurations i.e. ORCA2-LIM-PISCES configuration (Madec, 2008) with a 2^{o} x 2^{o} cos(Ø) horizontal resolution, 31 vertical levels, and PERIANT05 configuration (Amount, 2012) with 0.5^{o} x 0.5^{o} cos(Ø) horizontal resolution and 46 vertical levels. The model output was extracted in a netcfd format and processed using MATLAB software. Details of the model run information, including spin up time, surface boundary conditions, lateral boundary conditions, bottom boundary conditions, run duration

and initial conditions are summarized in appendix B for each configuration. In ORCA2 ΔpCO_2, SST, wind speed (U_{10}) 10m above sea level and MLD were extracted from the model output, InK_0 was calculated using (3.2) and the transfer velocity coefficient (*k*) was estimated using 3.4 (Wanninkhof et al., 2013). The Schmidt (Sc) number was calculated using 3.2 (Wanninkhof et al., 1992). For PERIANT05, similar parameters were extracted from the model output except for the wind speed (U_{10}), where instead, wind stress was provides by the model output and converted to wind speed using 3.5 (Karal et al., 2007).

$$\tau = \rho_{air} \times C_D \times U_{10}^2 \qquad (3.5)$$

Where τ is the shear stress, ρ_{air} is the air density and C_D is the wind-drag coefficient .The global wind –drag coefficient ($C_D = 1.23 \times 10^3$) was used for this study, also representative of most of the SO and has less spatial variability (Karal et al., 2007). From the model output, the interplay of major variables in driving the air-sea CO_2 flux seasonal cycle was investigated, specifically looking at ΔpCO_2, CO_2 solubility coefficient (K_0), SST, MLD and the gas transfer velocity coefficient (*k*).

In the subsequent analysis, the air-sea CO_2 flux seasonal cycle is investigated at three different boundaries of the SO (shown in section 3.2) using T09 observations for year 2000 and then compared with Lenton et al., 2013 results at the RECCAP boundaries. Lenton et al., 2013 was published as a spatial assessment of the SO carbon variability during 1990 -2009. This was done under the global carbon project as part of the Regional Carbon Cycle Assessment and Processes project (RECCAP; Canadell et al., 2011). In Lenton et al., 2013 the Atmospheric Tracer Transport Model Inter-comparison Project (TRANSCOM) boundaries was used to define sub-domains of the SO. These are a specific set of geographical boundaries consistent with the RECCAP protocol. This study present an extension of Lenton et al., 2013, investigating the air-sea CO_2 flux seasonal cycle at the Lenton 2013 RECCAP boundaries, geographic and dynamic boundaries (section 3.2) and the seasonal interplay of major variables driving of the air-sea CO_2 flux.

3.2 Calculations and assessment of the air-sea CO_2 fluxes

The air –sea CO_2 flux seasonal cycle in T09 was calculated from monthly mean observations and annual CO_2 fluxes were summations of the monthly fluxes for the different sub-regions. The ORCA2 air-sea CO_2 flux dataset was converted into a 5 day average format to standardize with the PERIANT05 model output, which was given in 5 day averages before computing the seasonal cycle and the standard deviation. The period of study (1993 – 2006) was selected because it represented a common period in two model outputs. Annual CO_2 fluxes were computed from the mean decadal annual flux for period 1993 – 2002 and the calculated standard deviation represents the decadal

interannual variability. The comparison analysis in the results focuses on the phase, magnitude and drivers of the air-sea CO_2 flux in the model output and T09 observations. The seasonal cycle phasing of the model outputs was assessed by means of a correlation coefficient (r^2) relative to the T09 observations in all sub-regions expect for the SO basins. This was due to the coarse resolution of the data (4^o latitude x 5^o longitude) and hence sparse spatial basin coverage. Drivers of the air-sea CO_2 flux seasonal cycle were investigated by assessing the seasonal variability of ΔpCO_2, MLD, SST, K_0 and *k* (equation 3.4 & 5). MLD was included to account for the effect of winter entrainment. For comparison purposes the air-sea CO_2 flux into the ocean is expressed as a negative value by convention. This is consistent with the RECCAP protocol (Canadell et al., 2011).

3.3 Study region

The Southern Ocean sub-domains were defined using three boundaries *viz.*

I. Lenton 2013 RECCAP boundaries (44^oS – 58^oS, south of 58^oS), following the RECCAP protocol. Lenton 2013 boundaries are shown by the red lines in figure 3.1a.
II. Geographical boundaries (40^oS – 50^oS and south of 50^oS), shown by the black dotted lines in figure 3.1a.
III. Dynamic boundaries, where the Sub-Antarctic Zone (SAZ) is defined by the region between the Subtropical Front (STF) and the Polar Front (PF), shown by the green area in figure 3.1a. Frontal positions here were estimated using SST criteria (Rintoul and Trull 2001), the defined SAZ was compared with the frontal positions from Orsi et al., 1995 and found to give a good approximation. The Antarctic Zone (AZ) was defined as the blue area south of the SAZ.

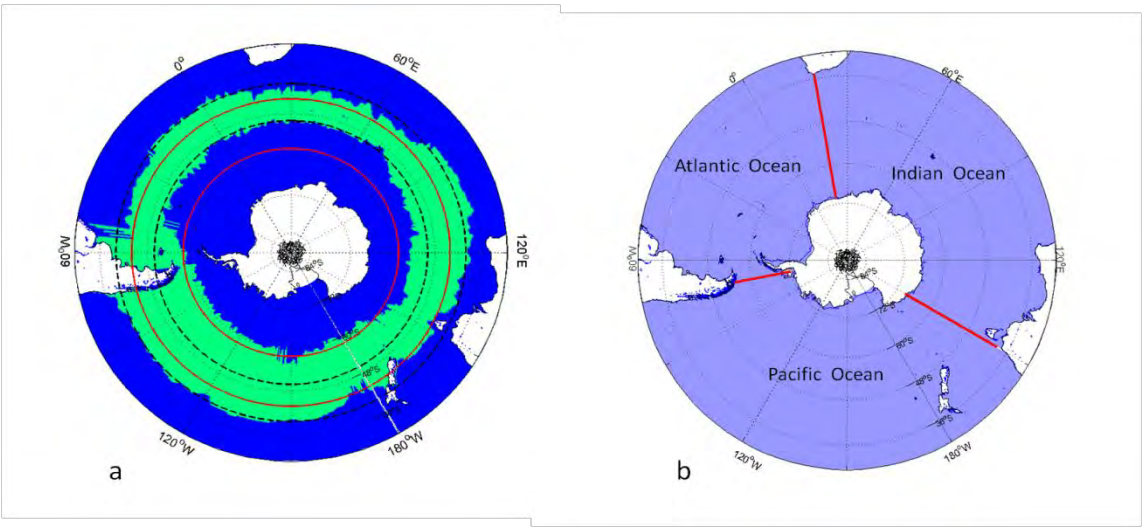

Figure 3.1 The right figure (a) shows the sub-domains of the Southern Ocean used in this study. The red lines show the Lenton 2013 RECCAP boundaries (44^{o}S – 58^{o}S and south of 58^{o}S), the black dotted lines show the geographic boundaries (40^{o}S – 50^{o}S and south of 50^{o}S south), the green zone shows the Sub-Antarctic Zone (SAZ), the northern boundary is defined as the climatological subtropical front and southern boundary by the Polar front, (fronts were defined using the SST criteria (Rintoul and Trull 2001)) and the Antarctic zone (AZ) is blue area south of the SAZ. The left figure (b) shows the Southern Ocean basins as defined in this study.

4. Results

The results section is divided into five subsections.

(i) Climatology of long term (1993- 2006) air – sea CO_2 flux for the ORCA2 and PERIANT05 configuration,

(ii) The seasonal cycle of air-sea CO_2 flux at 44^oS – 58^oS and 58^oS south. The objective here is to make a comparison of the findings of this study with Lenton et al., 2013 and the Takahashi et al., 2009 (T09) observations in the same latitudinal zones. Zonal boundaries 44^oS – 58^oS and 58^oS south where used in Lenton et al., 2013 to define the SO sub-domains. This study refers to these zones as the Lenton 2013 RECCAP boundaries for comparison purposes.

(iii) Seasonal cycle: boundary sensitivity analysis, presenting an air-sea CO_2 flux seasonal cycle comparison of the geographic boundaries (50^oS – 40^oS and 50^oS south) , Lenton 2013 RECCAP boundaries and dynamic boundaries (Sub-Antarctic (SAZ) and Antarctic zone (AZ) defined by frontal positions),

(iv) Seasonal cycle: basin sensitivity analysis, assessing the SO basins contribution to the zonal mean air-sea CO_2 flux seasonal cycle and annual fluxes in ORCA2 and PERIANT05.

(v) Wind speed climatology comparison of ORCA2 and PERIANT05.

In each sub-region a comparison analysis considers the phase, magnitude and drives of the air-sea CO_2 flux seasonal cycle.

4.1 Air-sea CO_2 flux long term Climatology

Here the climatologies for the period 1993 – 2006 for ORCA2 and PERIANT05 model outputs have been contrasted and compared with the T09 observations for the year 2000.

The ORCA2 air-sea CO_2 fluxes climatological mean over 1993 – 2006 shows a range of -8 to -15 $gCm^{-2}yr^{-1}$ for the majority of Southern Ocean (SO), see figure 4.1. In certain zones however the CO_2 flux is stronger. Examples are: south of Africa near the Agulhas retroflection, southeastern Atlantic Ocean, eastern coast of Australia and along the western boundary currents (reaching up to -40 $gCm^{-2}yr^{-1}$),see figure 4.1. It also shows the following CO_2 outgassing hotspots at specific sub-regions; central south Indian Ocean basin, west of the Kerguelen Plateau; south of the Agulhas retroflection; western Indian Ocean and the southeastern Pacific Ocean. Note that this sub-regions coincide with zones of deeper winter MLD and high Eddy Kinetic Energy (EKE) in the SO, (Rintoul and England, 2001; Sallèè et al., 2006). It is anticipated that high EKE might be a key driver of the positive CO_2 fluxes observed in these sub-regions in ORCA2. This possibility is considered though at 2^o x 2^o

resolution eddies are resolved however because ORCA2 is highly eddy parameterized (Madec, 2008), vertical diffusion might be driving bottom DIC into the surface waters at high EKE regions. ORCA2 air-sea CO_2 fluxes spatial variability features are generally different from T09 observations south of 48^{o}S, however shows similar features north of 48^{o}S i.e. the northern western part of the Atlantic Ocean, Indian Ocean and most part of Pacific Ocean.

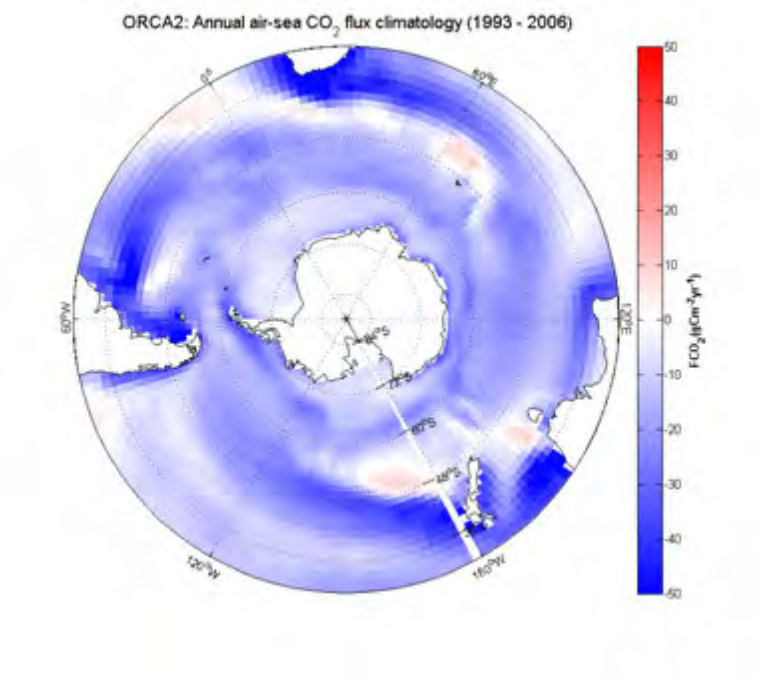

Figure 4.1 ORCA2 air-sea CO_2 flux climatology in $gCm^{-2}yr^{-1}$. Negative reflects influx into the ocean. ORCA2 shows a negative bias of the CO_2 flux, it has an average CO_2 flux of -10 $gCm^{-2}yr^{-1}$ for most part of the SO, only a few zones show positive flux hotspots. Most features of ORCA2 depicted in this figure are not present in the T09 observations CO_2 flux spatial map in figure 4.3

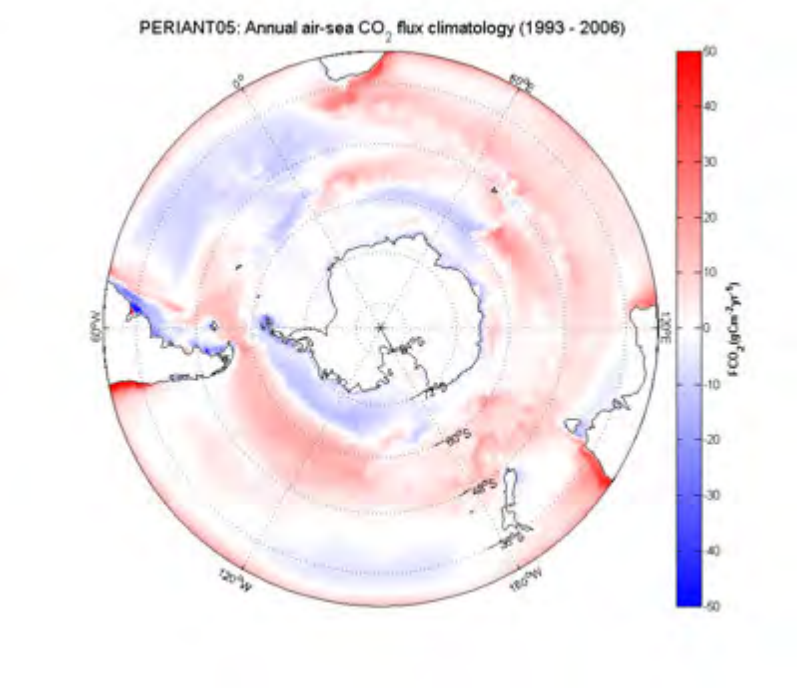

Figure 4.2 PERIANT05 air-sea CO_2 flux climatology in $gCm^{-2}yr^{-1}$. Negative reflects influx into the ocean. PERIANT05 generally shows a CO_2 outgassing bias. Most of features of PERIANT05 in Atlantic Ocean coincide with the CO2 flux of the T09 observation at figure 4.3. PERIANT05 shows a general good agreement with T09 observations south of 48°S.

PERIANT05 air-sea CO_2 fluxes spatial map (figure 4.2) is different from that of ORCA2, figure 4.1. The most explicit difference in the two climatological data sets is the enhanced spatial contrasts of the in-gassing /outgassing features of PERIANT05 compared to ORCA2. PERIANT05 generally depicts strong CO_2 outgassing features in most of parts of the SO, showing a uniform outgassing of about 10 – 25 $gCm^{-2}yr^{-1}$ in the majority of the Indian Ocean and the region between 48°S – 60°S in the Pacific Ocean. The region south of 58°S PERIANT05 is dominated by uniform CO_2 in-gassing features which are also observed in the T09 observations in figure 4.3. PERIANT05 and ORCA2 shows similar CO_2 in-gassing features in the eastern coast of South America and the central Atlantic Ocean, ORCA2 however shows a stronger CO_2 in-gassing reaching up to -45 $gCm^{-2}yr^{-1}$ compared to only -20 $gCm^{-2}yr^{-1}$ in PERIANT05 (see figure 4.1 and 4.2).

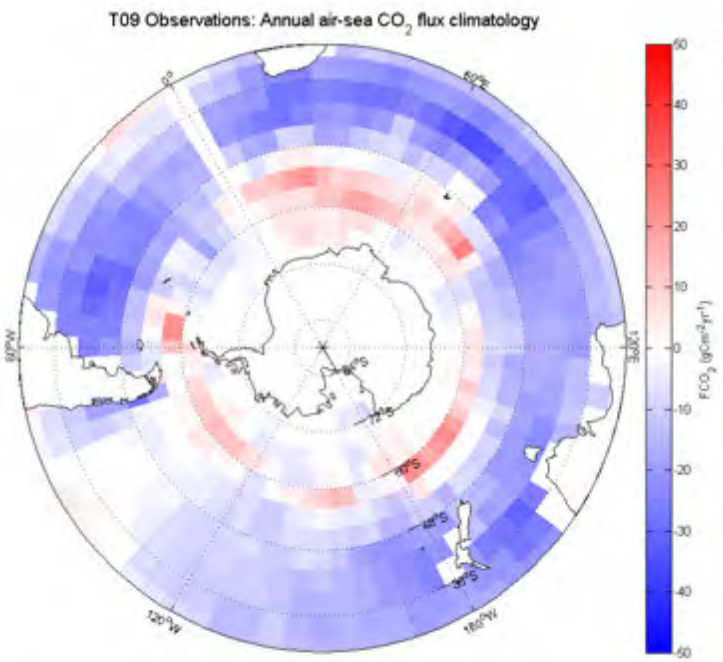

Figure 4.3 Climatological observations of mean annual CO_2 air-sea flux for 2000, based on 3 million surface measurements since 1970**.** Note that the colour bar comparable to the CO_2 fluxes of ORCA2 and PERIANT05 model output in figure 4.1 and 4.2 is marked by the dotted box (reconstructed from the Takahashi et al., 2009 dataset).

The climatological air-sea CO_2 flux of PERIANT05 is comparable to T09 observations in most parts of the Atlantic Ocean. The Atlantic Ocean basin in the SO is known to be dominated by seasonal and intra-seasonal primary production (e.g. Thomalla et al., 2011), hence the presence of the CO_2 in-gassing features present in PERIANT05 and T09 observations is attributed to biological CO_2 drawdown. In contrast to ORCA2, PERIANT05 model output shows a good agreement with T09 climatological air-sea CO_2 fluxes south of 48^{o}S but shows poor comparison north of 48^{o}S. In some regions PERIANT05 air-sea CO_2 flux shows a sharp contrast to T09 observations. For example, the Indian Ocean is dominated by strong CO_2 outgassing but yet T09 observation shows the opposite. The good comparison of PERIANT05 model output with observations south of 58^{o}S present an uncommon feature in Ocean modelling, this because Ocean models are known to better resolve observations air-sea CO_2 fluxes at the Sub-Antarctic zone and but poorly does so south of 58^{o}S (e.g. Gruber et al., 2009; Lenton et al., 2013).

Annual CO_2 fluxes in figure 4.4 shows that ORCA2 air-sea CO_2 flux climatological annual means overestimates the SO (here defined as south of 40^{o}S) annual uptake with relative to T09 observations, and PERIANT05 generally shows an outgassing bias. PERIANT05 has a climatological mean annual CO_2 flux of 0.24 PgCyr^{-1}, ORCA2's -1.0 gCyr^{-1} and T09 observations give a figure of -0.66 PgCyr^{-1}. Note that the total winter-summer air-sea CO_2 fluxes in both T09 observations and model

outputs contribute about two thirds of the total annual flux. Spring is responsible (not shown) for the other third as will be shown in the seasonal cycle phasing. The weakened CO_2 in-gassing observed during the winter season in the T09 observations has been reported previously (e.g. Metzl et al., 2006, 2009; Sokolov et al., 2008) and is attributed to the entrainment of enriched CO_2 waters below the mixed layer in winter weakening the net CO_2 influx. The enhanced CO_2 in-gassing in summer observed in the T09 observations have been previously reported to be associated with primary production (biological CO_2 uptake), (Metzl et al., 2006, 2009). The SO CO_2 climatological mean annual fluxes of ORCA2, PERIANT05 and T09 observations are summarized in Table 4.1 below.

PERIANT05 air-sea CO_2 flux seasonal cycle for the whole SO (south of 40°S) show a poor correlation with T09 observations ($r^2 = 0.14$) and ORCA2 shows a strongly negatively correlated ($r_2 = -0.60$), see table 4.2.

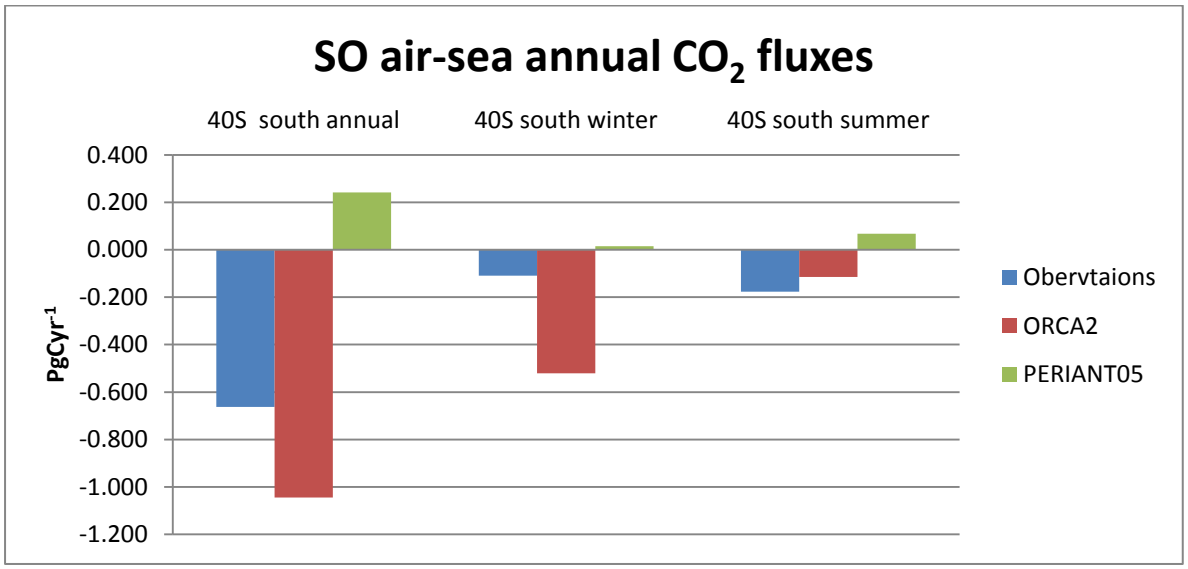

Figure 4.4 Decadal (1993- 2002) CO_2 fluxes for the total annual, winter and summer fluxes. ORCA2 generally overestimates the annul influx relative to observations while PERIANT05 underestimate the fluxes**.** Southern Ocean is here defined as south of 40°S.

Table 4.1 Climatological mean annual of air-sea CO_2 flux in the Southern Ocean (SO) of the period 1993 – 2002 for PERIANT05, ORCA2 and T09 observations for 2000 (Takahashi et al., 2012),in $PgCyr^{-1}$. SO here defined is as south of 40^oS

Region	T09 observations	ORCA2	PERIANT05
Annual flux	-0.66	-1.0±0.05	0.24±0.10
Winter mean flux	-0.11	-0.52±0.02	0.02±0.01
Summer mean flux	-0.18	-0.12±0.03	0.07±0.02

Table 4.2 Correlation coefficient (r^2) of the SO (south 40^oS) seasonal cycle of the air-sea CO_2 flux with T09 observations

Region	ORCA2	PERIANT05
SO(South of 40^oS)	-0.60	0.14

4.2 Characterization of the air-sea CO_2 flux seasonal cycle using the RECCAP boundaries

This section compares the seasonal cycle of the air-sea CO_2 flux in ORCA2, PERIANT05 and T09 observations at the Lenton 2013 RECCAP boundaries. The Regional Carbon Cycle Assessment and Project (RECCAP; Canadell et al., 2011) boundaries are chosen as they were used in Lenton et al., 2013 to defined sub-domains of the SO under the global carbon project for assessing the variability of the global carbon cycle over the period 1990 – 2009. This section compares findings of this study with T09 observations and Lenton et al., 2013 results at the sub-regions defined by these boundaries. The Lenton 2013 RECCAP boundaries are defined as 44^oS – 58^oS for the SAZ and south of 58^oS at the polar zone.

The seasonal cycle of air-sea CO_2 flux from the T09 observations dataset is shown in the figures 4.6a and 4.7b with ancillary variables driving the flux in equation 4.1, (Wanninkhof et al., 2009). Where *k* is the CO_2 gas transfer velocity coefficient, which is a function of the mean wind speed (U_{10}) 10m above sea level and the Schmidt number [kinematic viscosity of water)/ diffusion coefficient of CO_2 in sea water], (Sc/660), K_0 is the CO_2 solubility coefficient in seawater and is a function of temperature and salinity (Weiss, 1974) and ΔpCO_2 is the air-sea CO_2 partial pressure gradient. The air-sea pCO_2 gradient provides the thermodynamic driving potential controlling the CO_2 flux and *k*, the kinetic forcing as a function of CO_2 solubility in sea water (K_0(Sc/660)).

$$F_{CO_2} = K_0 \times k \times \Delta pCO_2 = K_0 \times 0.251(Sc/660)^{-0.5} \times U_{10}^2 \times \Delta pCO_2 \qquad (4.1)$$

The CO_2 sink in the zone 44°S – 58°S of T09 observations (figure 4.6) weakens at a constant slope from -0.045 $gCm^{-2}day^{-1}$ in January to -0.03 $gCm^{-2}day^{-1}$ end of March, maintain a constant flux of -0.03 $gCm^{-2}day^{-1}$ between Mar-Apr and then further weakens from May until ultimately outgases in September. The weakening of the CO_2 sink from January to March in the 44°S – 58°S zone is consistent with the decrease in CO_2 solubility (k_0) linked to the increase in SST, (see figure 4.6). Note that as the MLD deepens towards winter, it induces entrainment of the CO_2 saturated waters below the mixed layer, which weakens the net CO_2 influx (Figure 4.6a). From September when MLD shoals, CO_2 in-gassing increases almost consistently until reaches a maximum flux of -0.045 $gCm^{-2}day^{-1}$ in midsummer. This observation is consistent with expected increase in CO_2 uptake associated with primary production in summer (e.g. Solokov and Rintoul 2008; Metzl et al., 2006, 2009). Note that the seasonal cycle of the air-sea CO_2 flux follows similar phasing with ΔpCO_2 throughout the year. This observation strongly supports ΔpCO_2 (the thermodynamic forcing) as a major driver of the air-sea CO_2 flux in equation 4.1 and further suggests that primary production controls the summer CO_2 uptake and entrainment dominates the winter CO_2 outgassing (Metzl et al., 2006 and Lenton et al., 2006.

South of 58°S the seasonal cycle of air-sea CO_2 flux (T09 observations) has a slightly different phasing compared to 44°S – 58°S, figure 4.7. For example, during winter CO_2 outgassing is enhanced south of 58°S and last longer (six months, Jun-Dec) compared to only one month (Oct-Sept) at the zone 44°S – 58°S, cf. figures 4.6 & 4.7. Furthermore, the summer biological uptake of CO_2 continues until Feb compared to Dec in the zone 44°S – 58°S. The CO_2 uptake in summer south of 58°S is weaker (max CO_2 in-gassing -0.035 $gCm^{-2}day^{-1}$ compared to 44°S – 58°S (max CO_2 in-gassing -0.044 $gCm^{-2}yr^{-1}$, figures 4.6 & 4.7. The maximum MLD south of 58°S only reaches 60m which is relatively shallow compared to a mean 160m in zone 44°S – 58°S. In contrast to 44°S -58°S, the CO_2 flux in south of 58°S has a magnitude that strengthens from -0.01 $gCm^{-2}day^{-1}$ to -0.035 $gCm^{-2}day^{-1}$ between Jan – Feb as opposed to a seasonally weakening CO_2 flux trend. Note that despite the decrease in K_0 during Sept – Dec south of 58°S, CO_2 uptake increases, suggesting that biological activity is probably dominating the flux in agreement with the findings of Sokolov (2008).

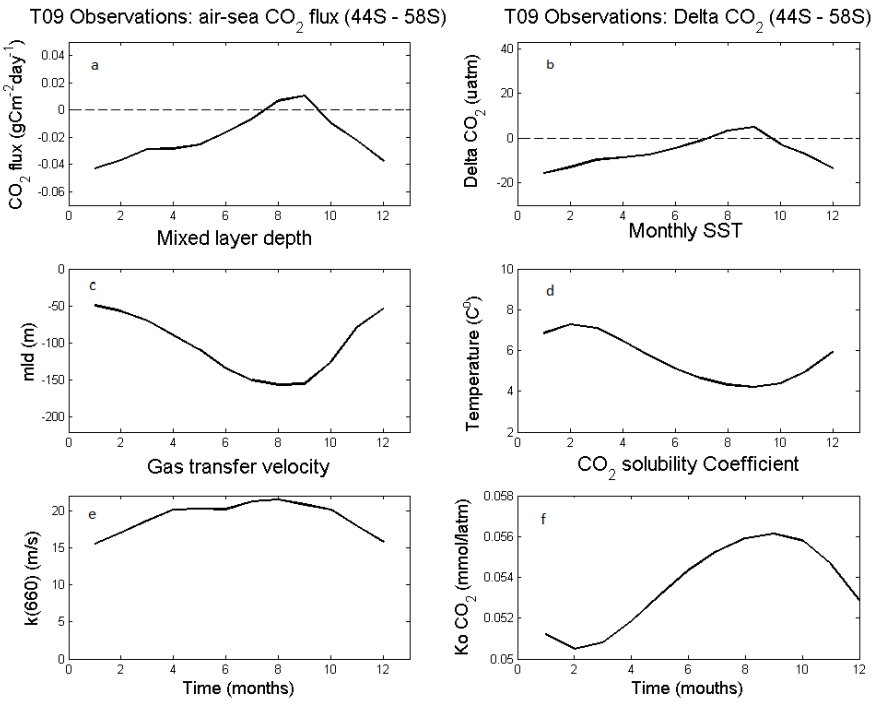

Figure 4.6 The seasonal cycle of air – sea CO_2 flux and ancillary variables in the 44°S - 58°S zone from T09 observations (a) CO_2 flux ($gCm^{-2}yr^{-1}$) negative indicates flux into the ocean , (b) Delta pCO2 (µatm) , (c) Mixed layer depth (MLD m) , (d) Sea Surface Temperature (SST), (e) Gas transfer velocity (ms^{-1}) , (f) CO_2 solubility Coefficient ($mmolL^{-1}atm^{-1}$) The x-axis in all figures reflect annual period in days. The dotted line in each figure above show the T09 observations

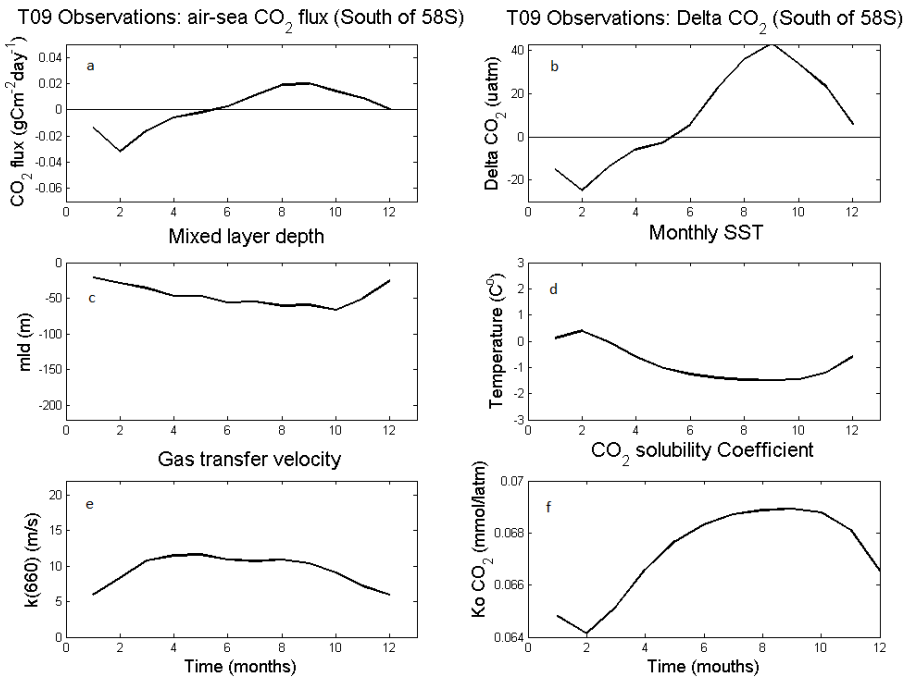

Figure 4.7 The seasonal cycle of air – sea CO_2 flux and ancillary variables south of 58°S zone from the PERIANT05 model. (a) CO_2 flux ($gCm^{-2}yr^{-1}$) negative indicates flux into the ocean , (b) Delta pCO2 (µatm) , (c) Mixed layer depth (MLD m) , (d) Sea Surface Temperature (SST), (e) Gas transfer velocity (ms^{-1}) , (f) CO_2 solubility Coefficient ($mmolL^{-1}atm^{-1}$) . The x-axis in all figures reflects annual period in days. The dotted line in each figure above show the T09 observations

T09 observations south of 58°S has a mean annual outgassing CO_2 flux of 0.049 $PgCyr^{-1}$, which is similar to 0.04 ±0.02 $PgCyr^{-1}$ reported in Lenton et al., 2013, figures 4.8 & 4.9. For the zone 44°S – 58°S T09 observations give an annual flux of -0.44 $PgCyr^{-1}$ and Lenton et al., 2013 give a figure of -0.32±0.16 $PgCyr^{-1}$. These annual means are statistically comparable due to the higher standard deviation (0.16) in Lenton et al., 2013.

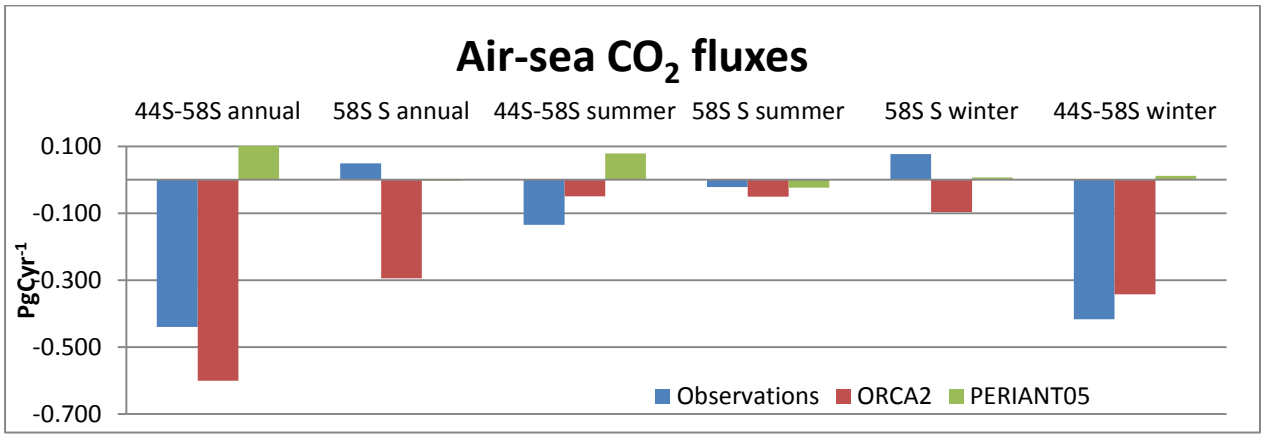

Figure 4.8 Show decadal (1993- 2002) climatological annual CO_2 fluxes the, winter and summer fluxes at 44°S – 58°S and south of 58°S. ORCA2 generally overestimates the annul influx relative to the T09 observations, PERIANT05 shows an outgassing bias at the zone 44°S – 58°S. Note that PERIANT05 annul is equivalent to T09 observations south of 58°S summer.

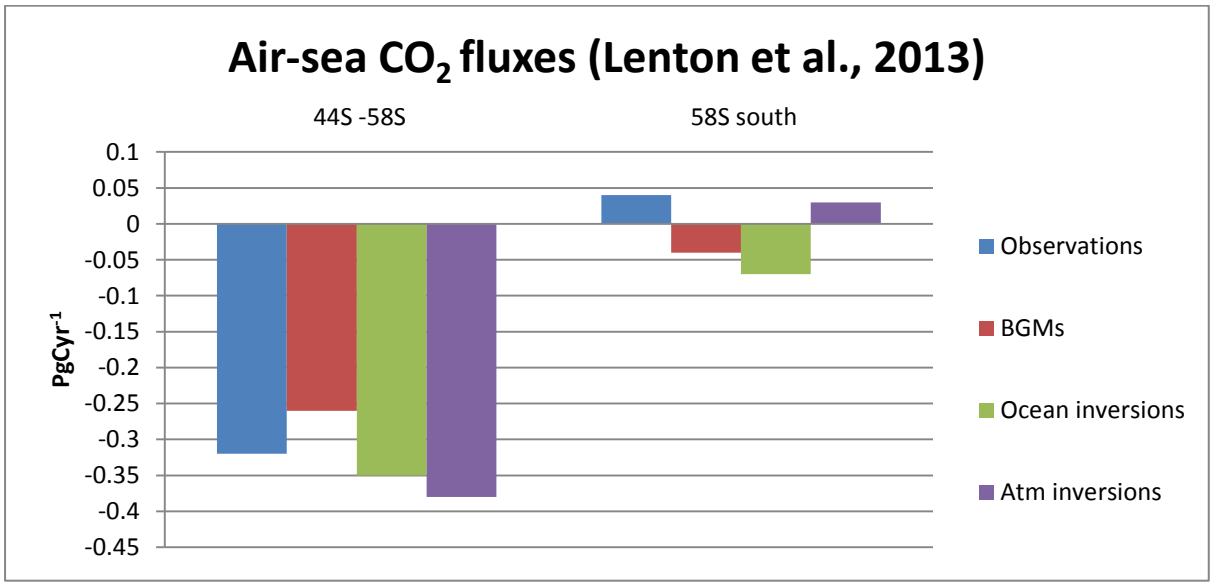

Figure 4.9 Show the median absolute deviation (MAD) of the annual fluxes of T09 observations, biogeochemistry models (BGMs), ocean inversions (green) and atmospheric inversions (purple) from Lenton et al., 2013.

The ORCA2 seasonal cycle of air-sea CO_2 at the zone 44°S – 58°S is out of phase with T09 observations for majority of the year except for period Jan-Feb where CO_2 in-gassing flux is decreasing driven by increase of SST causing weakening of surface CO_2 solubility K_0, figure 4.10(a). In contrary to T09 observations, ORCA2' s seasonal cycle of the air-sea CO_2 flux at the zone 44°S – 58°S

gives a maximum CO_2 in-gassing in September (-0.075 $PgCm^{-2}day^{-1}$) and minimum outgassing (0.01 $PgCm^{-2}day^{-1}$) at the end of summer in February. This result implies that ORCA2 acts as a CO_2 sink from beginning of autumn until end of year (December) for the zone 44°S – 58°S, this results is however in contrast to T09 observation and known literature (e.g. Metzl et al., 2006; 2009), figure 4.10. Also in sharp contrast to T09 observations, the maximum CO_2 in-gassing zone in ORCA2 (44°S – 58°S) coincides with the deepest MLD (200m), lowest SST and the maximum transfer velocity coefficient ($18ms^{-1}$). ORCA2 seasonal cycle of SST was found to be highly correlated with air-sea CO_2 fluxes (r^2 = 0.97) at the zone 44°S – 58°S, which suggest that the air-sea CO_2 flux in ORCA2 might be solely driven by CO_2 solubility (K_0), this postulation is further discussed in chapter 5.

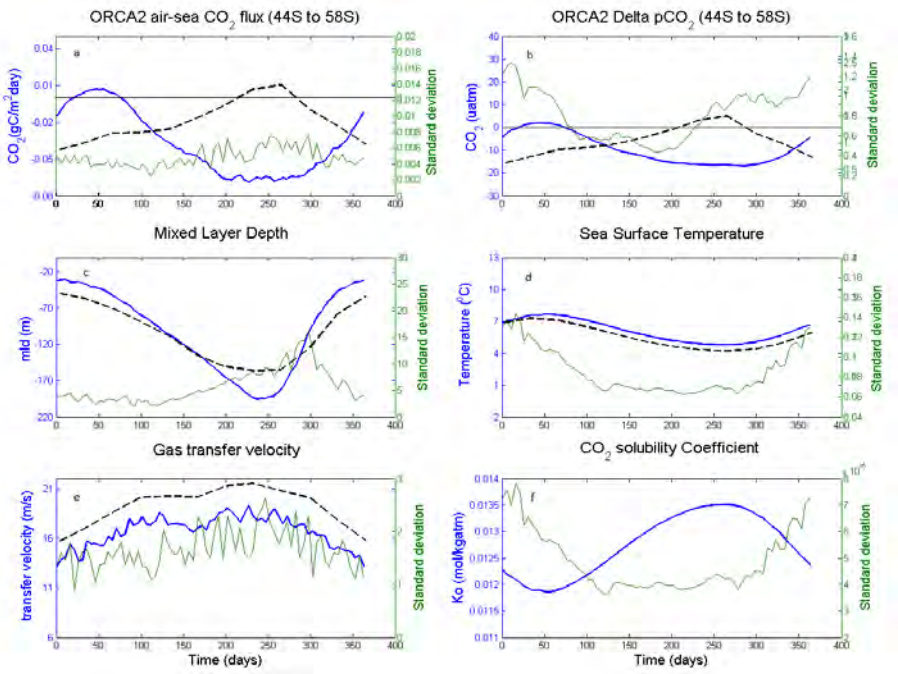

Figure 4.10 The seasonal cycle of air – sea CO_2 flux and ancillary variables in the 44°S - 58°S zone from the ORCA2 model.(a) CO_2 flux ($gCm^{-2}yr^{-1}$) negative indicates flux into the (b) Delta pCO2 (µatm) , (c) Mixed layer depth (MLD m) , (d) Sea Surface Temperature (SST), (e) Gas transfer velocity (ms^{-1}) , (f) CO_2 solubility Coefficient ($mmolL^{-1}atm^{-1}$). The x-axis in all figures reflects annual period in days. The dotted line in each figure shows T09 observation.

South of 58°S the seasonal cycle of air-sea CO_2 flux in ORCA2 depicts a negative flux throughout the year and shows a relatively similar phasing with T09 observations between Mar-Dec, figure 4.11. In contrary to 44°S – 58°S, between Jan-Mar the seasonal cycle (air-sea CO_2 flux) is out of phase with T09 observations (Fig. 4.11). One of the major differences between ORCA2 and T09 observations south of 58°S is the absence of the CO_2 outgassing feature occurring between Jun-Dec in T09 observation but not present in ORCA2. SST and gas transfer velocity (*k*) of ORCA2 south of 58°S are relative similar to T09 observations, (figure 4.11). Note that though ORCA2's seasonal cycle phasing of air-sea CO_2 flux is moderately similar to T09 observations south of 58°S between Apr-Dec, the

MLD and ΔpCO_2 show huge differences in both phase and magnitudes with comparison to T09 observations.

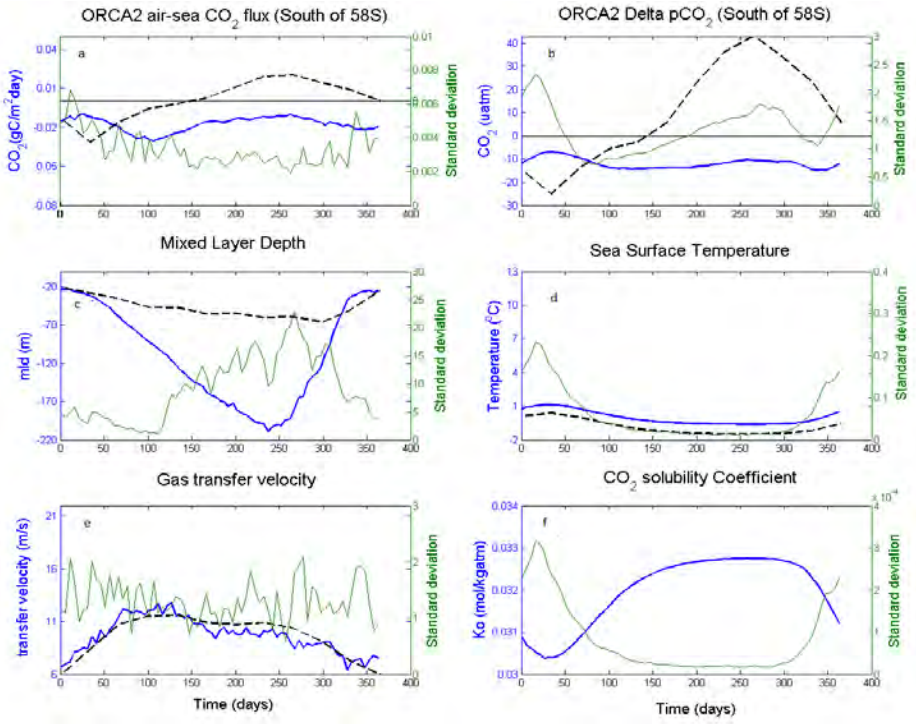

Figure 4.11 The seasonal cycle of air – sea CO_2 flux and ancillary variables in the south of 58°S zone from the ORCA2 model. (a) CO_2 flux ($gCm^{-2}yr^{-1}$) negative indicates flux into the ocean (b) Delta pCO2 (µatm) , (c) Mixed layer depth (MLD m) , (d) Sea Surface Temperature (SST), (e) Gas transfer velocity (ms^{-1}) , (f) CO_2 solubility Coefficient ($mmolL^{-1}atm^{-1}$). The x-axis in all figures reflects annual period in days. The dotted line in each figure shows T09 observations.

As observed in ORACA2, PERIANT05 seasonal cycle shows a similar phasing with T09 observations between Jan – Mar however have different magnitudes. However in contrast to ORCA2, PERIANT05 seasonal cycle of air-sea CO_2 fluxes is similar to observations in phase and magnitude during the winter season (Aug – Sept), see figure 4.12. Note that the winter where PERIANT05 air-sea CO2 flux is similar to T09 observations is known to be the time zone where subsurface DIC saturated waters mix (convective mixing) with surface waters as results of entrainment (Metzl et al., 2006, Salléé et al., 2012). In PERIANT05 the transfer velocity (*k*) shows a sharp reduction in early winter and recovers immediately the following month, coinciding with the maximum CO_2 in-gassing at the zone 44°S – 58°S. The implications of the correlation of the seasonal cycle of air-sea CO_2 flux with SST in late summer (Jan – Feb observed in both PERIANT05 and ORCA2 is discussed in chapter 5.

PERIANT05 and T09 observations CO_2 outgassing peaks in September coinciding with the deepest MLD which is consistent with the postulation made above that convective mixing is responsible for the winter CO_2 outgassing. Note that the seasonal of air-sea CO_2 flux in PERIANT05 is out of phase

with T09 observations during summer (Oct – Dec), suggesting that PERIANT05 might have a weaker biological CO_2 with relative to observations.

PERIANT05 seasonal cycle south of 58°S was found to show a good correlation with T09 observations (r^2 = 0.62), (see table 4.3). In contrast to the zone 44°S – 58°S, PERIANT05 seem to capture summer biological CO_2 drawdown between Nov – Feb south of 58°S. Note that PERIANT05 model output in this region (south of 58°S) is in sharp contrast to the findings of Lenton et al., 2013 (L13), where the five biogeochemical models in the study showed a poor correlation with observations south of 58°S. PERIANT05 seasonal cycle is thought to respond to the winter entrainment of DIC however underestimate the winter CO_2 outgassing and the summer biological CO_2 uptake (see figure 4.8). In chapter 5 the seasonal cycle of PERIANT05 is further discussed.

Table 4.3 Correlation coefficients (r^2) of the decadal (1993- 2002) CO_2 climatology of mean seasonal cycle of air-sea FCO_2 Lenton RECCAP 2013 boundaries with T09 observations. PERIANT05 is negatively correlated (-0.42) at 44°S – 58°S and strongly positively correlated with observations south of 58°S. ORAC2 shows the opposite, weakly correlated with T09 observations south of 58°S and strong negatively correlation 44°S -58°S.

Region	ORCA2	PERIANT05
44°S – 58°S	-0.60	-0.41
South of 58°S	0.18	0.62

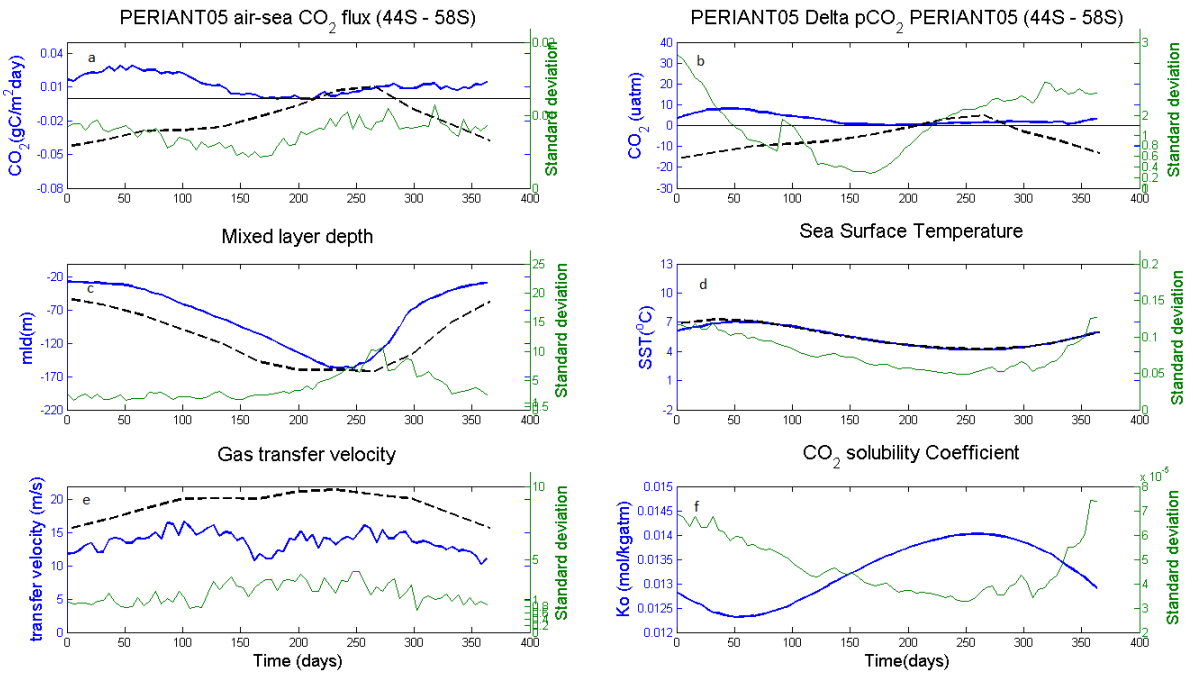

Figure 4.12 The seasonal cycle of air – sea CO_2 flux and ancillary variables in the 44°S - 58°S zone from the PERIANT05 model. (a) CO_2 flux ($gCm^{-2}yr^{-1}$) negative indicates flux into the ocean (b) Delta pCO_2 (µatm) , (c) Mixed layer depth (MLD m) , (d) Sea Surface Temperature (SST), (e) Gas transfer velocity (ms^{-1}) , (f) CO_2 solubility Coefficient ($mmolL^{-1}atm^{-1}$). The x-axis in all figures reflects annual period in days. The dotted line in each figure above show the T09 observations

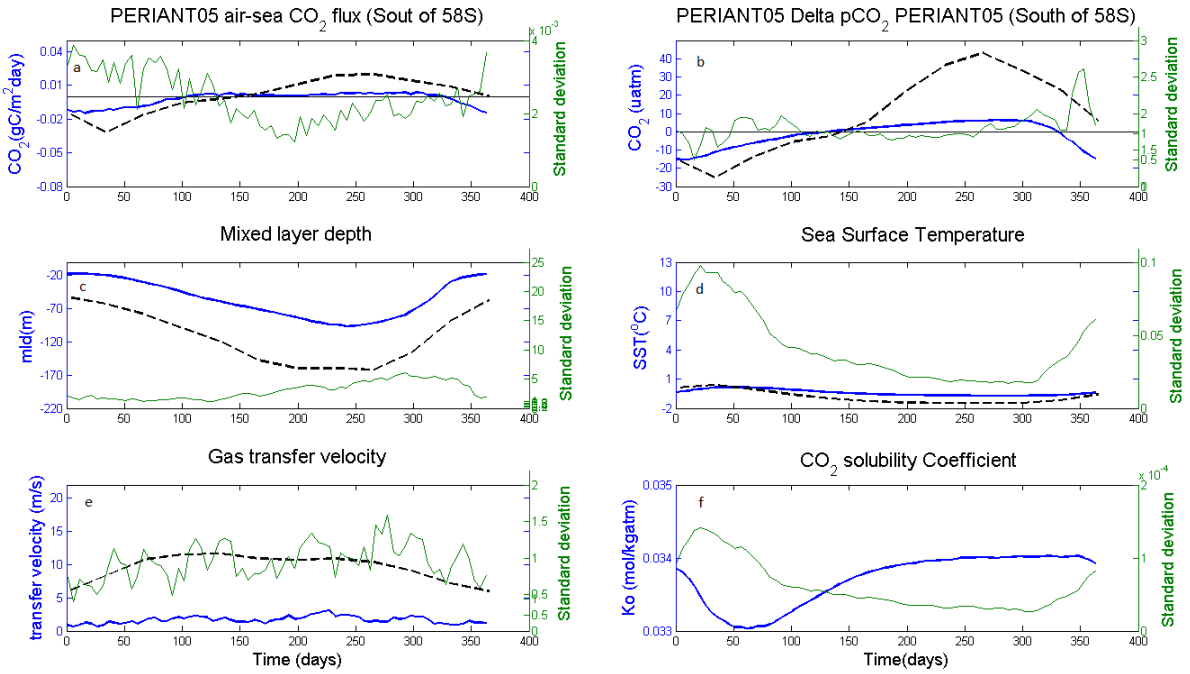

Figure 4.13 The seasonal cycle of air – sea CO_2 flux and ancillary variables in the south of 58°S zone from the PERIANT05 model. (a) CO_2 flux ($gCm^{-2}yr^{-1}$) negative indicates flux into the ocean (b) Delta pCO_2 (µatm) , (c) Mixed layer depth (MLD m) , (d) Sea Surface Temperature (SST), (e) Gas transfer velocity (ms^{-1}) , (f) CO_2 solubility Coefficient ($mmolL^{-1}atm^{-1}$). The x-axis in all figures reflects annual period in days. The dotted line in each figure above show the T09 observations

ORCA2 CO_2 annual flux (-0.60±0.02 $PgCyr^{-1}$) was found to overestimate annual oceanic CO_2 uptake with relative to T09 observations (-0.439 $PgCyr^{-1}$) in the zone 44°S – 58°S. ORCA2 mean annual air - sea CO_2 flux for the zone 44°S – 58°S was find to be statistically greater than the Median Absolute Deviation (MAD) of the biogeochemical models (BGMs) (-0.26±0.2 $PgCyr^{-1}$) , the ocean (-0.35±0.02$PgCyr^{-1}$) and atmospheric (-0.38±0.1$PgCyr^{-1}$) inversion models used in L13, see table 4.4 and 45. MAD is the measure of the variability of a univariate sample of quantitative data, and is defined as the median of the absolute deviation from the data's median. South of 58°S ORCA2 was found to have the mean annual CO_2 flux of -0.30 $PgCyr^{-1}$, much larger than the MAD of the BGMs (0.04 $PgCyr^{-1}$) in L13.

PERINAT05's annual CO_2 flux in the 44°S – 58°S zone (0.22 ±0.08 $PgCyr^{-1}$) was found to be different from the L13 BGMs climatological MAD i.e. -0.26±0.16 $PgCyr^{-1}$. However south of 58°S, PERIANT05 air-sea CO_2 annual flux (-0.002±0.03 $PgCyr^{-1}$) was found comparable to -0.04 $PgCyr^{-1}$ found in L13. These results therefore shows that both PERIANT05 and ORCA2 could not reproduce L13 mean findings, however PERIANT05 seasonal cycle south of 58°S was found to better compares with T09 observations of which none of the BGMs in L13 was able to achieve. It worth mention that the comparison made with L13 annual fluxes here was based on the mean MAD of all BGMs in L13 and this is because except for NEMO-Plankton 5 and NEMO-PISCES, individual BGMs annual CO_2 fluxes

are not provided in L13. The overestimation of mean annual CO_2 fluxes observed in ORCA2 is consistent with the results obtained for NEMO-Plankton 5 and NEMO-PISCES model outputs in L13. The mean annual CO_2 fluxes of NEMO-Plankton 5 and NEMO-PISCES were found to have higher annual fluxes relative to the other three BGMs (i.e. CCSM_BEC, CCSM_ETH and CSIRO) in L13, see figure 4.8. Annual fluxes of L13 are summarized in table 4.3.

Table 4.4 Mean Absolute Deviation (MAD) annual mean air-sea CO_2 flux of the Biogeochemistry models (BGMs), ocean inversions and Atmospheric (Atm) inversions models from Lenton et al., 2013. Note that the observations of Lenton et al, 2013 are lower than that the current study (table 4.1) however comparable with the standard deviation.

Region	observations	BGMs	Ocean Inversions	Atm inversions
44°S -58°S	-0.32±0.16	-0.26±0.2	-0.35±0.02	-0.38±0.1
58°S south	0.04±0.02	-0.04±0.09	-0.07±0.01	0.03±0.03

Table 4.5 Climatological air-sea CO2 flux of the period 1993 – 2006 and T09 observations for 2000 (Takahashi et al., 2012), shows annual fluxes for the SAZ (Sub-Antarctic zone) and the polar zone for Lenton 2013 RECCAP boundaries. Summer is here defined as Nov-Feb and Winter May-Aug

Region	T09 observations	ORCA2	PERIANT05
Annual air-sea CO_2 fluxes at the SAZ			
44S-58S annual	-0.439	-0.600±0.02	0.219±0.07
44S-58S winter	-0.416	-0.342±0.01	0.012±0.01
44S-58S summer	-0.135	-0.049±0.01	0.078±0.02
Annual air-sea CO_2 fluxes at the polar zone			
58S S annual	0.049	-0.294±0.03	-0.002±0.03
58S S winter	0.077	-0.096±0.01	0.007±0.00
58S S summer	-0.022	-0.051±0.02	-0.024±0.01

4.3 Seasonal cycle: Boundary sensitivity analysis

In this section the model output of ORCA2 and PERIANT05 are used to investigate the sensitivity of the air-sea CO_2 seasonal cycle to zonal boundary definition in the SO. This is done by comparing the air-sea CO_2 flux and annual CO_2 fluxes for the Lenton 2013 RECCAP boundaries (44°S – 58°S and 58°S south), geographical boundaries (40°S – 50°S and 50°S south) and dynamic boundaries (Sub-Antarctic Zone (SAZ) and Antarctic Zone (AZ) defined by mean climatological frontal positions using the SST criteria. This approach seeks to investigate whether the poor agreement between the model outputs air-sea CO_2 flux seasonal cycle and observational data is a result of the boundary definition. The observations data used here is the Takahashi et al., 2009 CO_2 surface in situ measurements, (http://www.ldeo.columbia.edu/res/pi/CO2/carbondioxide/pages/air_sea_flux_2000.html).

4.3.1 Seasonal cycle

The seasonal cycle phasing of air-sea flux CO_2 in ORCA2 was found to remain relatively similar between the zones 44°S – 58°S, 40°S -50°S and the SAZ. The only observable difference in seasonal cycle phasing occur for the period between winter-spring, where the seasonal cycle amplitude extend up to -0.075 $gCm^{-2}day^{-1}$ at the 40°S -50°S zone but only reaches up to -0.070 $gCm^{-2}day^{-1}$ for 44°S – 58°S and the SAZ, figure 4.15. This observation is attributed to the strong CO_2 in-gassing feature around 40°S in the ORCA2 air-sea CO_2 fluxes spatial map in figure 4.1. ORCA2 seasonal cycle of air-sea CO_2 flux generally show a poor correlation with T09 observations around SAZ region, shows a strong negative correlation at the zone 44°S – 58°S (r^2 = - 0.63), negatively correlated at 40°S – 50°S (r^2 = -0.21) and not correlated at the SAZ (r^2 =0.07). In contrast to ORCA2, T09 observations seasonal cycle shows significant differences between the three sub-regions (see figure 4.15). For example the zone 40°S – 50°S and the SAZ shows a strengthened CO_2 in-gassing throughout the year with relative to the 44°S – 58°S zone. Furthermore T09 observations show a CO_2 outgassing window between Oct-Sept at the zone 44°S – 58°S however this feature is not observed in both 40°S – 50°S and SAZ. The strengthened CO_2 in-gassing at the geographic and dynamic boundaries in T09 observations is consisted with reported literature at these sub-regions (e.g. Thomalla et al., 2011, Solokov 2008).

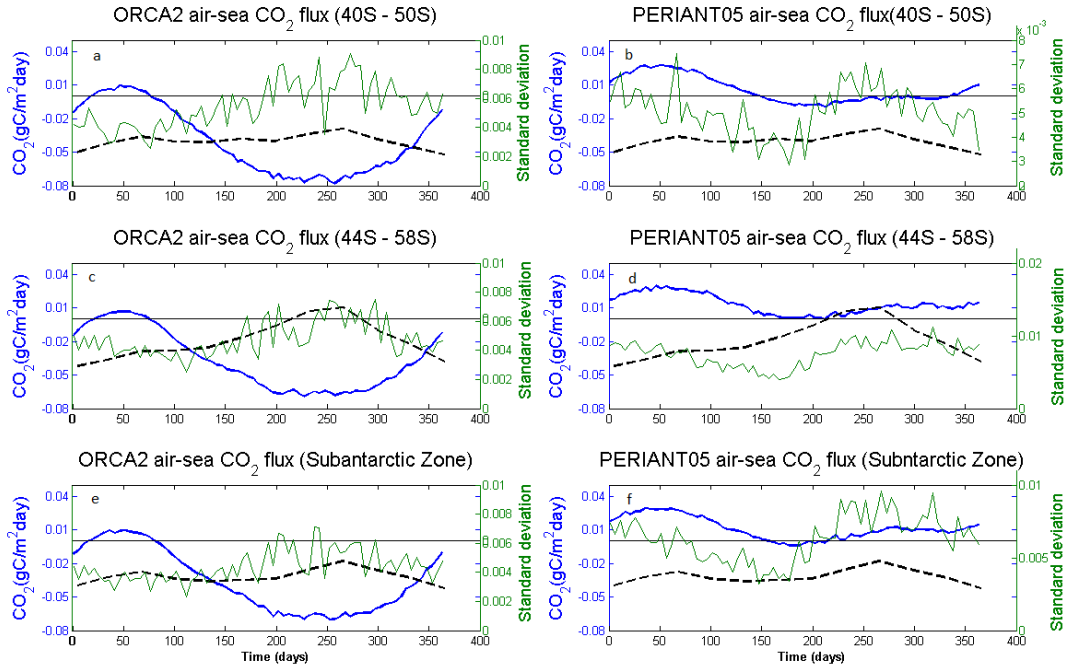

Figure 4.15 The air – sea CO_2 flux Seasonal cycle of flux at the Lenton 2013, geographic and dynamic boundaries for the Permanent Open Ocean Zone (POOZ). The x-axis in all figures reflects time in days. The dotted line in each figures above show the T09 observations. It shows that the seasonal cycle of air-sea CO_2 flux phasing is relatively similar between the three sub-regions in both ORCA2 and PERIANT05 however T09 observations show significant differences between the three sub-regions.

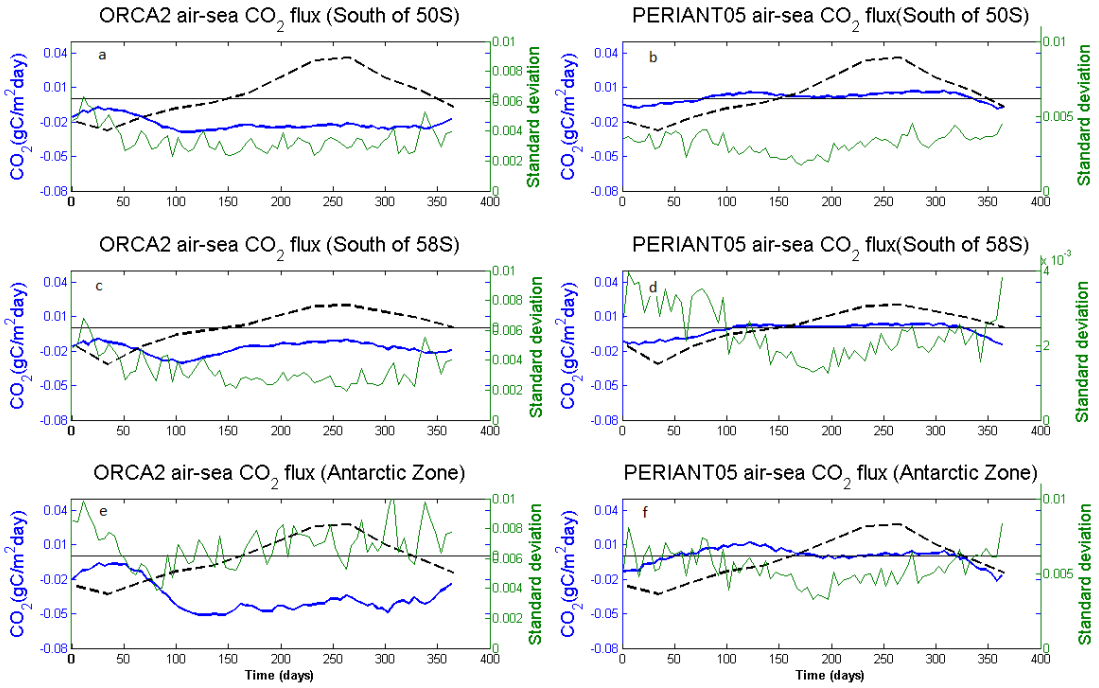

Figure 4.16 The air – sea CO_2 flux Seasonal cycle of flux at the Lenton 2013, geographic and dynamic boundaries for the Marginal Ice Zone (MIZ). The x-axis in all figures reflects time in days. The dotted line in each figures above show the T09 observations. Both ORCA2 and PERIANT05 oppose observations these sub-regions. Note that T09 observations seasonal cycle maintain a similar phasing between the three sub-regions have has different amplitudes

In PERIANT05 the seasonal cycle of air-sea CO_2 flux is similar in phase and amplitude in the zone 44°S – 58°S and the SAZ, but a little different in the zone 40°S – 50°S. The zone 44°S - 58°S and the SAZ shows a weak sink CO_2 in June and however maintain a weak constant CO_2 outgassing between Jun – Nov, (see figure 4.15). The enhanced CO_2 sink observed in the geography boundary is attributed to the CO_2 in-gassing zone at the central Atlantic Ocean, given that the geographic boundary is most northerly extend it covers much of the Atlantic Ocean CO_2 in-gassing zone compared to the other two boundaries in PERIANT05. Note that in T09 observations, CO_2 outgassing peak twice in the seasonal cycle for all three sub-regions, first in March associated with SST as stated above and in September associated with convective mixing (Metzl et al., 2006, 2009, Lenton et al., 2006), (see figure 4.15). PERIANT05 seasonal cycle reproduce both these CO_2 outgassing peaks , however after the second peaking in September the CO_2 flux does not retreat as primary production initialize towards summer. Furthermore the CO_2 outgassing increases significantly from December in all three sub-regions in PERIANT05, this increase might be associated with the increase in SST, this postulation is further discussed in Chapter 5.

In contrast to ORCA2 the seasonal cycle (air-sea CO_2 flux) of PERIANT05 though is not on phase with T09 observations it captures the seasonal cycle trend better at the dynamic boundary compared to the Lenton 2013 RECCAP and geographic boundaries (with different magnitudes). Note the

correlation of PERIANT05 decreases from r_2 = -0.42 the Lenton 2013 RECCAP to the dynamic boundary in r^2 = -0.005 in (see figure 4.17). In all three boundary definitions, the geographic boundary in PERIANT05 has the largest difference in seasonal cycle amplitude comparison to T09 observations seasonal cycle of air-sea CO_2 flux.

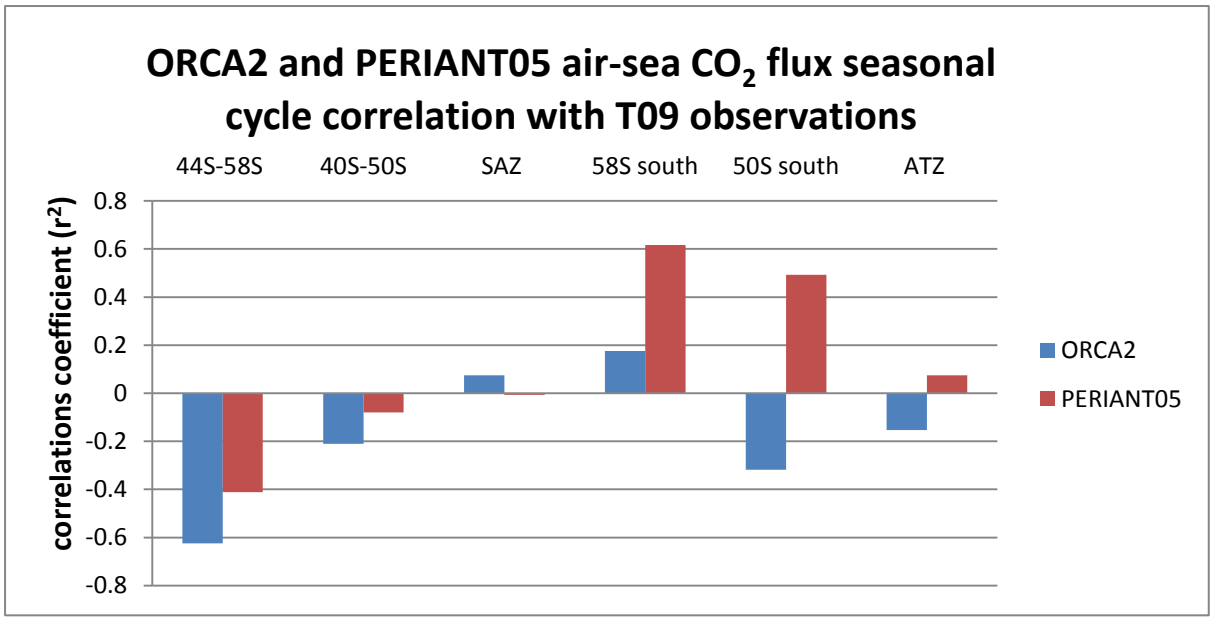

Figure 4.17 Show correlations coefficients of the decadal (1993- 2002) CO_2 climatology of mean annual fluxes for the geographic, Lenton and dynamic boundaries with T09 observations. ORCA2 and PERIANT05 show a general positive with observation at the SAZ and negative correlations at the Marginal Ice Zone (MIZ). ORCA2 correlations are inconsistent at the different sub-regions of the SO.

At the polar zone the seasonal cycle of air-sea CO_2 flux in ORCA2 maintain a roughly similar phasing between the Lenton 2013 RECCAP boundaries and geographic however the dynamic boundaries has a larger amplitude in comparison to other two (figure 4.16). The amplitude of the seasonal cycle at the dynamic boundaries reaches up to -0.05 $pCm^{-2}day^{-1}$ and only up to -0.03 $pCm^{-2}day^{-1}$ south 50°S and south of 58°S. The T09 observations air-sea CO_2 fluxes also maintain similar seasonal cycle phasing between the three sub-regions (south of 58°S, south of 50°S and the AZ) but has different amplitudes and all opposes ORCA2. ORCA2 seasonal cycle generally shows a poor correlation with T09 observations south of the polar front; south of 58°S (r^2 = 0.18), south of 50°S (r^2 = -0.32) and at the AZ (r^2 = -0.15). Note that the amplitude of the CO_2 outgassing window observed during the period Jun –Dec in the T09 observations in the polar zone is similar at the Lenton RECCAP 2013 and dynamic boundaries (0.02 $gCm^{-2}day^{-1}$), however larger in the geographic boundary (0.035 $gCm^{-2}day^{-1}$). In the polar zone all three boundary definitions has roughly similar onset of CO_2 outgassing in June, however the dynamic boundary offset the $_{CO2}$ outgassing in month earlier (November) compared to the other two (December) , see figure 4.16. These results show that ORCA2's seasonal

cycle of air-sea flux CO_2 is not sensitive to boundary. T09 observations however show some observable differences between the three boundary definitions.

In PERIANT05 the seasonal cycle of air-sea CO_2 flux shows a better comparison with observations at the polar zone compared to the SAZ region (see figure 4.17); south 58°S (r^2 = 0.62), south of 50°S (r^2 = 0.49) and AZ (r^2 = 0.07). PERIANT05's air-sea CO_2 flux seasonal cycle at the polar does show some minor differences in the seasonal cycle phasing however maintain three similar features in all three boundaries definition; (i) constant CO_2 flux around zero between Mar - Nov, (ii) an increase in CO_2 uptake between Nov – Dec and (iii) a decreasing CO_2 influx between Jan – Mar.

In conclusion the use of dynamic boundaries has shown not to improve significantly the seasonal cycle of air-sea CO_2 flux comparison with observations in both ORCA2 and PERIANT05.

4.3.2 Annual fluxes

The similarity of the CO_2 flux seasonal cycle phasing at 44°S – 58°S and the SAZ in ORCA2 observed above is also evident in their relative annual CO_2 fluxes, -0.60±0.03 PgC yr^{-1} and -0.58±0.02 $PgCyr^{-1}$ respectively. Interestingly though this two sub-regions has similar annual fluxes, the SAZ seasonal cycle is not correlated to T09 observations at the SAZ (r^2 = 0.01) but strongly negatively correlated at 44°S – 58°S (r^2 = -0.62). The 40°S – 50°S zone (-0.46±0.03 $PgCyr^{-1}$) in ORCA2 has the lowest annual CO_2 uptake compared to 44°S – 58°S and SAZ. Note that the zone 40°S – 50°S has the smallest surface area in comparison to 44°S – 58°S and the SAZ, thus the smaller annual CO_2 influx at this zone might be surface area based, section 4.4 further explores these phenomena.

PERINAT05 provides an annual CO_2 flux of 0.215±0.07 $PgCyr^{-1}$ at the SAZ, 0.219±0.07 $PgCyr^{-1}$ at the zone 44°S – 58°S and 0.094±0.04 $PgCyr^{-1}$ at 40°S – 50°S. Note that the annual CO_2 flux at the zone 40°S – 50°S is less than half that of 44°S – 58°S and the SAZ in PERINAT05, the reduction CO_2 uptake at this zone is attributed to the in-gassing zone at the Atlantic Ocean as stated above, see figure 4.18. T09 observations also show a strong CO_2 in-gassing at the zone 40°S – 50°S (-0.71 $PgCyr^{-1}$) compared to 44°S – 58°S (-0.44 $PgCyr^{-1}$) and the SAZ (-0.64 $PgCyr^{-1}$), this strong CO_2 in-gassing in the geographic boundary is thought to be due (*inter alia)* enhanced biological activity around this region. This matter is discussed further in chapter 5.

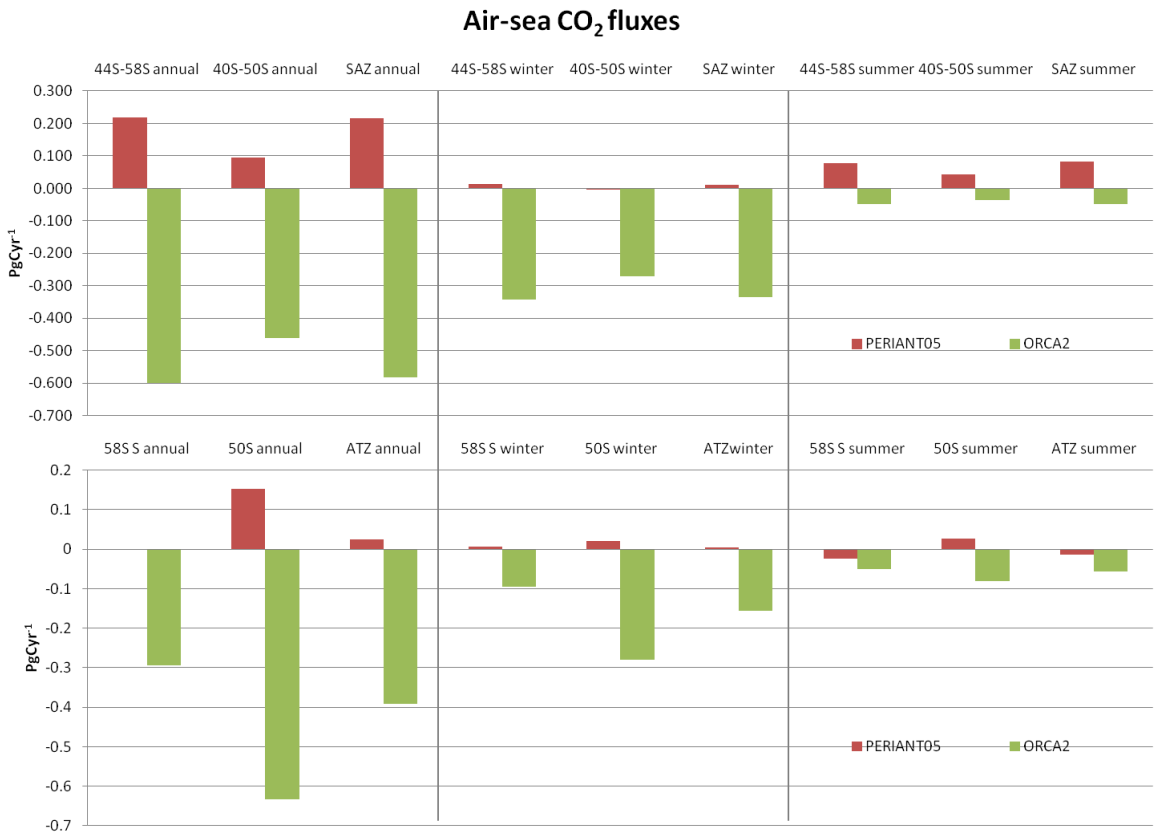

Figure 4.18 Shows the decadal (1993- 2002) CO_2 climatology of mean annul fluxes for the Lenton 2013 , geography and dynamic boundaries. Note ORCA2 has negative flux for all sub-regions for annual, winter and summer.

Table 4.7 Climatological mean annual of air-sea CO_2 flux of the period 1993 – 2006 and observations for 2000 (Takahashi et al., 2012), SAZ (Sub-Antarctic zone) and AZ (Antarctic Zone). Negative reflect the flux into the Ocean. The annual flux is given in $PgCyr^{-1}$. The gray shaded area shows the mean annual CO_2 fluxes.

Region	T09 observations	ORCA2	PERIANT05
Annual air-sea CO_2 fluxes at the SAZ			
40°S-50°S annual	-0.706	-0.460±0.03	0.094±0.04
40°S-50°S winter	-0.21	-0.270±0.01	-0.005±0.01
40°S-50°S summer	-0.138	-0.037±0.01	0.043±0.02
44°S-58°S annual	-0.439	-0.600±0.02	0.219±0.07
44°S-58°S winter	-0.416	-0.342±0.01	0.012±0.01
44°S-58°S summer	-0.135	-0.049±0.01	0.078±0.02
SAZ annual	-0.642	-0.582±0.02	0.215±0.07
SAZ winter	-0.20	-0.335±0.02	0.010±0.01
SAZ summer	-0.124	-0.048±0.01	0.083±0.02
Annual air-sea CO_2 fluxes at the polar zone			
58°S S annual	0.049	-0.294±0.03	-0.002±0.03
58°S S winter	0.077	-0.096±0.01	0.007±0.00
58°S S summer	-0.022	-0.051±0.02	-0.024±0.01
50°S annual	0.043	-0.633±0.04	0.152±0.06
50°S winter	0.101	-0.281±0.02	0.020±0.01
50oS summer	-0.039	-0.081±0.03	0.027±0.01
ATZ annual	-0.082	-0.391±0.04	0.025±0.04
ATZ winter	0.087	-0.157±0.01	0.005±0.00
ATZ summer	-0.072	-0.056±0.02	-0.014±0.00

Table 4.3 Mean Absolute Deviation (MAD) annual mean air-sea CO_2 flux of the Biogeochemistry models (BGMs) , ocean inversions and Atmospheric (Atm) inversions models from Lenton et al., 2013. Note that the observations of Lenton et al, 2013 are lower than that the current study (table 4.1) however comparable with the standard deviation.

Region	observations	BGMs	Ocean Inversions	Atm inversions
44S -58S	-0.32±0.16	-0.26±0.2	-0.35±0.02	-0.38±0.1
58S south	0.04±0.02	-0.04±0.09	-0.07±0.01	0.03±0.03

4.4 Seasonal cycle: Basin sensitivity analysis

This section examines the differences in the contribution made by each basin to the zonal magnitude and phasing of the air-sea CO_2 flux seasonal cycle. T09 observations are not included in this analysis

due to the coarse resolution of the data (4^{o} latitude x 5^{o} longitude) and hence sparse spatial basin coverage.

4.4.1. Seasonal cycle

The seasonal cycle of air-sea CO_2 flux of ORCA2 at the Atlantic and Indian Ocean basin follow a relatively similar phasing with the zonal mean seasonal cycle of the zone $44^{o}S$ – $58^{o}S$ with some minor differences. For example the Atlantic Ocean show a strengthening CO_2 in-gassing between Jan-Apr relative to the zonal mean seasonal cycle, see figure 4.19. In contrast to the other two basins (Pacific and Indian Ocean), the Atlantic Ocean in ORCA2 does not have a CO_2 outgassing window, instead the Atlantic Ocean acts as a CO_2 sink throughout the year. In the Pacific Ocean the seasonal cycle of air-sea CO_2 flux shows a weaken CO_2 in-gassing relative to the zonal mean seasonal cycle in the zone $44^{o}S$ – $58^{o}S$. Note that in the zone $44^{o}S$ – $58^{o}S$, the Pacific Ocean has a weaker CO_2 influx relative to the zonal mean seasonal cycle i.e. the amplitude of the seasonal cycle only reaches up to -0.02 $gCm^{-2}day^{-1}$ in September compared to -0.07 $gCm^{-2}day^{-1}$ in the zonal mean seasonal for the same period, (figure 4.19). The CO_2 out-gassing window at the Pacific Ocean is two months longer (Jan-Apr) compared to the zonal mean seasonal cycle (Feb-Mar) at the zone $44^{o}S$ – $58^{o}S$ in ORCA2.

At the SAZ (figure 4.20) the seasonal cycle of air-sea CO_2 flux in ORCA2 has a similar seasonal trend in all three basins (Pacific, Atlantic and Indian Ocean), with some minor difference occurring at the Atlantic Ocean. The Atlantic Ocean shows a strengthened CO_2 in-gassing of an order of 0.01 $gCm^{-2}day^{-1}$ throughout the year in SAZ. In contrary to the zone $44^{o}S$ – $58^{o}S$, in the SAZ the seasonal cycle of air-sea CO_2 flux in the Pacific Ocean maintain a similar seasonal trend with the zonal mean SAZ seasonal cycle.

In PERIANT05 the seasonal cycle of air-sea CO_2 flux in the Indian Ocean is similar to the zonal mean seasonal cycle for zone $44^{o}S$ – $58^{o}S$, the Atlantic Ocean shows a strengthened CO_2 in-gassing and the Pacific Ocean depicts a weakened CO_2 in-gassing with relative to the zonal mean seasonal cycle. The strengthened CO_2 influx at the Atlantic Ocean is attributed to the CO_2 in-gassing zone of the Atlantic Ocean in PERIANT05 as stated above (figure 4.2). This strengthened CO_2 influx of PERIANT05 at the Atlantic Ocean is particularly evident between Jul-Dec in the seasonal cycle (figure 4.19). In the zonal mean seasonal cycle of PERIANT05 ($44^{o}S$ – $58^{o}S$), the elevated CO_2 in-gassing at the Atlantic Ocean is compensated by the weakenedCO_2 in-gassing at the Pacific Ocean resulting in the net CO_2 influx in the seasonal cycle of air-sea CO_2 flux shown in the dotted line, figure 4.19.

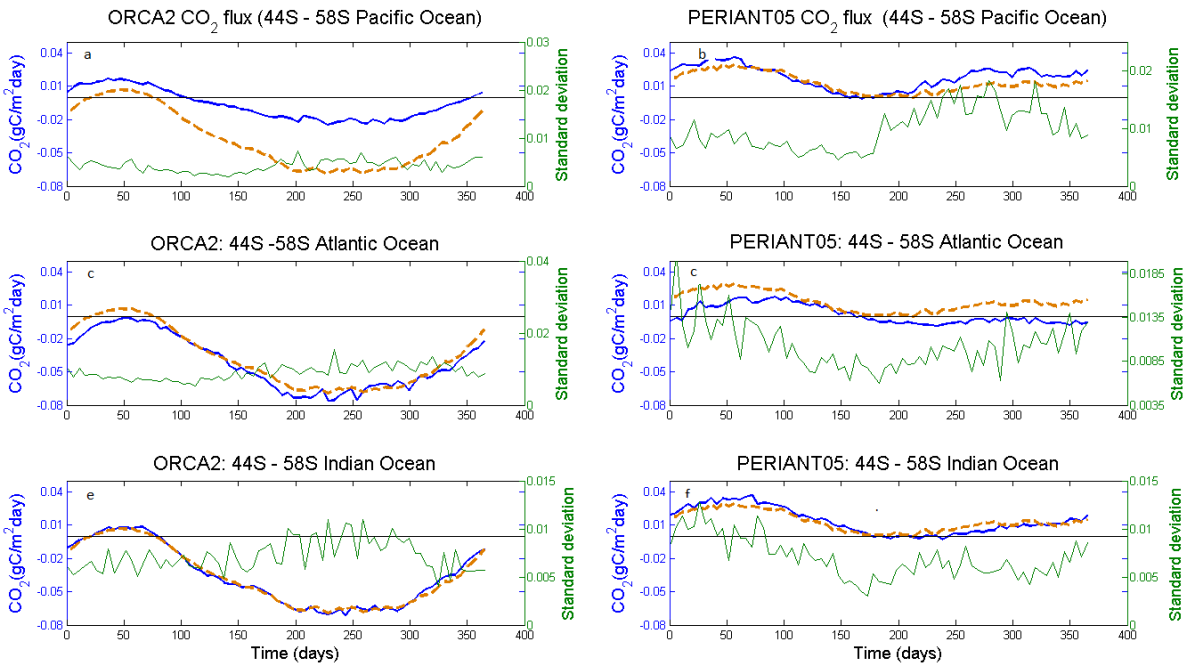

Figure 4.19 CO_2 flux at 44°S – 58°S for the Pacific, Atlantic and Indian Ocean, in $gCm^{-2}day^{-1}$. The brown dotted line shows the zonal mean seasonal cycle, blue line shows the basin seasonal cycle and the green line is the standard deviation of the basin seasonal cycle. Negative indicates influx in the Ocean. ORCA2 shows a weaken CO_2 in-gassing at the Pacific Ocean relative to the zonal mean seasonal cycle CO_2. In PERIANT05 note that the CO_2 in-gassing has strengthened in the Atlantic Ocean and weakened in the Pacific Ocean with relative to zonal mean seasonal cycle.

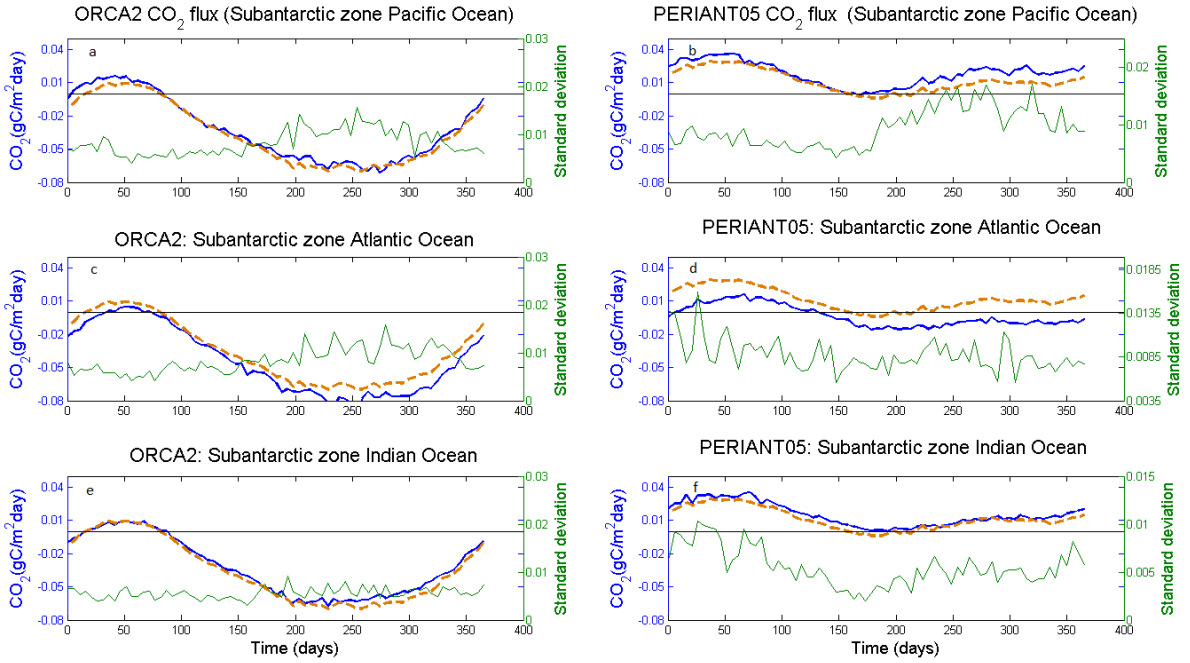

Figure 4.20 Shows the CO_2 flux at Sub Antarctic Zone for the Pacific, Atlantic and Indian Ocean, in $gCm^{-2}day^{-1}$. The brown dotted line shows the zonal mean seasonal cycle, blue line shows the basin seasonal cycle and the green line is the standard deviation of the basin seasonal cycle. Negative indicates influx in the Ocean. Negative indicate influx in the Ocean. ORCA2 shows a relatively seasonal cycle phasing all three basins. In PERIANT05 note that the CO_2 influx of the Atlantic Ocean is an order of 0.02 $gCm^{-2}day^{-1}$ stronger compared to the mean zonal seasonal cycle.

4.4.2 Annual fluxes

The criteria of basins annual air-sea CO_2 flux contributions to the total zonal mean CO_2 flux are different in ORCA2 and PERIANT05. In ORCA2 basins contribution to the zonal mean CO_2 flux is surface area based. To illustrate this note that in ORCA2 the basins contribution to the zonal means annual CO_2 flux is almost equal for the Lenton 2013 RECCAP and geography boundary, however different in the dynamic boundary. The Pacific Ocean basin (-0.25 $PgCyr^{-1}$) for example has a larger contribution to zonal mean annual CO_2 flux compared to the Atlantic (-0.17 $PgCyr^{-1}$) and Indian Ocean (-0.16 $PgCyr^{-1}$) in the dynamic boundary, see figure 4.21. This is because the surface area coverage of the Pacific Ocean in the dynamic boundary is significantly larger than the Pacific and Indian Ocean, whereas in the other two boundaries definition (Lenton 2013 RECCAP boundary and the geography boundary) surface coverage is roughly equal for all three basins. These observations further illustrate the proposition previously stated (section 4.3) that since the air-sea CO_2 fluxes of ORCA2 are dominantly K_0 driven and are uniform in most parts of the SO, annual air-sea CO_2 fluxes will be surface area based in ORCA2.

In PERIANT05 basins contribution to the zonal mean CO_2 flux are not surface area based but influenced by regional processes. For example at the Atlantic Ocean, the dynamic (-0.01 $PgCyr^{-1}$) and geographic boundary (-0.02 $PgCyr^{-1}$) act as CO_2 sinks, however the Lenton RECCAP boundary (0.02 $PgCyr^{-1}$) act as a CO_2 sources, figure 4.21. In PERIANT05 the Pacific Ocean is has the strongest CO_2 outgassing all three boundary definitions. This observation is congruent to previously reported literature i.e. Pacific Ocean has been reported to have less primary production based on observations (less biological CO_2 uptake) with relative to the Indian and Atlantic Ocean (e.g. Solokov and Rintoul, 2007; Thomalla et al., 2011).

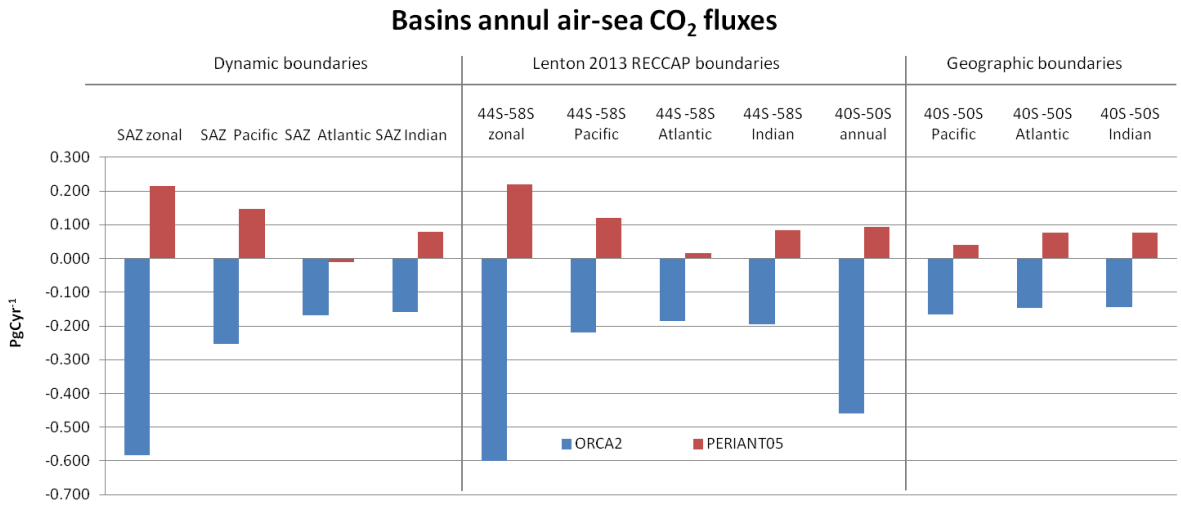

Figure 4.21 Annual air-sea CO_2 fluxes of the pacific, Atlantic and Indian Ocean at the SAZ, 44°S – 58°S and 40°S – 50°S. ORCA2 annual means are almost double at 44°S – 58°S relative to the SAZ expected for the Indian Ocean. Note that the basin air-sea CO_2 flux contribution to the zonal mean is not based on PERIANT05. The Atlantic Ocean generally acts as CO_2 weak source in Atlantic Ocean in PERIANT05.

Table 4.3 Air-sea CO_2 flux ($PgCyr^{-1}$) annual means for the Pacific (P), Atlantic (A) and Indian (I) at 44°S – 58°S, 40°S – 50°S, Sub Antarctic Zone (SAZ). ORCA2 annual means are almost as double at 44°S – 58°S relative to the SAZ expect for the Indian Ocean. In PERIANT05 annual means show minimal difference between Atlantic -Indian Oceans at the 44°S – 58°S relative to the SAZ and in contrast to ORCA2 at 44°S – 58°S is doubles in Indian Ocean

Region	ORCA2	PERIANT05
SAZ zonal mean	**-0.582±0.02**	**0.215±0.07**
SAZ Pacific	-0.253±0.02	0.146±0.05
SAZ Atlantic	-0.170±0.01	-0.0098±0.02
SAZ Indian	-0.160±0.01	0.0794±0.01
44S-58S zonal mean	**-0.60±0.02**	**0.219±0.07**
44S -58S Pacific	-0.219±0.01	0.121±0.03
44S -58S Atlantic	-0.186±0.02	0.015±0.03
44S -58S Indian	-0.196±0.01	0.084±0.02
40S-50S zonal mean	**-0.460±0.03**	**0.094±0.04**
40S -50S Pacific	-0.167±0.01	0.0391±0.02
40S -50S Indian	-0.145±0.01	0.0753±0.01
40S -50S Atlantic	-0.148±0.01	-0.0204±0.02

4.5 Wind Speed Climatology

This section compares the wind speed climatology over the 1993 – 2006 in ORCA2 and PERIANT05

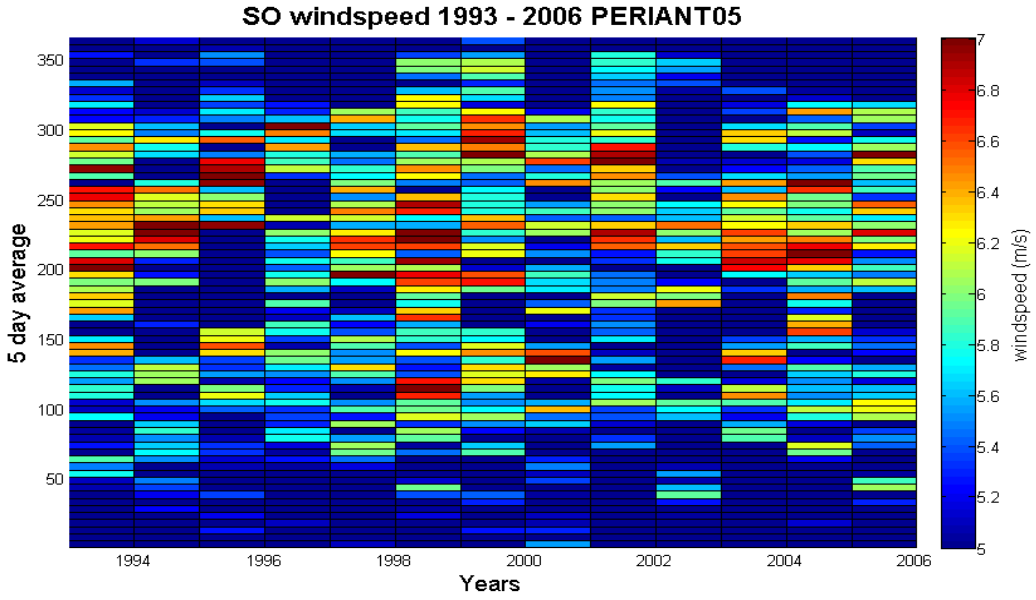

Figure 4.22 PERIANT05 Southern Ocean (SO) 5 day average wind speed (ms^{-1}) 1993 - 2006, SO here defined as south 30°S. PERIANT05 show slightly higher average wind speeds autumn-spring compared to summer (Wind product: ERA interim).

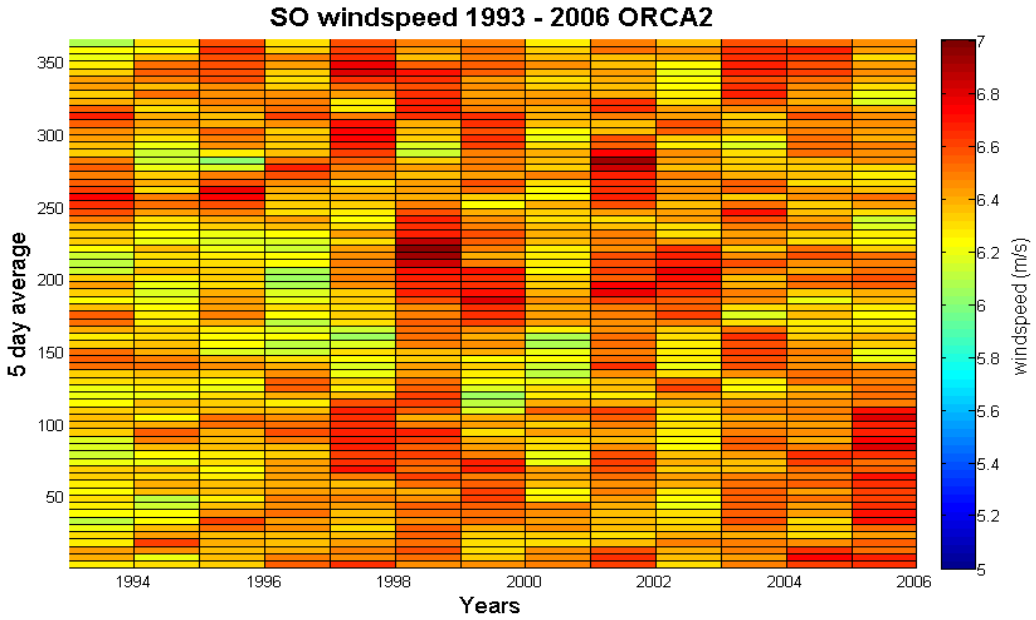

Figure 4.23 ORCA2 Southern Ocean (SO) 5 day average wind speeds (ms^{-1}) 1993 – 2006, SO here defined as south of 30°S, ORCA2 average winds are above 6 ms^{-1} in all the years. (Wind product: CORE IIb).

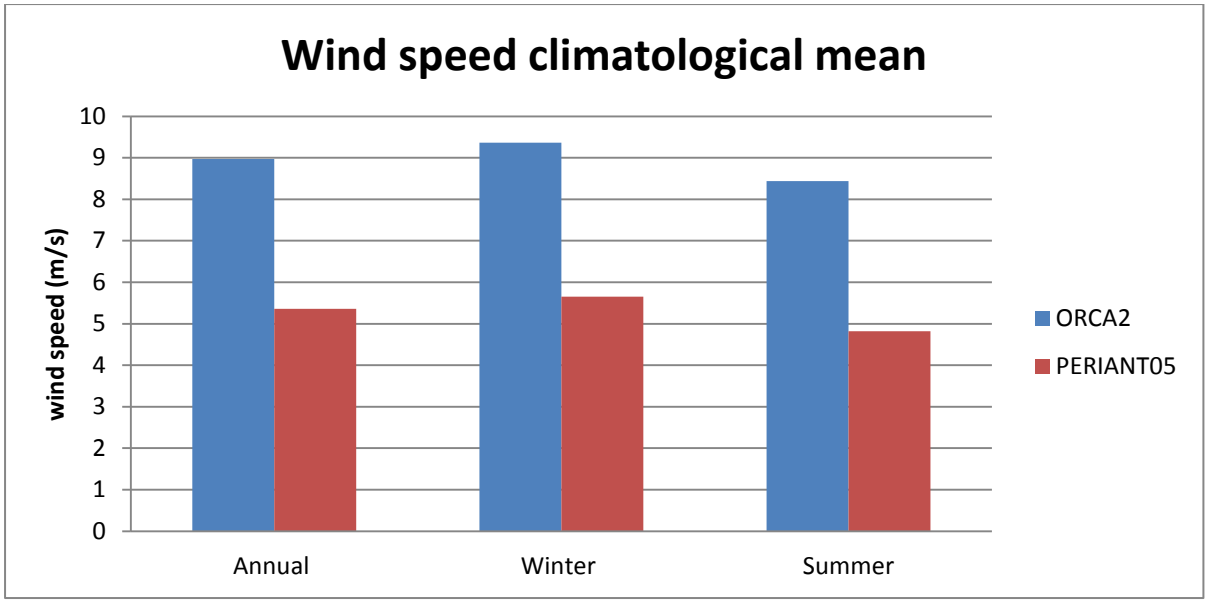

Figure 4.24 Wind speed (ms^{-1}) climatological means over 1993 – 2006 for ORCA2 and PERIANT05 model output. ORCA2 have higher average wind speed than PERIANT05, wind speeds are slightly higher in winter (May-Aug) relative to summer (Nov – Feb) in both ORCA2 and PERIANT05.

The climatological annual mean wind speed of ORCA2 (9 ms^{-1}) is relatively higher than that of PERIANT05 (5.7 ms^{-1}), figure 4.24. PERIANT05 consistently show underestimation of transfer velocity (*k*) with relative to T09 observations and ORCA2 (Figure 4.12-16) which emerges from low speeds as shown above (figure 4.22 – 23). Given that Ekman transport plays an important role in the air-sea CO_2 fluxes of the SO (Ito et al., 2010), these low wind speeds in PERIANT05 might be playing an important role in the misrepresentation of the spatial air-sea CO_2 fluxes variability in the SAZ (figure 4.2). Furthermore given that the strength of wind speed play a key role in the northward advection of subsurface CO_2 in SO (accounts for about 50% of the advected CO_2; Ito et al., 2010), the underestimated of wind speeds in PERIANT05 might have major implications on the subsurface transport and storage of anthropogenic CO_2 and hence poor representation of air-sea CO_2 variability. Although not explicitly quantified in study, it has been previously shown that piston velocity exert a major control in the seasonal variability of air-sea CO_2 fluxes (Bolin and Eriksson 1958; Sarmiento et al., 1992). Therefore by direct consequence the underestimation of transfer velocities (i.e. wind speed) in PERIANT05 with relative T09 observation might also be responsible for poor correlation of the seasonal cycle of air-sea CO2 flux with T09 observations at the SAZ (figure 4.17). In ORCA2 on the contrary is it speculated that elevated wind speed as shown above might be accelerating surface heat loss which further strengthen CO_2 uptake and hence the CO_2 in-gassing bias in ORCA2 , figure 4.2.

5. Discussion

This chapter will discuss the findings of this study in accordance with the above mentioned objectives. Sections of this chapter are organized as follows;

- Section 5.1 discusses a characterization of the air-sea CO_2 flux seasonal cycle and annual air-sea CO_2 fluxes at the Lenton 2013 RECCAP boundaries, comparing the model output of ORCA2, PERIANT05 and Lenton et al., 2013 results with respect to T09 observations.
- Section 5.2 discusses the effect of boundary definition in resolving the air-sea CO_2 flux seasonal cycle and annual air-sea CO_2 fluxes in ORCA2 and PERIANT05.
- Section 5.3 discusses basin scale contrasts to the mean zonal seasonal cycle: the contribution of the Pacific, Atlantic and Indian basins to the zonal mean air-sea CO_2 flux seasonal cycle and annual CO_2 flux in the SAZ.

5.1 Air-sea CO_2 flux seasonal cycle: a comparison to Lenton et al., 2013

In this section the seasonal cycle of air-sea CO_2 flux and annual CO_2 fluxes results are compared with findings of Lenton et al., 2013 (L13) in regions of similarly defined boundaries (Lenton 2013 RECCAP boundaries). The objective of this section is to assess the reproducibility of results of this study with reference to the biogeochemical models (BGMs) output in L13 (i.e. CCSM_BEC, CCSM_ETH, CSIRO, NEMO Plankton 5 and NEMO PISCES) and T09 observations for the year 2000. The subsequent analysis focuses on comparison of the phase, magnitude and drivers of the air-sea CO_2 flux seasonal cycle.

5.1.1 Seasonal cycle at 44°S – 58°S

In T09 observations CO_2 in-gassing was found to decline at a constant rate between Jan – Mar driven by weakening of CO_2 surface solubility (K_0) as Sea Surface Temperature (SST) increases in midsummer (see figure 5.1). Between Mar-Sept, CO_2 in-gassing was found to continue declining at weaker slope independent of the decrease in SST towards winter. At this point the influence K_0 to air-sea CO_2 fluxes is overpowered by strong ΔpCO_2 due to entrainment of subsurface DIC saturated water masses below the Mixed Layer Depth (MLD) as the buoyancy flux weakens towards winter. Air-sea CO_2 flux continues declining until towards end of winter when it outgasses for about a month (Sept-Oct) after which the CO_2 flux increases into the ocean at the onset of biological CO_2 uptake in spring. Between Sept-Dec CO_2 in-gassing strengthens as biological CO_2 uptake matures given the favorable conditions i.e. presence of sunlight, nutrients and stratification, see figure 5.1. This result is consistent with previous studies in the SO, suggesting that primary production plays a dominant role

in the air-sea CO_2 flux in summer and convective mixing dominates CO_2 outgassing in winter, (Metzl et al., 2006, 2009; Lenton et al., 2012; Solokov and Rintoul 2007).

The seasonal cycle of air-sea CO_2 flux in T09 observations computed in this study were generally found to be similar to those computed in L13. Given that both are computed from the same dataset, it is encouraging that L13 was reproduced in observations showing agreement with the computational methods used in this study.

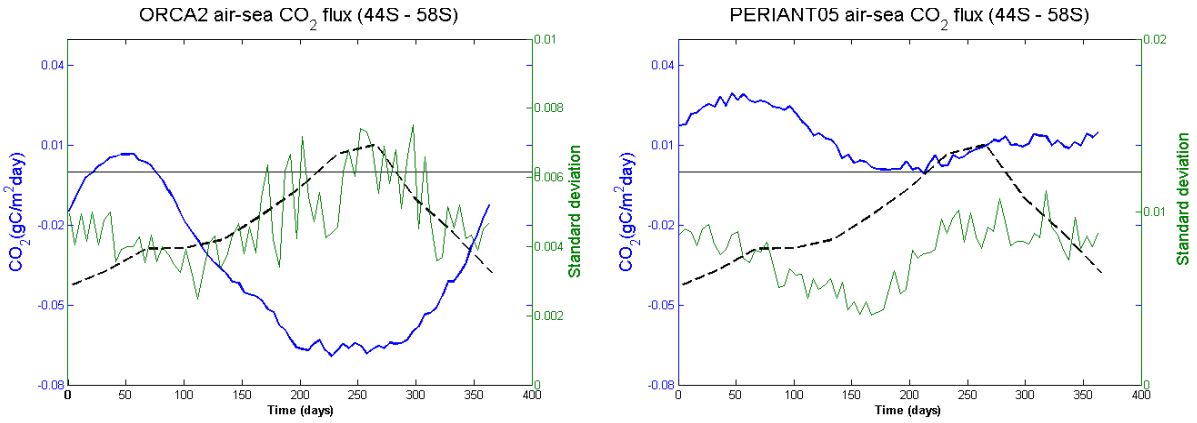

Figure 5.1 The air-sea CO_2 flux seasonal cycle of ORCA2 and PERIANT05 (blue) with the standard deviation (green) at the sub-region 44°S – 58°S. The dotted line shows T09 observations air-sea seasonal cycle for same sub-region. The seasonal cycle of ORCA2 is asymmetric to the observations for most of the year. PERIANT05 roughly simulate observations air-sea CO_2 flux seasonal cycle phasing Jan - Sept, however with different magnitudes. Negative reflect fluxes into the ocean.

In ORCA2 the seasonal cycle of air-sea CO_2 flux was found to be out of phase with respect to the T09 observations and the (Median Absolute Deviation) MAD of the BGMs from L13 for most parts of the year. Between Jan-Mar, ORCA2 seasonal cycle however has similar phasing with T09 observations but with different magnitudes, figure 5.2a. The period between Jan –Mar, where ORCA2 agrees with observations, air-sea CO_2 fluxes are dominantly driven by CO_2 surface solubility. The agreement in air-sea CO_2 flux phasing at this zone suggest that the seasonal variability of K_0 in ORCA2 and T09 observations are similar, however in the absence of other drivers of air-sea CO_2 fluxes, K_0 continues to drive the air-sea CO_2 fluxes seasonal cycle throughout the year in ORCA2. And hence the strong negative correlation of ORCA2 (r^2 = -0.62) seasonal cycle (air-sea CO_2 flux) with T09 observation is attributed to its poor seasonal interplay of drivers of air-sea CO_2 fluxes i.e. mixing and biological processes, see table 4.4. Instead ORCA2 air-sea CO_2 flux seasonal cycle does not show the effect of primary production in summer, as observed in the T09 observation; air-sea CO_2 fluxes instead decreases following SST variability. The effect of vertical mixing in winter is also not explicitly visible in ORCA2; during the winter season ORCA2 shows a counterintuitive increase of CO_2 in-gassing contrasting T09 observations and literature. The increase of ORCA2 air-sea CO_2 influx in winter is

however consistent with the decrease in SST and strengthening of K_0. To this extent the seasonal cycle of air-sea CO_2 flux in ORCA2 is strongly correlated with SST (r^2 = 0.97) and hence the main driver. This postulation explains the agreement of the air-sea CO_2 flux seasonal cycle of ORCA2 withT09 observations between Jan-Mar when the air-sea CO_2 flux is dominantly K_0 driven. This argument is further explored later in the text.

In PERIANT05 the seasonal cycle of air –sea CO_2 flux was also found to be negatively correlated with T09 observations at the zone 44^{o}S – 58^{o}S (r^2 = - 0.42). However though both ORCA2 and PERIANT05 are negatively corrected with observations at this zone, their corresponding seasonal cycles phasing are not similar. ORCA2 seasonal cycle shows a strong positive correlation with SST (r^2 = 0.97) while PERIANT05 is not as strongly correlated to SST (r^2 = 0.62) though both has a similar SST seasonal trend. The difference here is that ORCA2 seasonal cycle is similar to the SST trend throughout the year while PERIANT05 only shows correlation to SST seasonal cycle only for the first half of the year (Jan –Jun) and the month of December. As in ORCA2, PERIANT05 seasonal cycle (air-sea CO_2 flux) shows similar phasing with T09 observations between Jan – Mar where K_0 is the dominate driver. In contrast to ORCA2 however, PERIANT05 shows a strengthening of CO_2 outgassing between Jul- Sept making it similar to T09 observations in phase and magnitude for this time zone.

As stated in above the rise in CO_2 outgassing in winter is associated with convective mixing when the mixed layer depth deepen and subsurface rich DIC mix with surface waters. It is therefore evident that PERIANT05 seasonal cycle does pick up the effect of winter convective mixing. This postulation is also supported by the correlation of the winter CO_2 outgassing with the deepest MLD in both PERIANT05 and T09 observations, depicting optimum mixing when the buoyancy flux has weakened (see figure 4.12). Though PERIANT05 pick up the effect of winter convective mixing and late summer SST driven CO_2 fluxes, it also does not show the effect of biological CO_2 uptake during spring –summer. Instead during the period (Oct – Dec) where T09 observations shows a strengthened CO_2 in-gassing associated with biological CO_2 drawdown, PERIANT05 shows a constant CO_2 outgassing and eventually increases in December, see figure 5.1. The strengthening of CO_2 outgassing during December in PERIANT05 is thought to be due to the decrease of CO_2 solubility (K_0) in surface waters because SST increases as summer progresses. Note that at this time zone PERIANT05 seasonal cycle phasing is similar to ORCA2 and both are influenced by SST.

In conclusion the seasonal cycle of air-sea CO_2 flux in both ORCA2 and PERIANT05 was found not to reproduce the mean results of BGMs in L13 and T09 observations at the zone 44^{o}S – 58^{o}S. Furthermore ORCA2 and PERIANT05 CO_2 flux seasonal cycles were found show some differences in the seasonal cycle phasing between Jul – Sept, where PERIANT05 was found to be similar to be to

T09 observations , however not the case in ORCA2. This difference shows that PERIANT05 seasonal cycle is sensitive to the effect of winter convective mixing but not to biological CO_2 drawdown in summer; ORCA2 seasonal cycle is however insensitive to both convective mixing and biological CO_2 drawdown. It is worth mentioning that air-sea CO_2 flux seasonal cycle of ORCA2 is not distinctly present in L13 results. The comparison made here is based on the anomaly of all five BGMs applied in L13.

5.1.2 Seasonal cycle south of 58°S

In T09 observations the seasonal cycle of the air-sea CO_2 flux south of 58°S was found to be slightly different from that at 44°S- 58°S. For example the winter CO_2 outgassing window extended for 6 months (Jun-Dec) compared to a month at the zone 44°S -58°S (Oct-Sept), the spring -summer biological CO_2 uptake extended until end of summer in February as opposed to midsummer (December) for the zone 44°S -58°S, see figure 5.2.

In ORCA2 the seasonal cycle of air-sea CO_2 flux at this sub-region was found to be out of phase with T09 observations between Jan-Apr, but has similar phasing (with different amplitudes) for rest of the year (May-Dec). To this extent the ORCA2 seasonal cycle of air-sea CO_2 flux has a weak positive correlation with observations (r^2 =0.18), see table 4.4. The reason for agreement of the air-sea CO_2 flux seasonal cycle phasing of ORCA2 with observations between May-Dec remains unclear, it is however speculated that the deeper winter MLD of ORCA2 at this sub-region relative to T09 observations might be responsible.

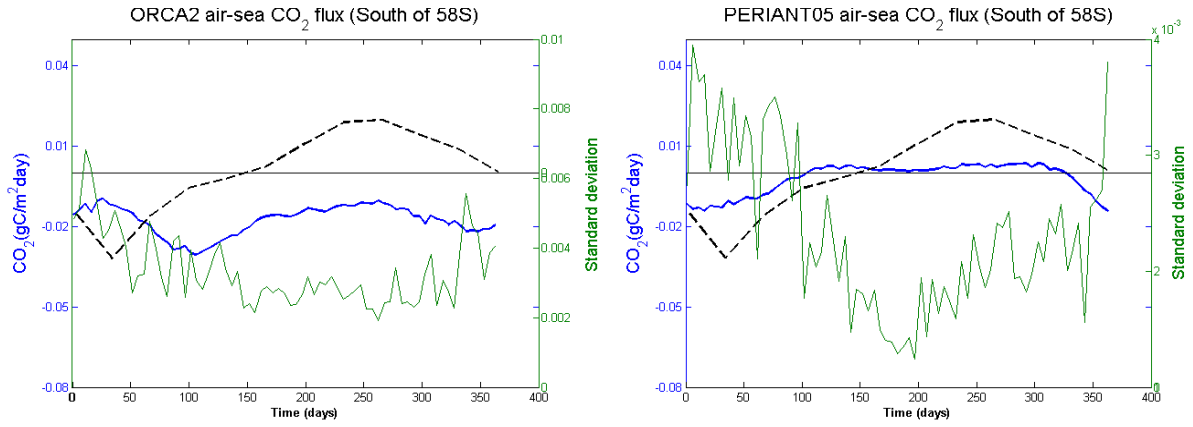

Figure 5.2 The air-sea CO_2 flux seasonal cycle of ORCA2 and PERIANT05 (blue) with the standard deviation (green) the sub-region south 58°S. The dotted line shows T09 observations air-sea seasonal cycle for same sub-region. The seasonal cycle of ORCA2 has a similar phasing with observations between Mar-Dec but with different amplitude. PERIANT05 CO_2 flux seasonal cycle shows a similar phasing for most part of the year observations. Negative reflect fluxes into the ocean.

The seasonal cycle of air-sea CO_2 flux in PERIANT05 was found to be positively correlated with observations (r^2 = 0.62) at this zone, table 5.1. This results contrast findings of L13 BGMs at this sub-

region, the BGMs used L13 generally showed a poor correlation with T09 observations at this zone (south of 58^{o}S), see figure 5.2 & 5.3. The poor simulation of air-sea CO_2 fluxes at the polar zone still remains an important challenge in most ocean models (Gruber et al., 2009; Metzl et al., 2009; Lenton et al., 2013). And hence the good correlation of PERIANT05 air-sea CO_2 fluxes with observation south of 58^{o}S might aid in the understanding of drivers of air-sea CO_2 fluxes in a seasonal scale. Though the PERIANT05 seasonal cycle is not completely analogous to T09 observations, it captures the three main features of the seasonal cycle depicted in T09 observations i.e. (i) weakening of the CO_2 in-gassing between Jan – Mar, (ii) constant CO_2 flux during the presence of ice: May – Oct in PERIANT05 (Sept in T09 Observations) and (iii) the increase of CO_2 uptake between Nov – Dec biologically driven. According to the conceptual model of Rysgaard et al 2011, the capping of air-sea CO_2 fluxes in Sept is caused by the closing of ice pores due to ice expunction and the increased in CO_2 uptake in summer is due to primary production mentioned above. Rysgaard et al., 2011 suggest that formation - dissolution of ice and brine solution is the main driver of the air-sea CO_2 fluxes in this zone. This postulation is confirmed in subsequent paper (Mongwe et al., 2014) following this study. The mechanistic understanding of the drivers of air-sea CO_2 fluxes south of 58^{o}S is still forms an important missing gape in global carbon budget and hence the use of PERIANT05 to harvest a deeper mechanistic understanding is an important future endeavor. The lack of in situ measurements in this area among others factors has been a key factor to the poor performance of ocean models in this sub-region and hence lack of mechanistic understanding in the processes driving the CO_2 flux at a seasonal scale. Therefore processes that models need to resolve are still poorly understood in this region (Gruber et al., 2009). Most of the observations available in these regions are only in summer with some regions yet to be sampled (Takahashi et al., 2009; Lenton et al., 2012). In a subsequent paper (Mongwe et al., 2014) following this study a more detailed analysis is covered including the role of DIC and Alkalinity in the seasonal cycle of air-sea CO_2 fluxes.

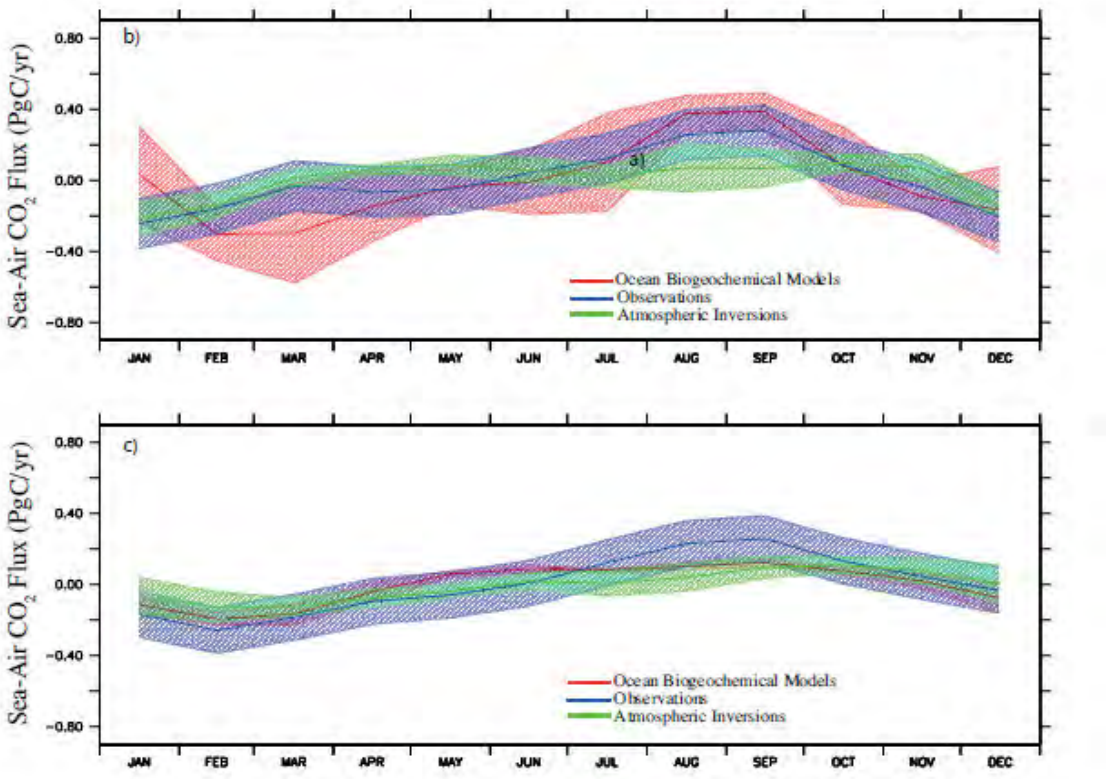

Figure 5.3 The air-sea CO_2 flux seasonal cycle anomaly from the observations (blue), ocean biogeochemical model (red) and atmospheric inversion models (green) from Lenton et al., 2013. The top figure (b) is the zone 44°S – 58°S and bottom (c) is the sub-region 58°S – 75°S. Negative reflect fluxes into the ocean.

5.1.3 Annual fluxes at 44°S – 58°S

For T09 observations a figure of -0.44 $PgCyr^{-1}$ was obtained for the mean zonal annual CO_2 flux for the zone 44°S – 58°S. This value is not significantly different from -0.32±0.16 $PgCyr^{-1}$ obtained in L13, given that both annual fluxes were calculated from the same data set i.e. Takahashi et al., 2009. Although the two values are not statically different given the large standard deviation (0.16) in L13, the reason for the difference of 0.12 $PgCyr^{-1}$ between the two values remain unclear given that both are calculated from the same dataset.

In ORCA2 an annual air-sea CO_2 flux of -0.60±0.02 $PgCyr^{-1}$ was obtained. This value is significantly larger than the MAD of the five BGMs from L13 (-0.26 ± 0.2 $PgCyr^{-1}$). ORCA2 overestimation of the annual flux at this zone is consistent with the model output of NEMO-Planton-5 and NEMO- PISCES BGMs in L13 (figure 2.8). Out of the five BGMs in L13 (CCSM_BEC, CCSM_ETH, CSIRO, NEMO-Plankton 5 and NEMO-PIESES), the annual CO_2 fluxes of NEMO-Planton-5 and NEMO- PISCES was found to be higher than the other three BGMs. For example NEMO-PISCES provided a mean annual CO_2 flux of -0.8 $PgCyr^{-1}$ for 44°S – 75°S in L13. In this study a value of -0.89 $PgCyr^{-1}$ was obtained for the mean accumulative annual CO_2 flux of the total climatological mean south of 44°S. The 0.09

PgCyr^{-1} difference can be attributed to the intrinsic variability of the model. It also worth mentioning that the climatological annual air-sea CO_2 fluxes in this study were computed over half the time period (1993 – 2002) used in L13 (1990 – 2009). The over overestimation of CO_2 annual uptake in ORCA2 is thought to due to its singular SST driven air-sea CO_2 fluxes creating a poor representation of world oceans spatial variability of air-sea CO_2 fluxes. For example the absence of the effect of convective mixes in the seasonal cycle of air-sea CO_2 flux by direct consequence increase the annual CO_2 in-gassing bias. ORCA2 misrepresentation of the impact mixing and biological processes to CO_2 fluxes challenges the accuracy of its annual fluxes and future predictions.

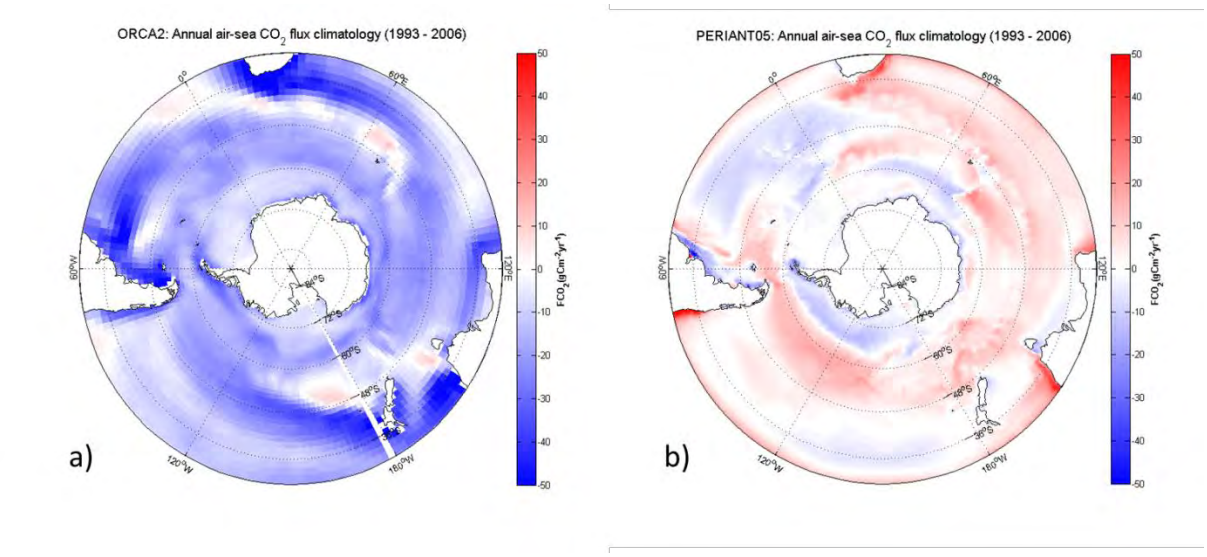

Figure 5.4 Spatial maps of the climatological annual mean air-sea CO_2 flux of PERIANT05 (0.5^o x 0.5^o); a) and ORCA2 (2^o x 2^o); b) of NEMO PISCES, in gCm^{-2}yr^{-1}. Note that the spatial distribution of air-sea CO_2 fluxes in ORCA2 and PERIANT05 different, ORCA2 compares better with T09 observations north of 50^{o}S and PERIANT05 compares better with observations south of 48^{o}S. Negative reflect fluxes into the ocean.

In PERIANT05 the mean annual of CO_2 flux of 0.219±0.07 PgCyr^{-1} was obtained for the zone 44^{o}S – 58^{o}S. This annual flux is not comparable to both the MAD of the five BGMs (-0.26±0.2 PgCyr-1) in L13 and T09 observations (-0.44 PgCyr^{-1}). PERIANT05 shows a general CO_2 outgassing bias in this zone, figure 5.4. It is therefore evident that magnitude of PERIANT05 air-sea CO_2 fluxes compares poorly to observations at the zone 44^{o}S – 58^{o}S in both the seasonal cycle and annual fluxes.

Interestingly note that NEMO PIESCES was able to partly resolve T09 observations air-sea CO_2 fluxes features south of 48^{o}S at the PERIANT05 (0.5^o x 0.5^o) configuration but does poorly so in the ORCA2 (2^o x 2^o) configuration. However instead ORCA2 better resolve observations air-sea CO_2 fluxes north of 50^{o}S in ORCA2 where PERIANT05 is showing an outgassing bias, figure 5.4. From the above results it is evident PERIANT05 air-sea CO_2 fluxes has improved the spatial variability of air-sea CO_2 fluxes south of 48^{o}S with relative to ORCA2. The improved spatial variability of the CO_2 fluxes in PERIANT05

however comes at the cost of a strong outgassing bias north of 48°S. These opposing effects cancel each other and to this extent simulations of air-sea CO_2 fluxes in the PERIANT05 (0.5° x 0.5°) configuration was not found to significantly improve resolving observations air-sea CO_2 fluxes relative the course resolution ORCA2 (2° x 2°) configuration at the zone 44°S – 58°S. PERIANT05 was however found captures two [(i) Jan - Mar K_0 driven air –sea CO_2 fluxes, (ii) effect of winter convective mixing] of the three main features [(i), (ii) and (iii) summer biological CO_2 uptake] of the seasonal cycle of air- sea CO_2 flux in this zone.

Table 5.1 Shows the correlation coefficients of the seasonal of air-sea CO_2flux of ORCA2 and PERIANT05 model output with T09 observations at the geographic, Lenton 2013 and dynamic boundaries. Note that ORCA2 shows a strong negative correlation with observations at the zone 44°S – 58°S and PERIANT05 also shows a negative correlation at this zone. Interestedly both ORCA2 and PERIANT05 show no correlation with T09 observation at the SAZ. This shows that the use of dynamic boundaries does not improve observations seasonal cycle of air-sea CO_2 in both ORCA2 and PERIANT05.

Region	ORCA2	PERIANT05
44°S-58°S	-0.63	-0.41
40°S-50°S	-0.21	-0.08
SAZ	0.07	-0.01
58°S south	0.18	0.62
50°S south	-0.32	0.49
ATZ	-0.15	0.07

5.1.4 Annual fluxes south of 58°S

T09 observations at this region provide a mean annual flux of 0.049 $PgCyr^{-1}$ which is not significantly different form 0.04±0.02 $PgCyr^{-1}$ obtained in L13, see table 5.1.

The annual mean CO_2 flux of ORCA2 (-0.29±0.03 $PgCyr^{-1}$) was also found to be comparable to the one obtained in L13 i.e. -0.25 $PgCyr^{-1}$ for NEMO-PISCES and both overestimate the annual CO_2 uptake with respect to the T09 observations. As consistent with the seasonal cycle, PERIANT05 air-sea CO_2 annual flux (-0.002 $PgCyr^{-1}$) was found well compares with T09 observations at this zone, see table 4.4.

The ORCA2's weakness with respect to entrainment of subsurface CO_2 enriched waters during the winter season has a profound effect in the annual CO_2 uptake simulated by the model. For example, during the autumn-winter seasons when the MLD deepens inducing entrainment at weakening of buoyance of flux, if the seawater below the mixed layer is not CO_2 saturated as in ORCA2, waters of net lower DIC concentrations are instead entrained. Entrainment of low DIC waters masses however has contrasting implications, instead the newly entrained waters enhances the ability of surface waters to dissolve more atmospheric CO_2 given the low CO_2 activity in the surface waters. Given that

ORCA2 has higher wind speeds (see figure 4.22 & 4.23) with relative to relative PERIANT05, high speeds accelerate surface heat loss in ORCA2 during the winter season which further strengthens K_0 and hence the strong CO_2 uptake. Furthermore high wind speeds in ORCA2 strengthens the gas transfer velocity (*k*) which further favours CO_2 in-gassing. This proposition is supported by the higher CO_2 uptake in the winter climatological mean CO_2 fluxes in ORCA2 compared to summer in the SO (figure 5.7). The disagreement of ORCA2 annual fluxes with T09 observations in figure 5.5 shows that ORCA2 air-sea CO_2 fluxes poorly simulate the true processes controlling CO_2 circulation in the SO.

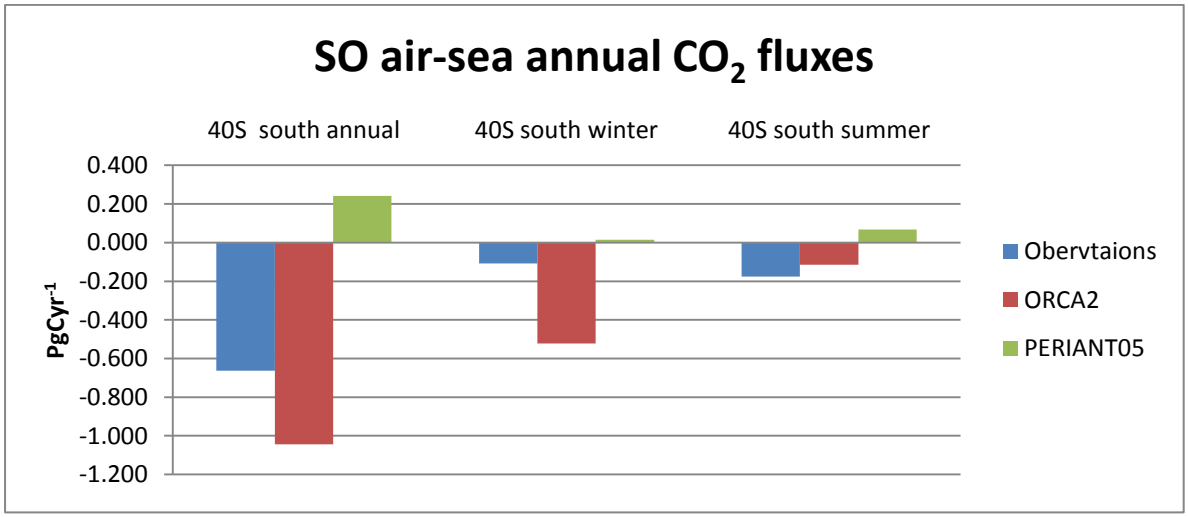

Figure 5.5 Decadal (1993- 2002) CO_2 fluxes for the total annual, winter and summer fluxes. ORCA2 generally overestimate the annul influx relative to observations while PERIANT05 underestimate the fluxes**.** Southern Ocean is here defined as south of 40°S.

From these results it is considered evident that L13 results were reproduced in ORCA2 and T09 observations in this study. PERIANT05 results have shown a sharp contrast to L13 BGMs mean behavior, the seasonal cycle of air-sea CO_2 flux in L13 BGMs was found to compares better to T09 observations in the SAZ and poorly so south of 58°S, however PERIANT05 shows the opposite. The poor comparison of ORCA2 seasonal cycle of air-sea CO_2 flux with T09 observations may be attributed to two main defaults i.e. the absence of vertical mixing in winter and primary production in summer. At this stage disentangling the effect of resolution from the absence of DIC entrainment and summer biological CO_2 uptake in the ORCA2 seasonal cycle of air-sea CO_2 flux remains a challenge.

In addition to the effect of resolution, appropriate boundary definition has been previously highlighted is a key factor in assessing CO_2 fluxes in SO due to the high spatial variability of CO_2 fluxes in the SO (Metzl et al., 2006, 2009; Lenton et al. ,2006, 2013). To this extent some studies have previously questioned the use of geographic boundaries since they do not delimit regions of distinct

air-sea fluxes (e.g. Séférian et al., 2012); the next section investigates this phenomena in ORCA2 and PERIANT05 model outputs.

5.2 Air-sea CO_2 flux seasonal cycle: boundary sensitivity

This section investigates the effect of boundary definition in resolving the air-sea CO_2 flux seasonal cycle and mean annual CO_2 fluxes in the Southern Ocean (SO). In doing so, the air-sea CO_2 flux seasonal cycle and annual CO_2 fluxes are assessed relative to the T09 observations for three different zonal boundary definitions in the SO i.e.

(i) Lenton 2013 RECCAP boundaries (44°S – 58°S and south of 58°S),

(ii) Geographic boundaries (40°S – 50°S and south of 50°S) and

(iii) Dynamic boundaries (SAZ and AZ), whereby the Sub-Antarctic Zone (SAZ) and Antarctic Zone (AZ) are defined using climatological frontal positions. SAZ in this study is defined as the region between the Subtropical Front (STF) and the Polar Front (PF) and the AZ is the region south of the PF to the Antarctic continent, figure 5.6.

The subsequent analysis focuses on a comparison of the phase, magnitude and drivers of the air-sea CO_2 flux seasonal cycle.

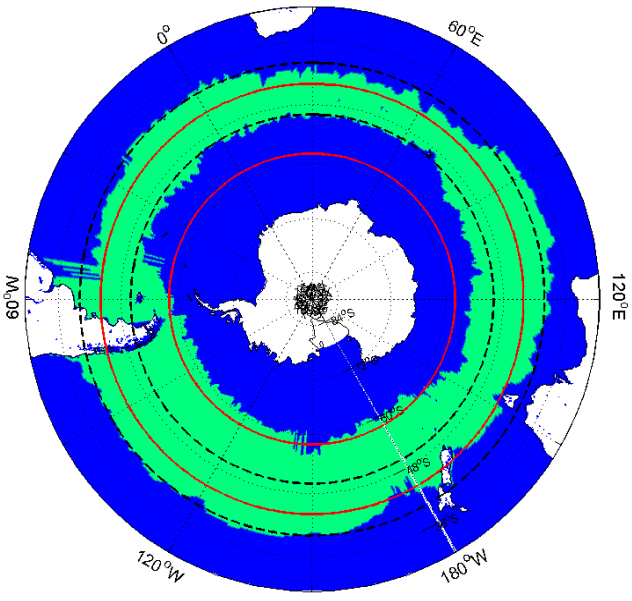

Figure 5.6 Zonal regions of the Southern Ocean used in this study. The red lines show the Lenton 2013 RECCAP boundaries (44°S – 58°S and south of 58°S); black dotted lines show the geographic boundaries (40°S – 50°S and south of 50°S south). The green sub-region shows the Sub-Antarctic Zone (SAZ), whereby the northern boundary is the subtropical front and southern boundary is the Polar front defined by the SST criteria (Rintoul and Trull 2001). Antarctic zone (ATZ) is blue area south of the SAZ.

5.2.1 Seasonal cycle at 44°S – 58°S, 40°S – 50°S and SAZ

In ORCA2 the seasonal cycle of the air-sea CO_2 flux was found to have a relatively similar phasing in all three sub-regions with some slight differences in amplitude, figure 4.15. For example in the zone 40°S – 50°S, CO_2 in-gassing reach up to -0.075 $gCm^{-2}day^{-1}$ in September and only up to -0.065 $gCm^{-2}day^{-1}$ in the zone 44°S – 58°S and the SAZ. The enhanced CO_2 in-gassing in the seasonal cycle amplitude of the zone 40°S – 50°S is attributed to the strong CO_2 in-gassing observed around 40°S in the western Pacific Ocean and the eastern Indian Ocean south of the Agulhas Return Current of ORCA2, see figure 5.5. The similarity of the seasonal cycle of air-sea CO_2 flux in the zone 44°S - 58°S and the SAZ shows that use of dynamic boundary opposed to the geographic does make a difference in the ORCA2 simulated air-sea CO fluxes. This is because ORCA2 air-sea CO_2 fluxes are relatively spatially uniform, showing CO_2 outgassing bias in most parts of the SO (see figure 5.4).

In T09 observations, the spatial meridional variability of air-sea CO_2 fluxes impose observable differences in the seasonal cycle phasing between three sub-regions defined by the Lenton 2013 RECCAP, geographic and dynamic boundaries, figure 4.15. To this extent, the seasonal cycle of air-sea CO_2 flux in ORCA2 is negatively correlated with T09 observations at the zone 44°S – 58°S (r^2 = -0.6), 40°S – 50°S (r^2 = -0.4) and not correlated with T09 observations at the SAZ (r^2 = 0.07), see Table 4.4. The rigidity of seasonal cycle phasing in ORCA2 between the three sub-regions is attributed to the uniform distribution of air-sea CO_2 fluxes in comparison to T09 observations as mention above.

The observed differences in the seasonal cycle phasing between the three sub-regions in the T09 observations are in agreement with zonal processes influencing the air-sea CO_2 fluxes in accordance to known literature. For example the zone 40°S – 50°S is the region where the subtropical low nutrient waters meet with Antarctic Intermediate Waters (AAIW) which are nutrients rich waters typical of the SO (Sallèè et al., 2006). The meeting of these two water masses therefore favours and sustains seasonal and intra- seasonal primary production strengthening biological CO_2 uptake at this sub-region (Thomalla et al., 2011; Sallèè et al., 2006), figure 5.7. This explains the strong CO_2 in-gassing throughout the year observed in seasonal cycle of T09 observation at this zone, figure 4.15. The absence of such features in ORCA2 further elucidates the lack of biological uptake in the seasonal cycle of air-sea CO_2 flux in ORCA2.

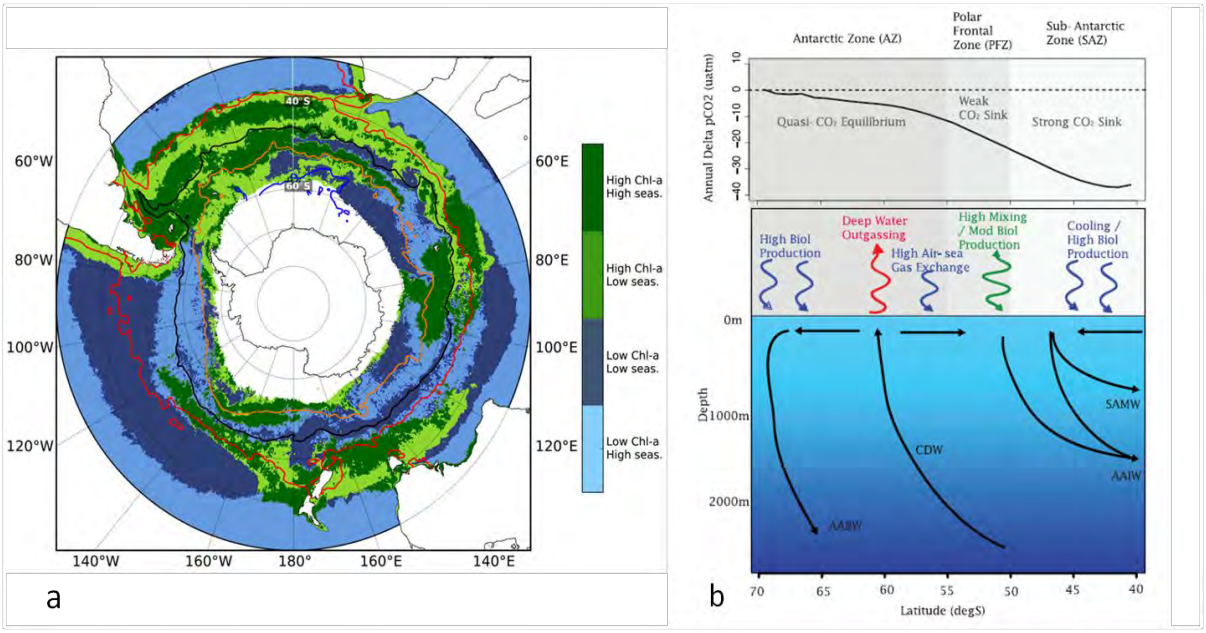

Figure 5.7 The figure on the left a) shows the phytoplankton biomass, blue represent region of low (<0.25 mgm-3) chlorophyll concentration with high seasonal cycle reproducibility (light blue), low seasonal cycle reproducibility (dark blue). Green represents a high chlorophyll concentration (> 0.25mgm-3), with dark green high seasonal cycle reproducibility and light green low seasonal cycle. Mean frontal positions (1998-2007), STF (red), SAF (blank), PF (yellow) and SACCF (pink), Taken from Thomalla et al., 2011. The right figure (b) shows the zonal air-sea CO_2 flux of the Southern Ocean between 40°S – 70°S.

In PERIANT05 the seasonal cycle phasing in zones 44°S – 58°S and SAZ was also found to be similar in phase and magnitude, figure 4.15. This similarity between these two zones is also attributed to the absence of discriminating features between the two boundaries, see figure 5.4. The air-sea CO_2 fluxes spatial map of PERIANT05 only shows contrasting features outside these two zones. For example, potential discriminating features i.e. the strong CO_2 in-gassing at the southern part of the SO only dominates south of 58°S (figure 5.4b) and the CO influx in the Atlantic Ocean includes both boundaries. In the zone 40°S – 50°S PERIANT05 shows some observable difference in the seasonal cycle of air-sea CO_2 flux relative to the zone 44°S – 58°S and the SAZ, this is thought to be because of the greater inclusion of the CO_2 in-gassing occurring at the Atlantic Ocean. This feature is particularly evident for the period Jun-Nov in the seasonal cycle, where the air-sea CO_2 flux remains negative (flux into the ocean) at the zone 40°S -50°S, however at the Lenton RECCAP boundary and dynamic boundary, the CO_2 flux is reversed to a source (positive) from August. Note that though the amplitude of seasonal cycle of air-sea CO_2 flux in PERIANT05 is not comparable to T09 observations, PERIANT05 was able to capture the high production area in the central Atlantic Ocean, this region has been previously reported to have elevated seasonal and intra-seasonal primary production as also stated above (Thomalla et al., 2009, Lenton et al., 2012). The high primary production in this area make it a region of strong CO_2 sink for the most of the year, figure 5.7a elucidate this features more clearly as also shown in observations air –sea CO_2 fluxes in figure 5.4b.

In conclusion it has been shown above that the use of dynamic boundary does not improve resolving the observations seasonal cycle of air-sea CO_2 flux in both ORCA2 and PERIANT05, however T09 observations show significant differences between the three sub-regions (44°S – 58°S, 40°S – 50°S and SAZ). It is therefore suggested that poor zonal boundary definition sensitivity in NEMO PISCES may be the result of poor simulation of observed air-sea CO_2 fluxes in the SO. If the model can better resolve the air-sea CO_2 fluxes in the SO, it is anticipated that boundary sensitivity will be evident in the seasonal cycle of air-sea CO_2 flux in the model outputs as in T09 observations.

5.2.2 Seasonal cycle at the AZ, south of 58°S and south 50°S

In ORCA2 the seasonal cycle of air-sea CO_2 flux was found to be different in the contrasting zones; south of 58°S, south of 50°S and the AZ, figure 5.13. The AZ was found to have comparatively greater amplitude in the seasonal cycle, reaching up -0.05 $gCm^{-2}day^{-1}$ between Apr-Nov compared to only -0.03 $gCm^{-2}day^{-1}$ south of 50°S for the same period. For south of 58°S the seasonal cycle phasing was found to be more similar to T09 observation between Apr-Dec, however with different magnitudes. The seasonal cycle of air-sea CO_2 flux was found to have a weak positive correlation with T09 observations south of 58°S (r^2 = 0.18), the reason for this positive correlation remains unclear. As consistent with L13 the seasonal cycle of air-sea CO_2 flux in ORCA2 at the sub-regions South of 50°S (r^2 = -0.31) and the AZ (r^2 = -0.15) is negatively correlated with T09 observations. Given that ORCA2 air-sea CO_2 fluxes has shown to be solely SST driven, it is speculated that the strong CO_2 uptake observed in this region is mainly due to longer periods of cold surface water influenced by the seasonal presence of ice. Given that this population holds, it will explains the increase of CO_2 flux only observed in summer when K_0 is weakened by warming of surface waters. The cause of the stronger negative amplitude in seasonal cycle amplitude of the dynamic boundary in ORCA2 relative to the two other boundaries remains unclear.

In PERIANT05, the seasonal cycle of air-sea CO_2 flux was found to be following a similar trend in all three zones with minor differences in magnitude, figure 5.16. For example the AZ shows a relatively stronger CO_2 outgassing window between Feb-May compared to two other zones. PERIANT05 seasonal of air-sea CO_2 flux at this sub-regions (polar zone) differ from ORCA2's, PERIANT05 is more in agreement with T09 observations in all three zones compared to ORCA2. As stated above the agreement of PERIANT05 seasonal cycle with T09 observations at this sub-region is an uncommon feature in ocean modeling, most ocean models as been reported to compares poorly with observations south of polar zone. The global ocean modelling community considers the cause of disagreement between the observations and modeled seasonal cycle of air-sea CO_2 fluxes at this sub-region (south of 58°S) an important challenge, (e.g. Gruber et al., 2009, Lenton et al., 2013). In

this study the proposed explanation for the behavior of air-sea CO_2 fluxes in PERAINT05 is that of Rysgaard et al., 2011 as mentioned above; PERAINT05 may be completely capping the air-sea CO_2 fluxes between autumn-spring when sea ice is present in SO. And when ice recedes in summer, primary production kick start the CO_2 biological uptake in the presence of sunlight and nutrients from the brine solution below the ice sheet. This process continues until midsummer when weakened by warming of surface water as summer matures, as K_0 decreases the CO_2 influx is weakened.

5.2.3 Annual fluxes at 44°S – 58°S, 40°S – 50°S and SAZ

In ORCA2 the mean annual CO_2 fluxes were found to generally overestimates CO2 uptake with relative to T09 observations and PERIANT05, -0.60 $PgCyr^{-1}$ 44°S – 58°S, -0.46 $PgCyr^{-1}$ 40°S – 50°S and -0.58 $PgCyr^{-1}$ at the SAZ, table 5.2. As previously stated, this result is consistent with NEMO-Plankton 5 and NEMO-PIESES results from Lenton et al., 2013, where these two model outputs were found to have higher annual CO_2 fluxes. The air-sea CO_2 annual flux of the dynamic boundary is not significantly different from that of the Lenton 2013 RECCAP boundary in as much as their respective seasonal cycles are similar in ORCA2. The difference of 0.02 $PgCyr^{-1}$ obtained between the two region's annual fluxes is attributed to the greater inclusion of the CO_2 outgassing features of ORCA2 south of the Agulhas Return Current in the Indian Ocean and the western Pacific Ocean. These CO_2 outgassing features of ORCA2 coincide with high (Eddy Kinetic Energy) EKE and deep winter MLD zones in the SO, see figure 5.12.

From these premises is suggested that in ORCA2, the saturated CO_2 waters expected to be below the mixed layer, (Sarmiento and Gruber, 2006) are found much deeper. Thus winter entrainment does not reach these waters in ORCA2 and instead only entrain low CO_2 concentrated waters, which ultimately results in more atmospheric CO_2 uptake. It is therefore postulated that the high EKE and deep winter MLD zones are the only regions where saturated CO_2 waters are be brought to the surface, weakening the net CO_2 influx and ultimately outgasses CO_2. From this premise it is further suggested that the weak or complete lack of summer biological CO_2 uptake in ORCA2 is associated with weak entrainment of nutrients from bottom water. This proposition is further supported by higher mean air-sea CO_2 fluxes in winter compared to the summer season in ORCA2 as previously stated. Note that though ORCA2 is not eddy resolving at 2^o x 2^o, it is eddy parameterized, (Madec, 2008). The eddy parameterization here implies that ORCA2 possesses a vertical eddy diffusivity profile (kz) which allow the vertical transport of DIC at high EKE zones though the model does not resolve eddies, figure 5.8.

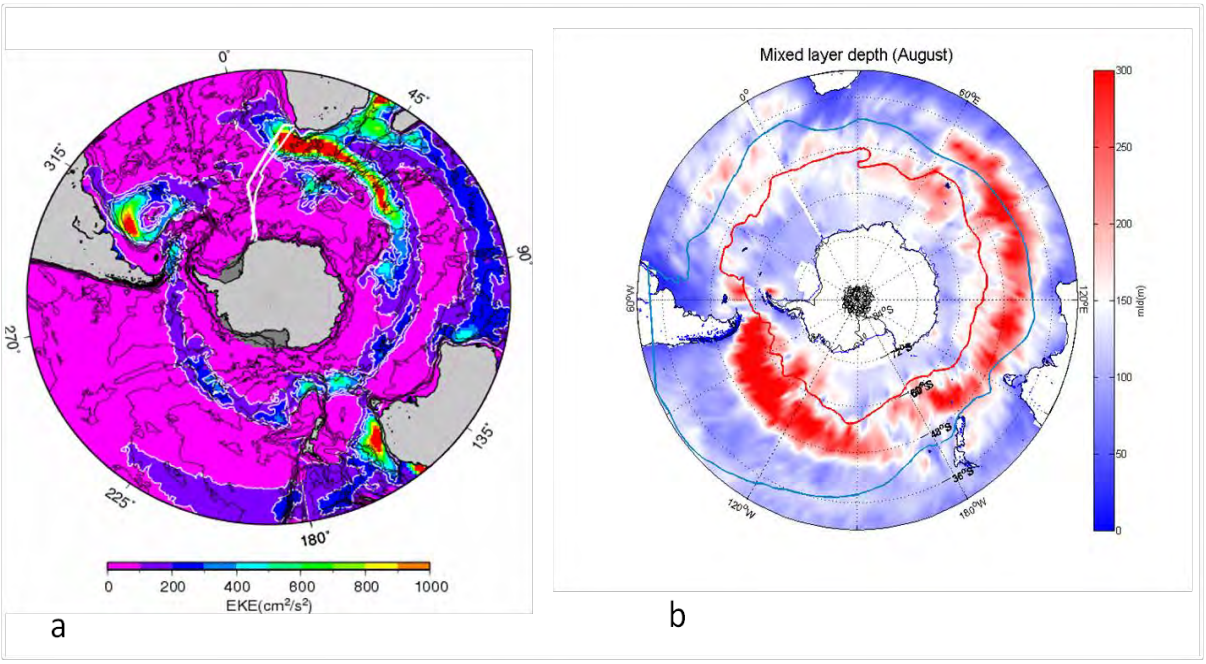

Figure 5.8 The figure (a) on the left show the Eddy Kinetic Energy (EKE) spatial variability in the Southern Ocean and the right figure (b) show the winter Mixed layer Depth in Southern Ocean. Note that the ORCA2 CO_2 outgassing features observed in figure 5.5a coincide with most of the EKE regions and some with deep winter MLD regions.

PERIANT05 gave the annual mean air-sea CO_2 flux of 0.219 $PgCyr^{-1}$ for the zone 44°S -58°S which is not significantly different from 0.215 $PgCyr^{-1}$ in the SAZ (table 5.1); these results are consistent with the observed similarity in seasonal cycle in these two zones. The 0.004 $PgCyr^{-1}$ annual CO_2 flux difference between the 44°S – 58°S and the SAZ is attributed to the more northern extension of the SAZ in the Atlantic Ocean, strengthening the annual fluxes in PERIANT05. The annual CO_2 flux of the zone 40°S – 50°S (0.094 $PgCyr^{-1}$) was found to be smaller compared to the other two regions and this difference is attributed to the in-gassing characteristics of the Atlantic Ocean described previously. The in-gassing-outgassing status of SO waters in the spatial distribution of air-sea CO_2 fluxes compensate each other in the two zones such that the total air-sea CO_2 flux is in quasi-equilibrium. However from the air-sea CO_2 flux spatial map of PERIANT05 in figure 5.4b, it is evident that air-sea CO_2 fluxes are not spatially uniform in the SO though the average zonal seasonal cycle and annual fluxes are similar. It is worth emphasizing that this finding are mainly because the first order problem i.e. the model's poor ability to resolve the air-sea CO_2 fluxes in phase and magnitude in the SO, it is anticipated that if ocean models can better resolve the spatial distribution of air-sea CO_2 fluxes in the SO, the effect of boundary definition will be explicit.

In the T09 observations, the seasonal cycle of air-sea CO_2 flux and annual CO_2 fluxes are different in the Lenton 2013 RECCAP boundaries, geographic and dynamic boundaries, this shows that the set of mechanisms controlling the air-sea CO_2 fluxes are distinct in this different sub-regions. However the

inability of NEMO PISCES to simulate some of these processes and compensation of the spatially heterogeneous in-gassing- outgassing features, limits the difference in annual CO_2 flux of the two regions.

Table 5.2 Summaries the climatological mean annual of air-sea CO_2 flux of the period 1993 – 2006 and observations for 2000 (Takahashi et al., 2012), SAZ (Sub Antarctic zone) and ATZ (Antarctic Zone) of this study and Lenton et al., 2013 results. Negative reflect the flux into the Ocean. The annual flux is given in $PgCyr^{-}1$.

Region	T09 observations	ORCA2	PERIANT05
Annual air-sea CO_2 fluxes at the SAZ			
44S-58S annual	-0.439	-0.600±0.02	0.219±0.07
44S-58S winter	-0.416	-0.342±0.01	0.012±0.01
44S-58S summer	-0.135	-0.049±0.01	0.078±0.02
40S-50S annual	-0.706	-0.460±0.03	0.094±0.04
40S-50S winter	-0.21	-0.270±0.01	-0.005±0.01
40S-50S summer	-0.138	-0.037±0.01	0.043±0.02
SAZ annual	-0.642	-0.582±0.02	0.215±0.07
SAZ winter	-0.2	-0.335±0.02	0.010±0.01
SAZ summer	-0.124	-0.048±0.01	0.083±0.02
Annual air-sea CO_2 fluxes at the polar zone			
58S S annual	0.049	-0.294±0.03	-0.002±0.03
58S S winter	0.077	-0.096±0.01	0.007±0.00
58S S summer	-0.022	-0.051±0.02	-0.024±0.01
50S annual	0.043	-0.633±0.04	0.152±0.06
50S winter	0.101	-0.281±0.02	0.020±0.01
50S summer	-0.039	-0.081±0.03	0.027±0.01
ATZ annual	-0.082	-0.391±0.04	0.025±0.04
ATZ winter	0.087	-0.157±0.01	0.005±0.00
ATZ summer	-0.072	-0.056±0.02	-0.014±0.00
Lenton et al., 2013 results			
Region	**T09 observations**	**BGMs**	**All models (n=26)**
44S- 58S	-0.32±0.16	-0.26±0.20	0.35±0.09
58S – 75oS	0.04±0.02	-0.04±0.09	0.04±0.07

5.3 Air-sea CO_2 flux seasonal cycle: basin contribution comparison

This section compares the contribution of each basin (i.e. Pacific, Atlantic and Indian Ocean) to the zonal mean seasonal cycle of air-sea CO_2 flux and annual CO_2 fluxes. T09 observations are not included in this analysis due to the coarse resolution of the data (4° latitude x 5° longitude) and hence sparse spatial basin coverage. The comparison analysis focuses on the phase, magnitude and drivers of the air-sea CO_2 flux seasonal cycle and annual means.

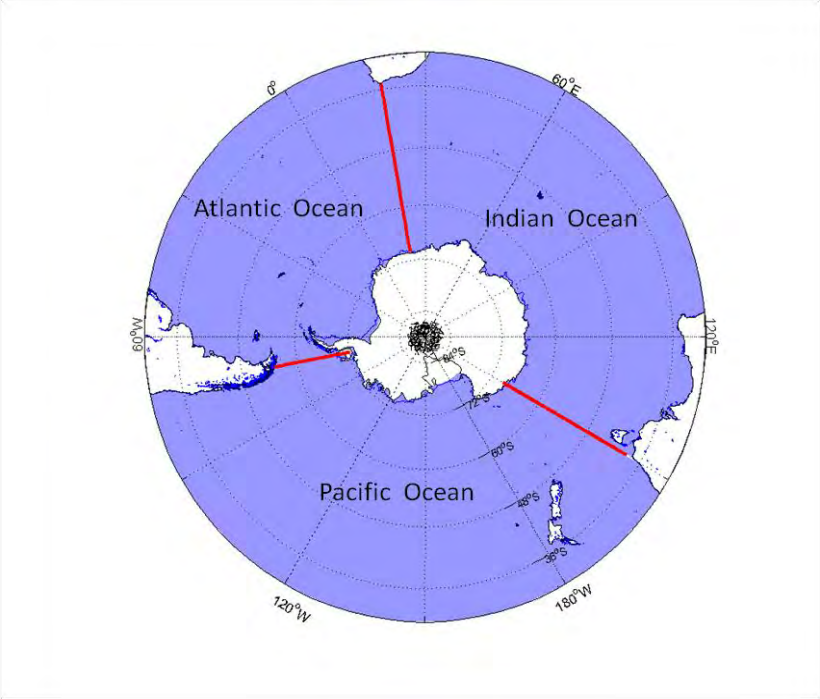

Figure 5.8 Shows the Atlantic, Indian and Pacific Ocean basins as defined in this study, the red lines show demarcations for each basin.

5.3.1 Seasonal cycle

In ORCA2 (44°S – 58°S) the seasonal cycle of air-sea CO_2 of the Pacific Ocean was found to be analogous to the zonal mean seasonal cycle of air-sea CO_2 flux in the Lenton 2013 RECCAP boundary and the dynamic boundary, figure 4.19. The Indian Ocean was found to have a strengthened CO_2 outgassing by an order about 0.02 $gCm^{-2}day^{-1}$ between Jan-Mar relative to the zonal mean seasonal cycle. This increase results in the extension of the CO_2 outgassing window from one month (Feb-Mar) to three months (Jan-Mar) in the Lenton 2013 RECCAP boundary. The same increase was observed in the dynamic boundary, however, instead the air-sea CO_2 flux increased by 0.01 $gC^{-2}day^{-1}$. For the zone 44°S – 58°S the seasonal cycle of the Pacific Ocean was found the most significant difference in the amplitude of the air-sea CO_2 flux seasonal cycle in ORCA2, showing a decrease of up to 0.05 $gCm^{-2}yr^{-1}$ in amplitude of seasonal cycle in spring. This decrease was only observed in the

Pacific Ocean of the zone 44°S – 58°S but not in the SAZ and 40°S – 50°S. The cause of this large decrease in the air-sea CO_2 flux remains unclear, figure 4.19-20.

In PERIANT05 the seasonal cycle of air-sea CO_2 flux was found to be analogous to the zonal mean CO_2 flux in the Indian Ocean, strengthened CO_2 in-gassing in the Atlantic Ocean and weakened CO_2 in-gassing in the Pacific Ocean, figure 4.19. The major cause of the different air-sea CO_2 flux seasonal cycles in the Pacific and Indian Ocean is thought to be mainly due to the PERIANT05 CO_2 in-gassing zone in the Atlantic Ocean. The strengthened CO_2 influx in the Atlantic Ocean may be compensated by the weakened CO_2 in-gassing in the Pacific Ocean when taking the zonal mean CO_2 flux into consideration. The dynamic boundary shows a strengthened CO_2 outgassing in the Atlantic Ocean and this is thought to be because of the more northerly extension of the dynamic boundary as previously stated. The similarity of the air-sea CO_2 flux seasonality in the Indian and Pacific Oceans is attributed to the uniform spatial distribution of air-sea CO_2 flux in these basins.

5.3.2 Annual air-sea CO_2 fluxes

In ORCA2, the basins' contribution to zonal CO_2 flux was found to be different from that of PERIANT05. The ORCA2 basins contribution to the zonal annual air-sea CO_2 flux was found to be roughly equal at the Lenton 2013 RECCAP boundary and geographic boundaries, though the Pacific Ocean had slightly higher annual fluxes, see figure 5.9. In the dynamic boundary however, the Pacific Ocean (-0.253 PgCyr-1) had a larger contribution compared to the Atlantic (-0.170 $PgCyr^{-1}$) and Indian Ocean (-0.16 $PgCyr^{-1}$). This is because the surface area coverage of the Pacific Ocean is significantly larger than that of the Indian and Pacific Ocean in the dynamic boundary, see figure 5.6. From these findings it was considered evident that the contribution of basins to zonal annual fluxes is surface area based in ORCA2, hence the Pacific Ocean annual air-sea CO_2 flux is slightly higher in all three regions. The surface area based annual fluxes in ORCA2 is not surprising given air-sea CO_2 fluxes are uniform in most past of the SO in ORCA2. This finding supports the premise that air-sea CO_2 fluxes of ORCA2 are predominately CO_2 solubility (K_0) driven throughout the year, as opposed to convective mixing in winter and primary production in summer, in accordance with previous studies, (Takahashi et al., 2009, 2012; Lenton et al., 2006, 2013; Metzl et al., 2006, 2009) .

In PERIANT05 the contribution of each basin to the annual air-sea CO_2 flux is not uniform or surface area based, consistent with previous propositions (e.g. Metzl et al., 2006; Lenton et al., 2006). The Atlantic Ocean generally acts as a weak CO_2 source to semi-CO_2 sink in the SAZ; 0.015 $PgCyr^{-1}$ 44°S – 58°S, 0.075 $PgCyr^{-1}$ 40°S – 50°S and -0.01 $PgCyr^{-1}$ SAZ in PERIANT05. The Pacific Ocean was found to be the greatest contributing basin, see table 5.2. The greater contribution of the Pacific Ocean in

PERINAT05 is because of the lack of CO_2 in-gassing features in this basin compared to the Indian and Atlantic Oceans; the air-sea CO_2 flux is rather uniform between 40°S – 60°S in the Pacific Ocean, see figure 5.5.

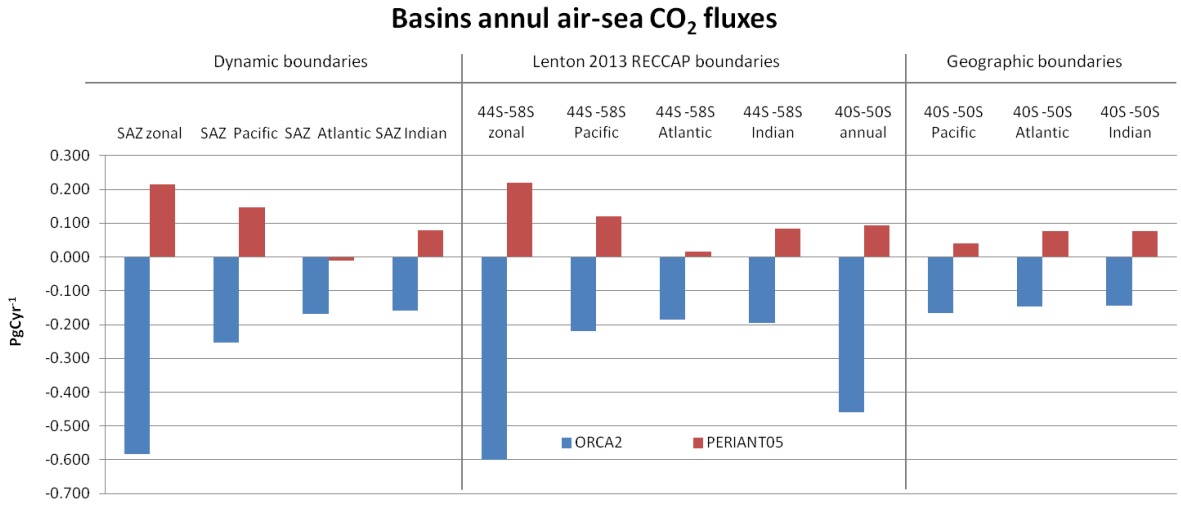

Figure 5.9 Annual air-sea CO_2 fluxes of the pacific, Atlantic and Indian Ocean at the SAZ, 44°S – 58°S and 40°S – 50°S. ORCA2 annual means are almost double at 44°S – 58°S relative to the SAZ expected for the Indian Ocean. Note that basin air-sea CO_2 flux contribution to the zonal mean is not based on PERIANT05. The Atlantic Ocean generally acts as CO_2 weak source in Atlantic Ocean in PERIANT05.

In summary the basins seasonal cycles of air-sea CO_2 flux in ORCA2 were found to be analogous in all three basins (Pacific, Atlantic and Indian basin) of the SO at the dynamic boundary and this due to the lack spatial variability in air-sea CO_2 fluxes of ORCA2. Annual CO_2 fluxes of ORCA2 were found to be surface based mainly due to the spatially uniformity of air-sea CO_2 fluxes in most parts of the SO. In PERIANT05 the seasonal cycle of air-sea CO_2 flux was found to show a strengthened CO_2 influx at the Atlantic Ocean and a weakened CO_2 influx in the Pacific Ocean relative to the zonal mean seasonal cycle at both 44°S – 58°S and the SAZ. Annual CO_2 fluxes of PERIANT05 were found not to be surface area base however influenced by regional processes. The seasonal cycle and annual CO_2 fluxes of PERIANT05 were found to be majorly influenced by the CO_2 in-gassing zone at the Atlantic Ocean in the PERIANT05 model output.

PERIANT05 has shown to simulate some of the observations air-sea CO_2 fluxes spatial features in the Takahashi et al., 2009 dataset. However PERIANT05 has also shown some weaknesses in simulating observations of air-sea CO_2 flux in some parts of the SO, showing a general outgassing bias, the Indian Ocean sector for example. Furthermore PERIANT05 air-sea CO_2 flux was found to compares better to T09 observations south of 48°S and poorly so north of 48°S. The use of the dynamic boundary definition was found not to improve resolving the observations seasonal cycle of air-sea CO_2 flux in both PERIANT05 and ORCA2. In ORCA2 the seasonal cycle of air-sea CO_2 flux was found to

be CO_2 solubility (K_0) solely driven and greatly underestimates the effect of primary production and convective mixing in the seasonal cycle. Boundary definition was found to affect the mean annual CO_2 fluxes of ORCA2 surface area based and play a minimal role resolving observations seasonal cycle of air-sea CO_2 flux. The course resolution in ORCA2 is considered to play a role in the poor air-sea CO_2 flux seasonal cycle sensitivity, however the absence of, or weak winter CO_2 entrainment and primary production in summer considered to be the first order problem of ORCA2 simulation of air-sea CO_2 fluxes in the SO.

Note: A post corrections contribution; upon completions of the analysis it was discovered that the atmospheric pCO_2 dataset use to force the NEMO PISCES model for the PERIANT05 configuration was about an order 10µatm lower than the mean global atmospheric pCO_2, see figure 8.9 in Appendix A. The PERIANT05 configuration used in the study was not ran locally however at the Laboratoire des Ecoulements Géophysiques et Industriels (LEGI),in France. The implications of the underestimated atmospheric pCO_2 forcing will only affect the magnitudes of the air-sea CO_2 fluxes however the seasonal cycle phasing and spatial variability are not affected. Therefore the PERIANT05 air-sea CO_2 fluxes presented here by direct consequence has an underestimation of CO_2 sinks and overestimation of sources and therefore the outcome of the PERIANT05 simulation presented here must be interpreted with this caution.

6. Conclusions

This study firstly investigated the seasonal cycle sensitivity of air-sea CO_2 fluxes to model resolution using the biogeochemical model NEMO PISCES. Secondly it assessed the impact of boundary definition on seasonal and annual air-sea CO_2 fluxes in the SO. A third outcome was an estimation of the contribution of each SO basin (i.e. Pacific, Atlantic and Indian Ocean) to the mean zonal seasonal cycle of air-sea CO_2 flux and annual CO_2 fluxes.

By the comparing the model output of the ORCA2-LIM-PISCES (2^o x 2^o cosØ) configuration and PERIANT05 (NEMO PISCES) (0.5^o x 0.5^o cosØ) configuration with respect to the Takahashi et al., 2009 (T09) observations, it was found that air-sea CO_2 fluxes are only better resolved south of 48^oS and some part of the Atlantic in the PERIANT05 configuration. North of 48^oS, PERIANT05 shows a general CO_2 outgassing bias and poor spatial comparison with relative to T09 observations. ORCA2 air - sea CO_2 fluxes on other hand were found to moderately compare with T09 observations north of 50^oS however poorly does so south of 50^oS. In the contrast ORCA2 air-sea CO_2 fluxes were found to show a general CO_2 in-gassing bias with respect to T09 observations.

The spatial map of ORCA2 air-sea CO_2 fluxes in the SO was found to poorly with T09 observations; it generally shows a CO_2 in-gassing bias with a few CO_2 outgassing hotspots zones not observed in observations air-sea CO_2 fluxes. The seasonal cycle of air-sea CO_2 flux in ORCA2 was found to be out of phase with T09 observations for almost all the selected sub-regions considered for the study. For the period between Jan-Mar however both ORCA2 and PERIANT05 seasonal cycles of air-sea CO_2 fluxes showed similar phasing with T09 observations but with different magnitudes. During this period (Jan – Mar) the observed values of air-sea CO_2 fluxes are predominantly SST driven by means of CO_2 surface solubility (K_0) variability. The ORCA2 seasonal cycle phasing similarity with observations in this period was found to be because ORCA2 air-sea CO_2 fluxes are solely SST driven (by means of K_0). Thus the SST component in the influence of air-sea CO2 fluxes is well represented in ORCA2, however other drivers (i.e. convective mixing and biological processes) are best minimal, but more likely, of no effect in the air-sea CO_2 flux seasonal cycle of ORCA2. In T09 observations, these processes are observed in accordance with the literature (e.g. Metzl et al., 2006, 2009; Sokolov et al., 2008; Thomalla et al., 2011).

The CO_2 outgassing hotspots observed in ORCA2 were found to coincide with regions of high Eddy Kinetic Energy (EKE) and deep winter Mixed layer Depths (MLD). It has been suggested that the CO_2 saturated waters, normally found below the mixed layer (Sarmiento and Gruber, 2006), are found much deeper in ORCA2, therefore only regions of high EKE and deep winter MLDs can reach these

waters and hence provide locations of CO_2 outgassing hotspots. This postulations is considered though ORCA2 is not eddy resolving at 2^o x 2^o because given that ORCA2 is highly eddy parameterized (Madec, 2008), it possess vertical diffusion at high EKE zones which will allow upward transport of DIC at this zones. Furthermore the lack or weak summer biological CO_2 uptake in ORCA2 was attributed to the absence of nutrient entrainment during the autumn-winter seasons when the MLD deepens. And hence K_0 continues to dominate air-sea CO_2 fluxes in the absence of primary production in spring. Basin contribution to the zonal mean air-sea CO_2 annual fluxes was found to be surface area based in ORCA2. This is mainly because the air-sea CO_2 fluxes of ORCA2 has a CO_2 in-gassing bias and are uniform for most parts of the SO and therefore integration of annual fluxes over a large area will give concomitant annual fluxes. The overestimates of air-sea CO_2 flux annual fluxes with relative to the T09 observations in ORCA2 is consistent with the model output of NEMO PISCES and NEMO-Plankton5 in L13.

In PERIANT05, the CO_2 outgassing bias observed as mention above among other factors was found to be due the underestimated pCO_2 atmospheric forcing used to run the simulation. The atmospheric pCO_2 forcing dataset used to run the PERIANT05 simulation was discovered to have been an order 10 µatm lower than the mean global atmospheric CO_2. However even when filtering the general underestimation of oceanic CO_2 in-gassing as a consequence of underestimated atmospheric forcing, PERINAT05 air-sea CO_2 fluxes were found to show some weakness in the representation of air-sea CO_2 fluxes spatial variability in the Sub-Antarctic zone. Some of the strong CO_2 outgassing zones in PERIANT05 were found to be appear as strong in-gassing zones in T09 observations, for example; the region along the Agulhas retroflection, northern Indian Ocean and the western northern Pacific Ocean. The seasonal cycle of air-sea CO_2 flux in PERIANT05 was found to generally show poor correlation with T09 observations at the SAZ (r^2 = -0.41 for 44^oS – 58^oS, r^2 = -0.08 for 40^oS – 50^oS and r^2 = -0.006 for the SAZ) however good correlated with observations south of 58^oS (r^2 = 62). Though PERIANT05 showed a poor correlation with observations at the SAZ, it was found to capture two [(i) late summer CO_2 outgassing driven by increase of Sea Surface Temperatures (SST) weakening CO_2 surface solubility (K_0), (ii) winter CO_2 outgassing driven by Convective mixing] of the three main features [(i),(ii) and (ii) summer biological CO_2 drawdown] of the seasonal cycle of air-sea CO_2 fluxes at the SAZ. The mean CO_2 annual fluxes of PERIANT05 in the SAZ were generally found to show a CO_2 outgassing bias with respect to T09 observations except for the polar zone and hence not comparable.

In comparison to findings Lenton et al., 2013 (L13), PERIANT05 model output was found to be different in sense that the biogeochemical models (BGMs) used in L13 showed better comparison

with observations at the zone 44°S – 58°S and poorly so south of 58°S, PERIANT05 however shows the opposite. PERIANT05's good comparison with T09 observations south of 58°S present an uncommon outcome in ocean modeling given that ocean models are generally known to perform very poorly south of 58°S (e.g. Gruber et al., 2009). A mechanistic understanding of the drivers of air-sea CO_2 fluxes south of 58°S is still an important missing gape in global carbon budget and hence the use of PERIANT05 with observations to harvest a deeper mechanistic understanding is an important future endeavor. In a subsequent paper following this study, such aspects are covered where a more detailed mechanistic description of the drivers of air-sea CO_2 fluxes is presented including the role DIC and Alkalinity seasonal variability in the seasonal cycle of air-sea fluxes

The use of dynamic boundaries was generally found not to improve the model's (NEMO PISCES) sensitivity to the observations seasonal cycle of air-sea CO_2 fluxes in both PERIANT05 and ORCA2. Basins' contribution to the zonal mean air-sea CO_2 fluxes was found to be non-uniform but influenced by regional process in PERIANT05. For example the Pacific and Indian Ocean were found to be CO_2 sources, however the Atlantic Ocean was found to lie between a sink CO_2 source and source influenced by the biological driven CO_2 uptake in the central Atlantic Ocean. From the results it was found evident that improvement of the spatial resolution in PERIANT05 (0.5^o x 0.5^o) from ORCA2 (2^o x 2^o) played a role in better resolving the seasonal cycle of air-sea CO_2 flux south of 48°S , however this results does not establish that resolution is the main default in ORCA2 . The absence of vertical mixing during autumn-winter and primary production in summer is considered the problem in the first order in ORCA2. At this stage disentangling the effect of resolution from the absence of DIC entrainment and summer biological CO_2 uptake in the ORCA2 seasonal cycle of air-sea CO_2 flux remains a challenge.

Given the findings of this study it is considered that the absence or weakness of the impact of boundary definition in the air-sea CO_2 fluxes in ORCA2 and PERIANT05 is mainly because the NEMO PISCES model is unable to resolve true ocean processes regulating air-sea CO_2 interaction. Thus it is anticipated that if ocean models can better resolve observations of air-sea CO_2 fluxes, the effect of boundary definition will be evident in the seasonal cycle and annual CO_2 fluxes. It should be noted that this study only focused on the Surface Ocean, however other processes in ocean interior also significantly affect the air-sea CO_2 fluxes i.e. subsurface CO_2 transport, ocean interior water masses transport and mixing, and etc. The scope of this study does not cover all processes driving air-sea CO_2 fluxes, but focused on the effect of boundary definition and model resolution of surface air-sea CO_2 fluxes. Other process might also play an important role in driving air-sea CO fluxes i.e. horizontal- vertical transport, meso-submesoscale, stratification and etc. Anticipated further caveat

is that the use the T09 observations as a baseline for comparison might create a bias in the analysis, given that observations are still very limited in the SO, where most observations are available for only three months of summer (Takahashi et al., 2009). The intrinsic variability of ORCA2, PERIANT05 and L13 results might also create another source of variability in the model outputs comparison. These aspects notwithstanding, this study has achieved its objective in highlighting some of the sources of variability between observations and model outputs in respect of air-sea CO_2 fluxes in the SO. Given that this studies only focused on the Surface Ocean, it is recommended that the findings presented here are further investigated in relation to the ocean interior.

7. References

Anav, A. et al. (2013): Evaluating the land and ocean components of the global carbon cycle in the CMIP5 earth system models. J. Climate, 26, 6801–6843.

Arrhenius, S. (1896). On the Influence of Carbonic Acid in the Air Upon the Temperature of the Ground. *Philosophical Magazine* 41: 237-76.

Aumont, O. and Bopp, L. (2006). Globalizing results from ocean in situ iron fertilization studies, *GlobalBiogeochem. Cycles* ., 20, GB2017, doi:10.1029/2005GB002591, 2006.

Bakker, D. C. E., Hoppema, M., Schroder, M., Geibert, W., and de Baar, H. J. W. (2008). A rapid transition from ice covered CO_2-rich waters to a biologically mediated CO2 sink in the eastern Weddell Gyre, *Biogeosciences*, 5, doi:10.5194 : 1373–1386.

Bolin, B. and Eriksson, E. (1958). Changes in the carbon dioxide content of the atmosphere and sea due to fossil fuel combustion, in: The Atmosphere and the Sea in Motion: Scientific Contributions to the Rossby Memorial Volume, edited by: Bolin, B., *New York, Rockefeller Institute Press*, 130–142.

Bates, N.R. (2001). Interannual variability of oceanic CO_2 and biogeochemical properties in the Western North Atlantic subtropical gyre, *Deep-SeaRes.II*., 48 (8–9): 1507–1528.

Bates, N. R. and Mathis, J. T. (2009). The Arctic Ocean marine carbon cycle: evaluation of the air-sea CO_2 exchanges, ocean acidification impacts and potential feedbacks. *Biogeosciences* 6: 2433–2459.

Borges, A.V. and Wanninkhof, R. (2007). 37th International Liege Colloquium on Ocean Dynamics, Liege, Belgium, May 2–6, 2005, 5th International Symposium on Gas Transfer at Water Surfaces. *J. Mar. Sys.* 66:1–3

Broecker, H.C., Peterman, J. and Siems, W. (1978). The influence of wind on CO_2 exchange in a wind wave tunnel, including the effects of monolayers. *J. Mar. Res.* 36:595–610

Broecker WS, Peng T-H, O¨ stlund G, Stuiver M. (1985). The distribution of bomb radiocarbon in the ocean. *J. Geophys. Res.* 99:6953–70

Broecker WS, Sutherland S, Smethie W, Peng T-H, O¨ stlund G. (1995). Oceanic radiocarbon: separation of the natural and bomb components. *Glob. Biogeochem. Cycles* 9:263–88

Caldeira, K., and Duff, P.B. (2000). The role of the Southern Ocean in uptake and storage of anthropogenic carbon dioxide, *Science*, 287: 620–622.

Canadell, J. G., Ciais, P., Gurney, K., Le Qu´ er ´ e, C., Piao, S., Raupach, M. R., and Sabine, C. (2011). An international effort to to quantify regional carbon fluxes, *EOS*, 92, 81 pp.

Carr, M.E. et al., (2006), A comparison of global estimation of marine primary production from ocean colour , *Deep-Ses Res., Part II*, 53, 741 – 770.

Cox, G. F. N. andWeeks,W. F (1983). Equations for determining the gas and brine volumes in sea-ice samples. *J. Glaciol.*, 29 : 306–316.

Dickson, A.G., 1981. An exact definition of total alkalinity and a procedure for the estimation of alkalinity and total inorganic carbon from titration data. *Deep-Sea Res*. 28A (6): 609–623.

Dickson, A.G. and Millero, F.J. (1987). A comparison of the equilibrium constants for the dissociation of carbonic acid in seawater media. *Deep-Sea Research Part a-Oceanographic Research Papers*. 34:1733-1743.

Fauchereau, N., Tagliabue, A., Monteiro, P., and Bopp, L. (2011). The response of phytoplankton biomass to transient mixiing events in the Southern Ocean*, Geophys. Res. Lett*., 38, L17601, doi:10.1029.

Fung, I. Y., Doney, S. C., Lindsay, K. and John, J. (2005). Evolution of carbon sinks in a changing climate, *Proc. Natl. Acad. Sci*., 202, doi:10.1073/pnas.0504949,102 : 11201– 11206.

Gnanadesikan, A., Gruber, N., Slater, R.D. and Sarmiento, J.L. (2002). Oceanic vertical exchange and new production: A comparison between model results and observations, *Deep Sea Res*. II, 49: 363–401.

Gruber, N., Sarmiento, J. L. and Stocker, T.F. (1996). An improved method for detecting anthropogenic CO2 in the oceans, *Global Biogeochem. Cycles*, 10(4), doi:10.1029/96GB01,608 : 809–837.

Gruber, N., Gloor, M., Fletcher, S. E. M., Doney, S. C., Dutkiewicz, S., Follows, M. J., Gerber, M., Jacobson, A. R., Joos, F., Lindsay, K., Menemenlis, D., Mouchet, A., Muller, S. A., Sarmiento, J. L., and Takahashi, T. (2009). Oceanic sources, sinks, and transport of atmospheric CO_2, *Global Biogeochem*. Cy*cles*., 23, GB1005, doi:10.1029/2008gb003349.

HLPE, (2012). Food security and climate change. A report by the High Level Panel of Experts on Food Security and Nutrition of the Committee on World Food Security, Rome 2012

Ho, D.T., Bliven, L.F.,Wanninkhof, R. And Schlosser, P. (1997). The effect of rain on air-water gas exchange. *Tellus B* 49:149–58

Ho, D. T., Law, C. S., Smith, M. J., Schlosser, P., Harvey, M. and Hill, P. (2006). Measurements of air-sea gas exchange at high wind speeds in the Southern Ocean: Implications for global parameterizations, *Geophys. Res. Lett*., 33, L16611, doi:10.10292006GL026817.

ICCCEA, Incorporating Climate Change Considerations in Environmental Assessment (2003), *The Federal-Provincial-Territorial Committee on Climate Change and Environmental Assessment*, ISBN 0-662-35454-0

Ito, T.,Woloszyn, M., and Mazloff, M. (2010). Anthropogenic carbon dioxide transport in the Southern Ocean driven by Ekman flow, *Nature*, 463, 80–84.

Iudicone, D., Madec,G., and McDougall, T.J. (2008). Water-mass transformations in a neutral density framework and the key role of light penetration. *J Phys Oceanogr*, 38(7):1357–1376. doi:10.1175/2007JPO3464.1

Keeling, C. D. (1970). "Is Carbon Dioxide from Fossil Fuel Changing Man's Environment?" *Proceedings of the American Philosophical Society* 114: 10-17

Keeling, C. D., Brix, H. and Grube, N. (2004). Seasonal and long-term dynamics of the upper ocean carbon cycle at Station ALOHA near Hawaii, *Global Biogeochem. Cycles*, 18, GB4006, doi:10.1029/ 2004GB002227

Lenton, A., Metzl, N., Takahashi, T., Kuchinke, M., Matear, R. J., Roy, T., Sutherland, S. C., Sweeney, C., and Tilbrook, B. (2012). The observed evolution of oceanic pCO(2) and its drivers over the last two decades, *Global Biogeochem. Cycles*., 26, GB2021, doi:10.1029/2011gb004095.

Lenton A., Tilbrook, B., Law, R., Bakker, D., Doney, S.C., Gruber, N., Hoppema, M., Ishii, M., Lovenduski, N.S., Matear, J.R., McNeil, B.I., Metzl, N., Mikaloff Fletcher, S.E., Monteiro, P., Rödenbeck, R., Sweeney, C. and Takahashi, T. (2013), Sea-air CO_2 fluxes in the Southern Ocean for the period 1990–2009, Biogeosciences Discuss., 10 : 285– 333.
Le Quèrè, C., Rodenbeck, C., Buitenhuis, E. T., Conway, T. J., Langenfelds, R., Gomez, A., Labuschagne, C., Ramonet, M., Nakazawa, T., Metzl, N., Gillett, N., and Heimann, M. (2007). Saturation of the Southern Ocean CO2 sink due to recent climate change, Science, 316, doi:10.1126/science.1136188: 1735– 1738.

Le Quèrè, C., Raupach, M. R., Canadell, J. G., Marland, G., Bopp, L., Ciais, P., Conway, T. J., Doney, S. C., Feely, R. A., Foster, P., Friedlingstein, P., Gurney, K., Houghton, R. A., House, J. I., Huntingford, C., Levy, P. E., Lomas, M. R., Majkut, J., Metzl, N., Ometto, J. P., Peters, G. P., Prentice, I. C., Randerson, J. T., Running, S. W., Sarmiento, J. L., Schuster, U., Sitch, S., Takahashi, T., Viovy, N., van der Werf, G. R., and Woodward, F. I. (2009).Trends in the sources and sinks of carbon dioxide, Nat. Geosci., 2, 10.1038/Ngeo689 : , 831–836, doi

Le Quèrè, C., Takahashi, T., Buitenhuis, E.T., Rödenbeck, C. and Surtherland, S.C. (2010). Impact of climate change and variability on the global oceanic sink of CO_2, 24, doi:10.1029/2009GB003599.

Liss, P.S., Heimann, M. and Roether, W. (1988). Tracers of air-sea gas exchange (and discussion). *Phil. Trans. R. Soc. London Ser. A Math. Phys. Sci.* 325:93–103

Liss, P.S. (1983). Gas transfer: experiments and geochemical implications. In *Air-Sea Exchange of Gases and Particles*, WG Slinn,: 241–99.

Lovenduski, N. S., and Gruber, N. (2005). Impact of the Southern Annular Mode on Southern Ocean circulation and biology*, Geophys. Res. Lett*., 32, L11603, doi:10.1029/2005GL022727.

Lovenduski, N., Gruber, N., Doney, S. C., and Lima, I. D. (2007). Enhanced CO_2 outagssing in the Southern Ocean from a positive phase of the Southern Annular Mode, Global Biogeochem Cy., 21, GB2026, doi:10.1029/2006GB002900.

Lovenduski, N. S., Gruber, N., and Doney, S. C. (2008). Toward a mechanistic understanding of the decadal trends in the Southern Ocean carbon sink, *Global Biogeochem. Cycles*., 22, GB3016, doi:10.1029/2007gb003139.

Loose, B., Schlosser, P., Perovich, D., Ringelberg, D., Ho, D. T. and co-authors (2011). Gas diffusion through columnar laboratory sea ice: implications for mixed-layer ventilation of CO2 in the seasonal ice zone. *Tellus* 63B, 23–39.

Madec, G. (2008). NEMO ocean engine. IPSL Note du Pole de Mode´ lisation 27/

Matear, R. J. and Lenton, A. (2005). Impact of historical climate change on the southern ocean carbon cycle, J. Climate, 21, doi:10.1175/2008JCLI2194.1 : 5820–5834.

Matsumoto, K. and Gruber, N. (2005). How accurate is the estimation of anthropogenic carbon in the ocean? An evaluation of the É*C*_ method, *Global Biogeochem. Cycles*., 19, GB3014, doi:10.1029/2004GB002397.

McNeil, B. I., Metzl, N., Key, R.M., Matear, R.J. and Corbiere, A. (2007). An empirical estimate of the Southern Ocean air-sea CO_2 flux, *Global Biogeochem. Cycles*, 21, GB3011, doi:10.1029/2007GB002991.

Millero, F.J., Byrne, R.H. Wanninkhof, R, Feely, R.A, Clayton, T. , Murphy, P. and Lamb, M.L. (1993) . The internal consistency of CO2 measurements in the equatorial Pacific , *Mar. Chem*., 44, 269-280.

Metzl, N., Brunet, C., Jabaud-Jan, A., Poisson, A., and Schauer, B. (2006). Summer and winter air-sea CO_2 fluxes in the Southern Ocean*, Deep-Sea Res*. Pt. I, 53, 1548–1563, doi:10.1016/j.dsr.2006.07.006.

Metzl, N. (2009). Decadal increase of oceanic carbon dioxide in Southern Indian Ocean surface waters (1991 – 2007), Deep-Sea Res, Pt. II, 56: 607 – 619.

Mehrbach, C., Culberson, C.H., Hawley, J.E. and Pytkowice, R.M. (1973). Measurement of the apparent dissociation constants of carbonic acid in seawater at atmospheric pressure, *Limnol. Oceanogr*, 18: 897-907.

Mikaloff Fletcher, S. E., Gruber, N., Jacobson, A. R., Doney, S. C., Dutkiewicz, S., Gerber, M., Follows, M., Joos, F., Lindsay, K., Menemenlis, D., Mouchet, A., Muller, S. A., and Sarmiento, J. L. (2006). Inverse estimates of anthropogenic CO2 uptake, transport, and storage by the ocean, *Global Biogeochem. Cycles*., 20, GB2002, doi:10.1029/2005GB002530.

Mikaloff Fletcher, S. E., Gruber, N., Jacobson, A. R., Gloor, M., Doney, S. C., Dutkiewicz, S., Gerber, M., Follows, M., Joos, F., Lindsay, K., Menemenlis, D., Mouchet, A., Muller, S. A., and Sarmiento, J. L. (2007). Inverse estimates of the oceanic sources and sinks of natural CO2 and the implied oceanic carbon transport, *Global Biogeochem. Cycles*., 21, GB1010, doi:10.1029/2006gb002751.

Monteiro, P., Schuster, U., Hood, M., Lenton, A., Metzl, N., Olsen, A., Rogers, K., Sabine, C., Takahashi, T., Tilbrook, B., Yoder, J., Wanninkhof, R., and Watson, A.: A global sea surface carbon observing system: assessment of changing sea surface CO_2 and air-sea CO_2 fluxes, edited by: Hall, J., Harrison, D. E., and Stammer, D., (2010). Proceedings of the "OceanObs'09: Sustained Ocean 5 Observations and Information for Society" Conference, Venice, Italy, 21–25 September 2009*, ESA Publication WPP-306*. A global sea surface carbon observing system: assessment of changing sea surface CO_2 and air-sea CO_2 fluxes, OceanObs'09: Sustained Ocean Observations and Information for Society, Venice, Italy.
Nomura, D., Yoshikawa-Inoue, H. and Toyota, T. 2006. The effect of sea-ice growth on air-sea CO2 flux in a tank experiment. *Tellus* **58B**, 418–426, doi:10.1111/j.1600-0889.2006.00204.x.

Omar, A., Johannessen, T., Bellerby, R. G. J., Olsen, A., Anderson, L. G., and co-authors (2005). Sea-ice and brine formation in Storfjorden: implications for Arctic wintertime air-sea CO2 flux. In: *The Nordic Seas: An Integrated Perspective* (eds Drange, H., Dokken, T., Furevik, T., Gerdes, R. and Berger W.) Geophysical Monograph 158*, American Geophysical Union*, Washington, DC: 117–187.

Orsi, A. H., Whitworth III, T. and owlin, W. D. (1995). On the meridional extent and fronts of the Antarctic circumpolar current, *Deep Sea Res*., 42: 641-673.

Pardo MA, Silverberg N, Gendron D, Beier E, Palacios DM (2013) Role of environmental seasonality in the turnover of a cetacean community in the southwestern Gulf of California. *Mar Ecol Prog Ser*, 487: 245–260

Revelle, R. (1985). Introduction: The scientific history of Carbon Dioxide. In *The carbon cycle and atmospheric CO2: natural variations Archean to present*, volume 1, pages 1-4.

Rysgaard, S., Nielsen, T. G. and Hansen, B.W (1999). Seasonal variation in nutrients, pelagic primary production and grazing in a high-Arctic coastal marine ecosystem, Young Sound, Northeast Greenland. *Mar. Ecol. Prog. Ser.* 179, 13–25.

Rysgaard, S., Glud, R. N., Sejr, M. K., Bendtsen, J. and Christensen, P. B. (2007). Inorganic carbon transport during sea ice growth and decay: a carbon pump in polar seas. *J. Geophys. Res.* 112, C03016, doi:10.1029/2006JC003572.

Rysgaard, S., Bendtsen, J., Delille, B., Dieckmann, G.S., Glud, R.N., Kennedy, H., Mortensen, J. Paradimitriou, S., Thomas, D.N. and Tison J. (2011). Sea ice contribution to the air–sea CO_2 exchange in the Arctic and Southern Oceans, *Tellus,* 63B: 823–830

Rintoul, S. R., and Trull T. W. (2001). Seasonal evolution of the mixed layer in the subantarctic zone south of Australia. *J. Geophys. Res., 107*, 31: 447–31 460.

Rintoul, S.R., and England, M. H. (2001). Ekman Transport dominates Local air-sea Fluxes in Driving Variability of subantarctic mode water, *American meteorological society*, vol 32:1308 – 1321.

Rodgers, K. B., Sarmiento, J. L., Aumont, O., Crevoisier, C., de Boyer Mont´egut, C., and Metzl, N. (2001). A wintertime uptake window for anthropogenic CO_2 in the North Pacific, *Global Biogeochem*. *Cycles*., 22, GB2020, doi:10.1029/2006GB002920.

Roy, T., Rayner, P. J., Matear, R. J., and Francey, R. (2003). Southern Hemisphere ocean CO_2 uptake: reconciling atmospheric and oceanic estimates, *Tellus*, 55B : 701–710.

Sabine, C. L., et al. (2004). The oceanic sink for anthropogenic CO_2, *Science*, 305:367– 371.

Sallèè, J. B., Matear, R. J., Rintoul, S. R., and Lenton, A. (2012). Localized subduction of anthropogenic carbon dioxide in the Southern Hemisphere oceans, *Nat. Geosci*., 5, doi:10.1038/Ngeo1523 : 579–584.

Sallée, J,Wienders, N., Morrow, R. and Speer, K. (2006). Formation of subantarctic mode water in the southeastern Indian Ocean. *Ocean Dyn.,* **56,** 525–542..
Sarmiento, J. L., and Gruber, N. (2002), Anthropogenic carbon sinks, *Phys. Today*, 55: 30– 36.

Sarmiento, J. L., Orr, J.C and Siegenthaler, U. (1992). A perturbation simulation of CO2 uptake in an ocean general circulation model, *J. Geophys. Res*., 97(C3) :621– 3645.

Sarmiento, J. L., Gruber, N., Brzezinski, M. A., and Dunne, J. P. (2004). High-latitude controls of thermocline nutrients and low latitude biological productivity, *Nature*, 427: 56–60.

Shcherbina, A. Y., Talley, L. D. and Rudnick, D. L. 2003. Direct observations of North Pacific ventilation: Brine rejection in the Okhotsk Sea. *Science* **302**, 1952–1955.

Schlitzer, R. (2002). Carbon export fluxes in the Southern Ocean: results from inverse modelling and comparison with satellite based estimates, Deep-Sea Res. Pt. II, 49: 1623–1644.

Sèfèrian, R., Iudicone, D., Bopp, L., Roy, T. and Madec, G. (2012). Water mass analysis of effect of climate change on air-sea CO_2 fluxes: the Southern Ocean, *America meteorological society*, vol 25 ,doi: 10.1175/JCLI-D-11-00291.1: 3894- 3908.

Sokolov, S. and Rintoul, S. R. (2007). On the relationship between fronts of the Antarctic Circumpolar Current and surface chlorophyll concentrations in the Southern Ocean, J. *Geophys. Res.*, 112, C07030, doi:10.1029/2006JC004072.

Sololov, S. (2008). Chlorophyll blooms in the Antarctic Zone south of Australia and New Zealand in reference to the Antarctic Circumpolar Current fronts and sea ice forcing, *J. Geophys. Res*., 113, C03022, doi:10.1029/2007JC004329.

Sorenson, R. P. (2011). "Eunice Foote's Pioneering Research on CO_2 and Climate Warming." *Search and Discovery*: Article:70092.

Sulzman, E.W. (2000). The carbon cycle, *university Corporation for Atmospheric Research*.

Speer, K.G , Isemer, H.J. and Biastoch, A. (1995). Water Mass Formation from Revised COADS Data. *Journal of Physical Oceanography*, 25(10):2444—2457.

Sverdrup, H. U. (1953). On conditions for the vernal blooming of phytoplankton*, J. Conseil*, 18: 287–295.

Takahashi, T., Sutherland, S. C., Sweeney, C., Poisson, A., Metzl, N., Tilbrook, B., Bates, N., Wanninkhof, R., Feely, R. A., Sabine, C., Olafsson, J. and Nojiri, Y. (2002). Global sea-air CO_2 flux based on climatological surface ocean *p*CO2 and seasonal biological and temperature effects, *Deep-Sea Research Pt. II*, 49: 1601–1622.

Takahashi, T., Takahashi, T.T., and Sutherland, S.C. (1995). Assessment of the role of the North Atlantic as a CO_2 sink. *Philos.Trans.R.So*c. LondonB348 : 143–152.

Takahashi, T., Sutherland, S. C., Wanninkhof, R., Sweeney, C., Feely, R. A., Chipman, D. W., Hales, B., Friederich, G., Chavez, F., Sabine, C., Watson, A., Bakker, D. C. E., Schuster, U., Metzl, N., Yoshikawa-Inoue, H., Ishii, M., Midorikawa, T., Nojiri, Y., Kortzinger, A., Steinhoff, T., Hoppema, M., Olafsson, J., Arnarson, T. S., Tilbrook, B., Johannessen, T., Olsen, A., Bellerby, R., Wong, C. S., Delille, B., Bates, N. R. and de Baar, H. J. W. (2009). Climatological mean and decadal change in surface ocean *p*CO2, and net sea-air CO2 flux over the global oceans, *Deep-Sea Research Pt. II*, 56, doi:10.1016/J.Dsr2.2008.12 : 554 577.

Takahashi, T., Sweeney, C., Hales, B., Chipman, D. W., Newberger, T., Goddard, J. G., Iannuzzi, R. A., and Sutherland, S. C. (2012),The changing carbon cycle in the Southern Ocean, Oceanography, 25: 26 37.

Tanhua, T., Körtzinger, A., Friis, K., Waugh, D.W. and Wallace, D.W.R. (2007). An estimate of anthropogenic CO_2 inventory from decadal changes in oceanic carbon content, *Proce. Natl. Acad*. Sci., 104(9), doi:10.1073pnas.0606574104 : 3037– 3042.

Thomalla, S. J., Fauchereau, N., Swart, S., and Monteiro, P. M. S. (2011). Regional scale characteristics of the seasonal cycle of chlorophyll in the Southern Ocean*, Biogeosciences*, 8, 2849–2866, doi:10.5194/bg-8-2849-2011.

Thompson, D. W. J. and Solomon, S. (2002). Interpretation of recent Southern Hemisphere climate change, *Science*, 296: 895–899.

Thompson, D.W.J., Solomon, S., Kushner, P.J., England, M.H., Grise, K.M. and Karoly, D.J. (2011). Signatures of the Antarctic ozone hole in Southern Hemisphere surface climate change. *Nature Geoscience.* doi:10.1038/ngeo1296.

Treguier, A.M., Böning, C.W., Bryan, F., Danabasoglu, G., Drange, H.,Taguchi, B., Pirani, A., (2014) CLIVAR WGOMD Workshop on high resolution ocean climate modelling: outcomes and recommendations, *CLIVAR Exchanges No.* 65, Vol. 19, No. 2

Milliman, J.D. (1993), Production and accumulation of calcium carbonate in the ocean: budget of nonsteady state, *Global Bio-geochem*. Cycles, 7, 927-957.

Wanninkhof, R. (1992), Relationship between gas exchange and wind speed over the ocean., *J. Geophys. Res*., 97: 7373–7381.

Wanninkhof, R., Asher, W. E., Ho, D. T., Sweeney, C. S., and McGillis, W. R. (2009). Advances in quantifying air-sea gas exchange and environmental forcing, Ann. *Rev. Mar. Sci*., 1, 213–244, doi:10.1146/annurev.marine.010908.163742..

Wanninkhof, R., Park, G.H., Takahashi, T., Sweeney, C., Feely, R., Nojiri, Y., Gruber, N., Doney, S. C., McKinley, G. A., Lenton, A., Le Qu´ er ´ e, C., Heinze, C., Schwinger, J., Graven, H., and Khatiwala, S.: Global ocean carbon uptake: magnitude, variability and trends, Biogeo10 sciences Discuss., 9, 10961–11012, doi:10.5194/bgd-9-10961-2012, 2012.

Weeks, W. F. and Ackley, S. F. (1986). The growth, structure and properties of sea ice. In: *The Geophysics of Sea Ice* (ed. Untersteiner, N.). Plenum, New York.

Weiss, R. F. (1974). Carbon dioxide in water and seawater: The solubility of a nonideal gas, *Mar. Chem*., 2: 203-215.

Wofl-Gladrow, D.A, Richard, E.Z., Klass, C., Körtziner, A. and Dickson, A.G. (2007). Total alkalinity: The explicit conservative expression and its application to biogeochemical processes, Marine *Chemistry*, 106 : 287–300

8. Apendix A

The seassonal cycel of air-sea CO_2 flux at the geographi and dynamic boundaries with ancillary variables driving the air-sea fluxes.

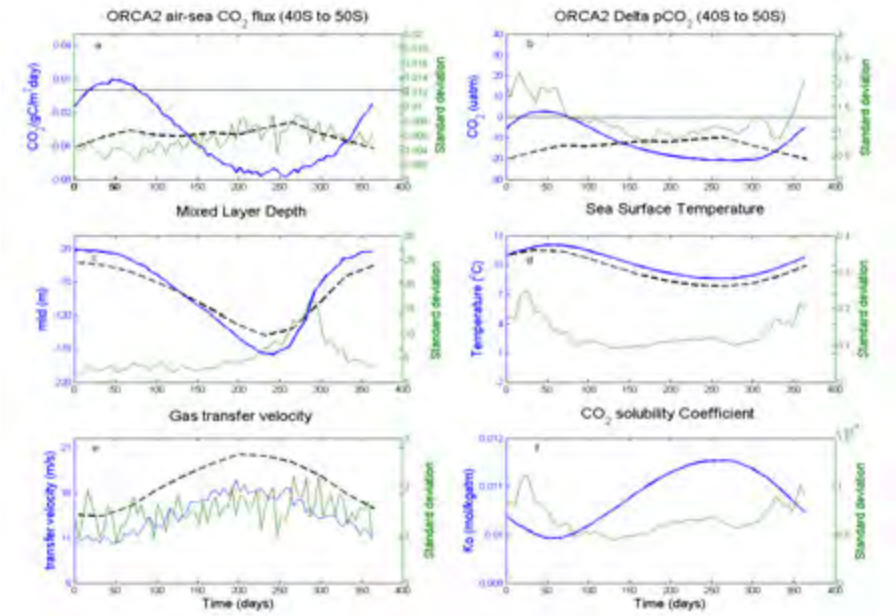

Figure 8.1 The seasonal cycle of air – sea CO_2 flux and ancillary variables in the 40°S - 50°S zone from the ORCA2 model. (a) CO_2 flux ($gCm^{-2}yr^{-1}$) negative indicates flux into the ocean (b) Delta pCO2 (µatm) , (c) Mixed layer depth (MLD m) , (d) Sea Surface Temperature (SST), (e) Gas transfer velocity (ms^{-1}) , (f) CO_2 solubility Coefficient ($mmolL^{-1}atm^{-1}$). The x-axis in all figures reflects annual period in days. The dotted line in each figure above show the T09 observations

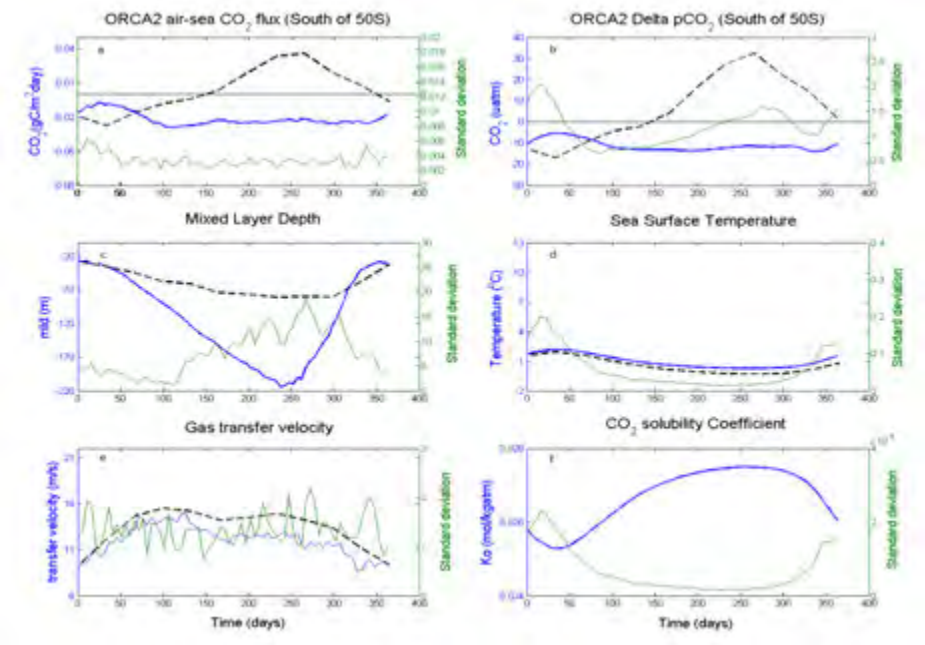

Figure 8.2 The seasonal cycle of air – sea CO_2 flux and ancillary variables in the south of 50°S zone from the ORCA2 model. (a) CO_2 flux ($gCm^{-2}yr^{-1}$) negative indicates flux into the ocean (b) Delta pCO2 (µatm) (c) Mixed layer depth (MLD m) , (d) Sea Surface Temperature (SST), (e) Gas transfer velocity (ms^{-1}) , (f) CO_2 solubility Coefficient ($mmolL^{-1}atm^{-1}$). The x-axis in all figures reflects annual period in days. The dotted line in each figure above show the T09 observations

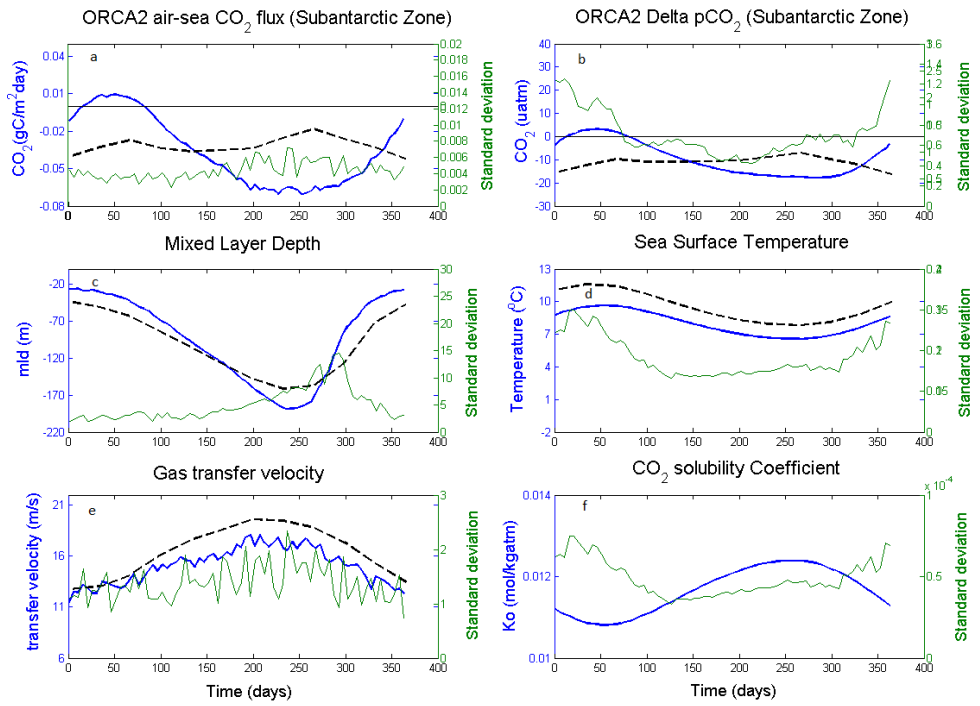

Figure 8.3 The seasonal cycle of air – sea CO_2 flux and ancillary variables in the sub-Antarctic zone from the ORCA2 model. (a) CO_2 flux ($gCm^{-2}yr^{-1}$) negative indicates flux into the ocean (b) Delta pCO2 (µatm) , (c) Mixed layer depth (MLD m) , (d) Sea Surface Temperature (SST), (e) Gas transfer velocity (ms^{-1}) , (f) CO_2 solubility Coefficient ($mmolL^{-1}atm^{-1}$). The x-axis in all figures reflects annual period in days. The dotted line in each figures above show the T09 observations.

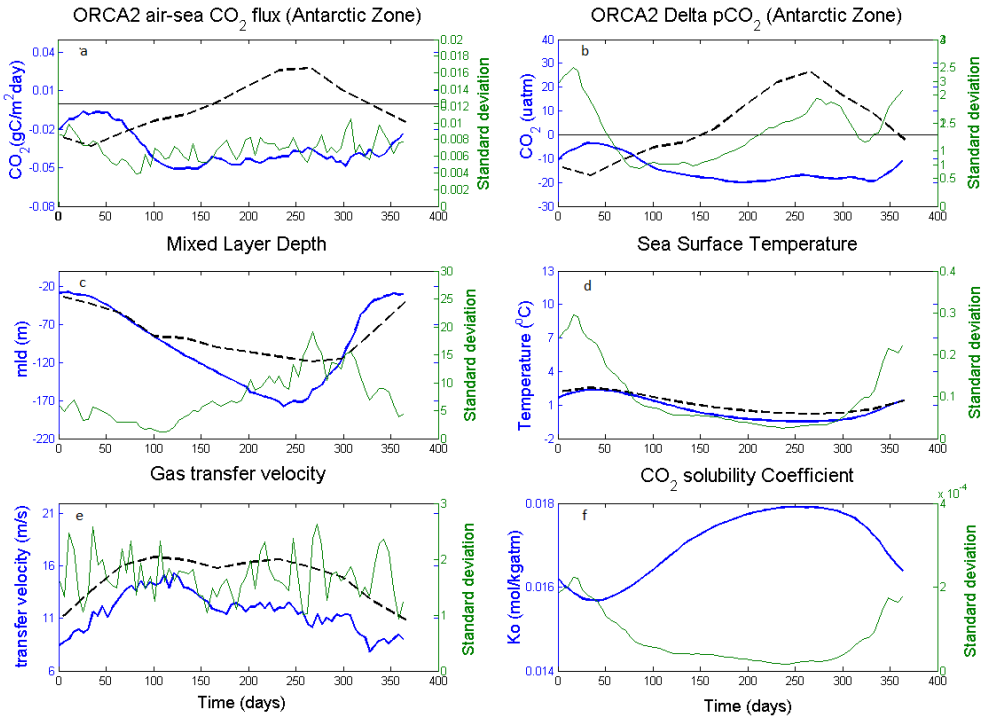

Figure 8.4 The seasonal cycle of air – sea CO_2 flux and ancillary variables in the Antarctic zone from the ORCA2 model. (a) CO_2 flux ($gCm^{-2}yr^{-1}$) negative indicates flux into the ocean (b) Delta pCO2 (µatm) (c) Mixed layer depth (MLD m) , (d) Sea Surface Temperature (SST), (e) Gas transfer velocity (ms^{-1}) , (f) CO_2 solubility Coefficient ($mmolL^{-1}atm^{-1}$). The x-axis in all figures reflects annual period in days. The dotted line in each figures above show the T09 observations.

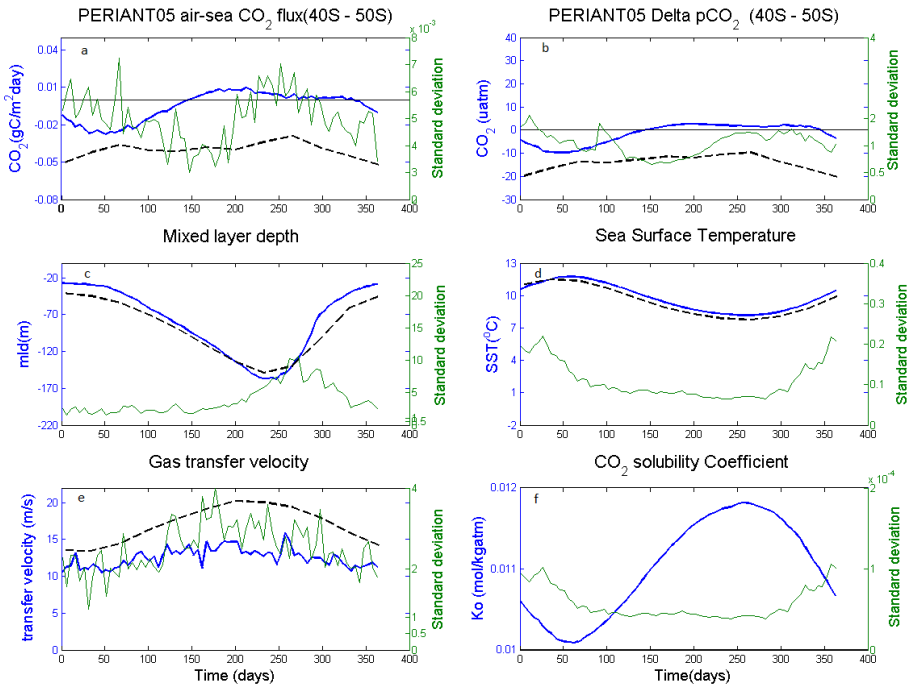

Figure 8.5 The seasonal cycle of air – sea CO_2 flux and ancillary variables in the 40°S - 50°S zone from the PERIANT05 model. (a) CO_2 flux ($gCm^{-2}yr^{-1}$) negative indicates flux into the ocean (b) Delta pCO2 (µatm) , (c) Mixed layer depth (MLD m) , (d) Sea Surface Temperature (SST), (e) Gas transfer velocity (ms^{-1}) , (f) CO_2 solubility Coefficient ($mmolL^{-1}atm^{-1}$). The x-axis in all figures reflects annual period in days. The dotted line in each figure above show the T09 observations

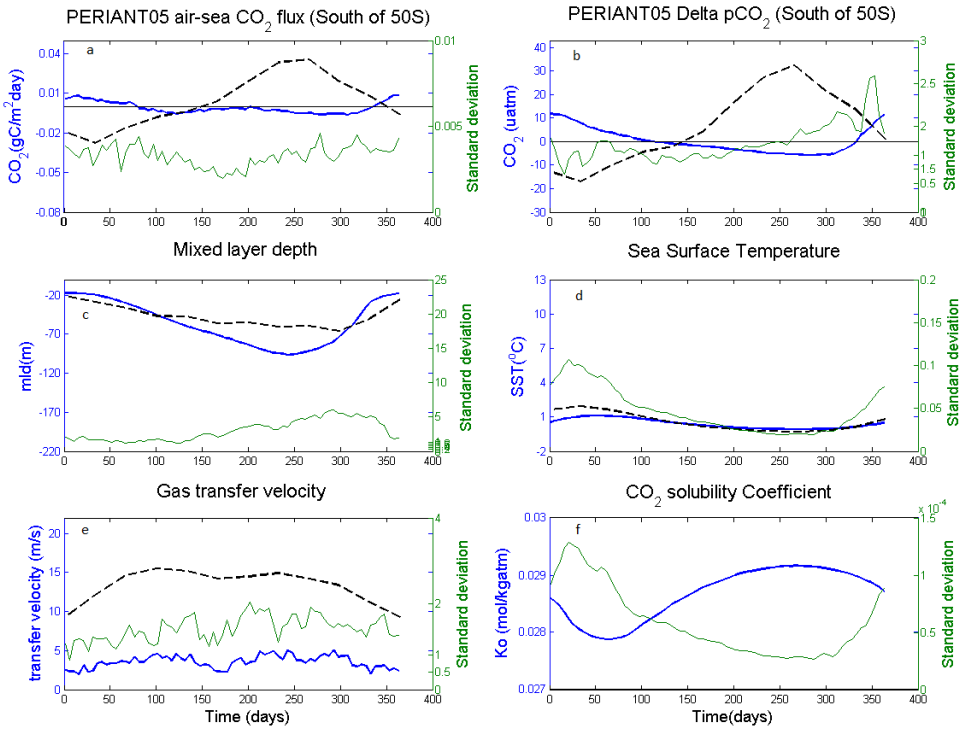

Figure 8.6 The seasonal cycle of air – sea CO_2 flux and ancillary variables south of 50°S zone from the PERIANT05 model. (a) CO_2 flux ($gCm^{-2}yr^{-1}$) negative indicates flux into the ocean (b) Delta pCO2 (µatm) , (c) Mixed layer depth (MLD m) , (d) Sea Surface Temperature (SST), (e) Gas transfer velocity (ms^{-1}) , (f) CO_2 solubility Coefficient ($mmolL^{-1}atm^{-1}$). The x-axis in all figures reflects annual period in days. The dotted line in each figure above show the T09 observation

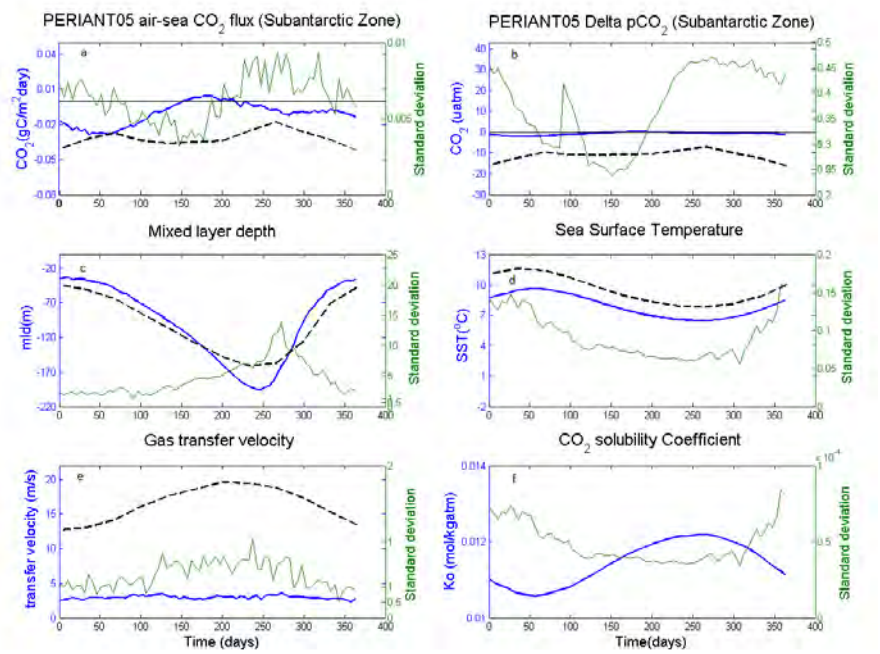

Figure 8.7 The seasonal cycle of air – sea CO_2 flux and ancillary variables in the sub-Antarctic zone from the PERIANT05 model. (a) CO_2 flux ($gCm^{-2}yr^{-1}$) negative indicates flux into the ocean (b) Delta pCO2 (µatm) , (c) Sea Surface Temperature (SST), (d) Gas transfer velocity (ms-1) , (e) CO_2 solubility Coefficient (mmolL-1atm-1) and (f) Mixed layer depth (MLD m) (c) Mixed layer depth (MLD m) , (d) Sea Surface Temperature (SST), (e) Gas transfer velocity (ms^{-1}) , (f) CO_2 solubility Coefficient ($mmolL^{-1}atm^{-1}$). The x-axis in all figures reflects annual period in days. The dotted line in each figure above show the T09 observations

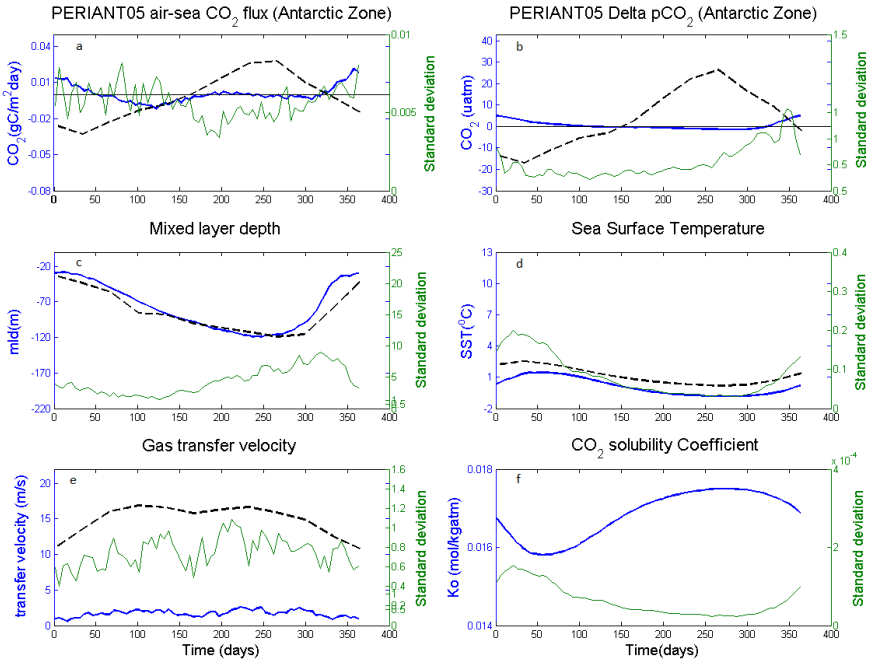

Figure 8.8 The seasonal cycle of air – sea CO_2 flux and ancillary variables in the Antarctic zone from the PERIANT05 model. (a) CO_2 flux ($gCm^{-2}yr^{-1}$) negative indicates flux into the ocean (b) Delta pCO2 (µatm) , (c) Mixed layer depth (MLD m) , (d) Sea Surface Temperature (SST), (e) Gas transfer velocity (ms^{-1}) , (f) CO_2 solubility Coefficient ($mmolL^{-1}atm^{-1}$). The x-axis in all figures reflects annual period in days. The dotted line in each figure above show the T09 observations

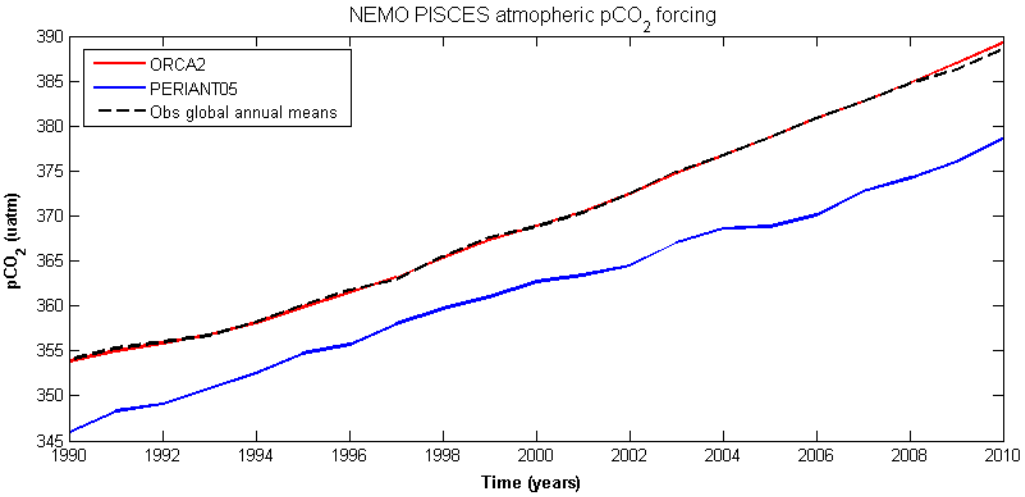

Figure 8.9 Shows the atmospheric partial pressure of CO_2 (pCO_2) forcing of NEMO PISCES for the ORCA2 and PERIANT05 configurations, given in µatm with respect to the mean global atmospheric pCO_2. Note that atmospheric pCO2 of PERIANT05 is about 10 µatm lower than that global mean atmospheric CO_2.

Appendix B

(i) Specifications for O2LP ORCA2-LIM-PISCES

Domain	Global -179.75 to 180.0°E, -78.19-89.61°N		
Horizontal grid	x=182, y=149, xy= 27,118, xyz=840,658 Resolution 2°, tripolar, two poles in Northern Hemisphere		
Vertical grid	31 vertical levels, z-coordinate with partial-bottom steps Upper 200m (16 levels: ~5, 15, 25, ...129, 142, 159, 182m) Upper 500m (19 levels: ~217, 272, 364, 512m)		
Bathymetry	2° global model		
Initial conditions	Started with dynamics and ice from O2L-SPIN01A Biology from climatology: glodap Alk, DIC, DOC, Fe, NO3, O2, PO4 and Si		
Run duration	1768-2007 (forcing CORE11b five times, to equilibrate carbon) Pre-industrial spin-up: 1768-1827 (constant 1828 carbon, annual average) Anthropogenic spin-up: 1828-2007 (interannual carbon, annual average)		
Lateral Boundary conditions	No open boundaries		
Surface boundary conditions	Atmospheric forcing	COREIIb applied to ORCA2 grid	
		10m u and v swrad, lwrad. tair, thumi (t2, q2) precip, snow	6 hours 24 hours 6 hours 1 month
	Damping	T and S are damped to climatologies	
	Runoffs	S and T, are included at a frequency of 24 hours. River treatments, mixing over upper 15m	

	Sea surface restoring	Salinity only - using Levitus climatology
	Penetration of light	Read from a climatology fron seawifs
	Dust ndeposition	1m climatology Annual
Bottom boundary conditions	Linear bottom friction. Includes geothermal heating read from file Diffusive bbl scheme.	
Model numerics	Advection scheme: TVD Eddy mixing parameterised (Gent and McWilliams 1990) Laplacian lateral diffusion for tracers along isoneutral surfaces Biplacian lateral diffusion of momentum along geopotential surfaces implicit time stepping vertical diffusion is handled by TKE scheme, with tke source below the ML, langmuir paramererisation, surface mixing length scale is a function of wind stress first vertical derivative of mixing length bounded by 1	

(ii) Specifications for PERIANT05-GAA95b

Domain	Regional Circumpolar 72.75-73.25°E, 78.59-29.59°S
Horizontal grid	x=722, y=202 Resolution 0.5°
Vertical grid	46 vertical levels, z-coordinate with partial-bottom steps Upper 200m (16 levels: ~5, 15, 25, ...129, 142, 159, 182m)

	Upper 500m (19 levels: ~217, 272, 364, 512m)		
Bathymetry	From PERIANT05 – physics model		
Initial conditions	Started from rest T and S from Levitus Ice from ORCA05-g70.112		
Run duration	1992-2011		
Lateral Boundary conditions	Only northern boundary open. OBC • 5d ocean dynamics from ORCA05-GAA95b • 1m tracer climatologies – Alk, DIC, DOC, De, NO3, O2, PO4, Si		
Surface boundary conditions	Atmospheric forcing	ERAInterim	
		10m u and v swrad, lwrad. tair, thumi (t2, q2) precip, snow	3 hours 24 hours 3 hours 24 hours
	Damping	T and S are damped to climatologies	
	Runoffs	S and T, are included at a frequency of 24 hours. River treatments, mixing over upper 10m	
	Sea surface restoring	Salinity only - using Levitus climatology	
	Penetration of light	2 bands, constant	
	PISCES Forcing	Dust, river input, bathy	
Bottom boundary conditions	Non-linear bottom friction.		
Model numerics	Advection scheme: TVD		

	Eddy mixing parameterised (Gent and McWilliams scheme) Laplacian lateral diffusion for tracers along isoneutral surfaces Biplacian lateral diffusion of momentum along geopotential surfaces implicit time stepping vertical diffusion is handled by TKE scheme, with tke source below the ML, langmuir paramererisation, surface mixing length scale is a function of wind stress first vertical derivative of mixing length bounded by 1